SAPIENZA
UNIVERSITÀ DI ROMA

Superfluidity in neutron star matter

Facoltà di Scienze Matematiche, Fisiche e Naturali

Corso di Laurea Magistrale in Fisica

Candidato

Giulia De Rosi

Matricola 1217074

Relatore

Prof. Omar Benhar Noccioli

Anno Accademico 2012/2013

Superfluidity in neutron star matter
Tesi di Laurea Magistrale. Sapienza – Università di Roma

Questa tesi è stata composta con LaTeX e la classe Sapthesis.

Email dell'autore: giuliacciadr@gmail.com

A mio nipote Diego

"Qualunque cosa tu possa fare, qualunque sogno tu possa sognare, comincia.
L'audacia reca in se genialità, magia e forza. Comincia ora"
Johann Wolfgang Göethe

Contents

Introduction

The description of the properties of neutron star matter requires the use of concepts and techniques belonging to different fields of Physics [1]. For example, the study of the superfluid and superconducting transitions that are believed to take place inside the star, encompasses nuclear and particle Physics, as well as condensed matter Physics [2].

In neutron stars, both conditions for the occurrence of superfluidity in fermion systems, i.e. strong degeneracy and the existence of an attractive interaction between the constituents, are fulfilled. The onset of a superfluid (and/or superconducting) phase does not have a significant impact on the equation of state, determining the equilibrium properties of the star, except in the very low density region of the crust. The condensation energy – i.e. the difference between the energies of the normal and superfluid states associated with the formation of Cooper pairs – is in fact negligible with respect to the typical energies of the normal phase.

The main effect of the superfluid transition is the appearance of a gap in the energy spectrum, in the vicinity of the Fermi surface. This leads to a strong reduction of the phase space available to particles undergoing scattering processes, which in turn results in a strong modification of the neutrino emission, scattering and absorption rates and of the transport coefficients, including the shear viscosity and thermal conductivity. As a consequence, a quantitative understanding of the superfluid phase is required to study both neutron star cooling and the stability of rotating stars, which is largely determined by dissipative processes.

This Thesis is part of a broad project, aimed at developing a consistent description of equilibrium and non equilibrium properties of neutron stars, based on a realistic model of nuclear dynamics at microscopic level. The main element of the proposed approach is an effective nucleon-nucleon interaction, derived from a realistic phenomenological Hamiltonian – strongly constrained by the available data – within the formalism of Correlated Basis Function (CBF) [3, 4]. Unlike the bare nucleon-nucleon force, this interaction is well behaved at short distances, and can be used to carry out perturbative calculations in the basis of eigenstates of the non-interacting system.

Previous applications of the CBF effective interaction approach include the calculations of the shear viscosity and thermal conductivity coefficients [3, 5, 6], as well as of the nuclear matter response to both charged- and neutral-current neutrino interactions [7, 8, 9].

We have used the same CBF effective interaction to compute the superfluid gap of pure neutron matter, arising from the formation of Cooper pairs of neutrons in states of relative angular momentum $\ell = 0$, in which the nuclear interaction is

attractive.

In Chapter 1, we outline the process leading to the formation of neutron stars and summarize the present understanding of their structure.

Chapter 2 is devoted to the discussion of the mechanism responsible for the formation of Cooper pairs, leading in turn to the appearance of a superconductive phase, while in Chapter 3 we describe the variational approach to superconductivity originally developed by Bardeen, Cooper and Schrieffer, that we have followed in our work.

In Chapter 4 we analyze the main features of nuclear structure and dynamics, while in Chapter 5 we focus on the complexity of the nucleon-nucleon interaction and the difficulties associated with the solution of the nuclear many-body problem.

Finally, in Chapter 6, we present our numerical results, including the momentum dependence of the solution of the gap equation, $\Delta(\mathbf{k})$, at fixed density, as well as the density dependence of $\Delta(k_F)$, k_F being the Fermi momentum. The calculations have been carried out for the case of pure neutron matter, focusing on Cooper pairs of neutrons in the $^1S_0$ state.

Throughout this Thesis we always use a system of units in which $\hbar = h/2\pi = c = 1$ where h is Planck's constant and c is the speed of light.

Chapter 1

Neutron stars

The study of neutron stars encompasses many different fields of Theoretical Physics. The primary interest is obviously astrophysical, because a neutron star is one of the possible outcomes of stellar evolution. In addition, neutron stars are interesting from the gravitational point of view, as their non radial oscillations give rise to emission of gravitational waves, the frequencies and damping times of which depend on the internal structure of the star. The detection of a gravitational signal emitted by a neutron star may in fact provide valuable information on the properties of matter in a density regime not attainable by terrestrial experiments. In this context, a critical role is played by the development of theoretical models of neutron star matter capable to provide quantitative predictions of the gravitational emission. Finally, neutron stars are very interesting from the point of view of nuclear and particle physics: they can be regarded as atomic nuclei of macroscopic, indeed gigantic, size, that may undergo transitions to exotic states, associated with the appearance of strange baryons and deconfined quarks.

Realistic models of neutron star matter, besides being based on an accurate description of nuclear dynamics, must take into account phenomena that are typical of condensed matter, such as the transition to a superfluid phase in fermion systems. The occurrence of a superfluid phase, the study of which is the subject of this work, leads to a sharp modification of the viscous properties of neutron star matter, thus dramatically affecting the onset of the so called Chandrasekhar instability [6]. In 1970, Chandrasekhar [10, 11] demonstrated that the emission of gravitational radiation from rotating stars may lead to instability. For a non-rotating star, the gravitational wave emission is purely dissipative and damps the oscillations. For a rotating star, on the other hand, there are two possibilities. If the oscillations propagates in the direction opposite to the star rotation, gravitational emission reduces the amplitude of the perturbation, in such a way as to conserve angular momentum. For a fast-rotating star, on the other hand, the oscillations are dragged to move in the same direction as the star rotation. In this case, conservation of angular momentum requires that the perturbation amplitude grow, thus leading to instability (Fig.1.1). Of particular relevance is the instability driven by the so called r-modes oscillations, the restoring force of which is the Coriolis force.

Chandrasekhar discovery implies that, in the absence of viscosity, all rapidly rotating stars are bound to become unstable. As a consequence, the study of viscosity,

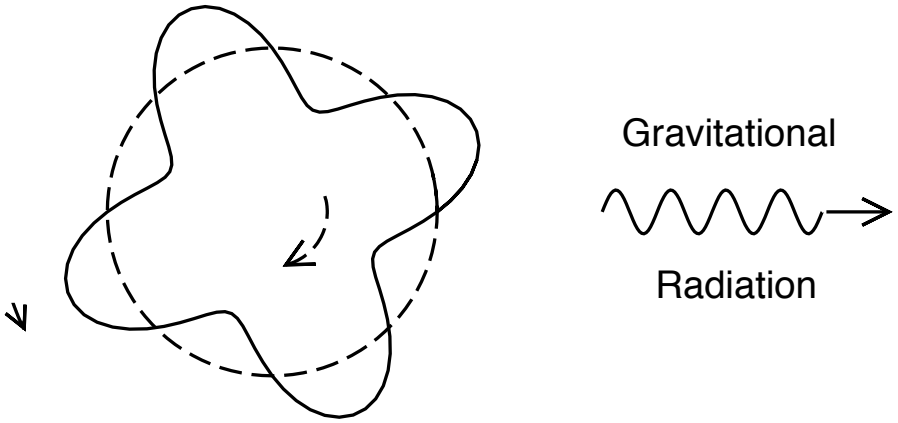

Figure 1.1. Oscillation mode (solid line) rotates in the direction opposite to the star rotation (dashed line). If the oscillation is dragged to move in the direction of star rotation, gravitational wave emission lead to instability.

and its modifications due to the onset of superfluidity, is of paramount importance for the determination of the stability of rotating neutron stars.

Besides playing a critical role in driving the viscous properties of neutron star matter, superfluidity affects both structure and dynamics of the star in many ways. For example, the appearance of the superfluid phase produces a change of the rotational period of a pulsar (a particular type of rotating neutron star), as well as a change of the neutrino emission rate, largely responsible for the cooling of the star.

In this Chapter, we will outline the process leading to the formation of a neutron star and summarize the present understanding of its internal structure.

1.1 Neutron star formation

Under the action of gravity, inter-stellar gas clouds, mainly composed of molecular hydrogen, collapse, thus triggering the formation of a star. The ongoing collapse increases the star temperature and the associated thermal pressure, that tends to balance the gravitational contraction. The core temperature grows until a critical value is reached, at which nuclear fusion reactions become possible. At this stage, hydrogen transforms into helium.

When all the hydrogen available for nuclear fusion is exhausted, the contraction due to gravitational forces resumes. As a result, a chain of exothermic reactions, such as fusion of helium into carbon and carbon into oxygen, can occur in the star core. At this point, the stellar evolution can lead to two possible outcomes:

- a *white dwarf*;
- a *neutron star* or a *black hole*.

In the first case, the star initial mass is relatively small: $M < 4\ M_\odot$[1], and the chain of exothermic nuclear fusion reactions stops before reaching the endpoint,

[1]The mass of the Sun is $M_\odot = 1.989 \times 10^{33}$ g.

corresponding to the formation of nuclei in the region of ^{56}Fe. Hence, the external layers become unstable and the core collapses, leading to the birth of a white dwarf. These systems are characterized by a density $\rho_{WD} \sim 3 \times 10^6\,\mathrm{g/cm^3}$ and a radius $R_{WD} \sim 2 \times 10^3\,\mathrm{Km}$. Referring to Sirius B, the first observed white dwarf, Sir Arthur Eddington wrote, in his 1920 book *The internal Constitution of the Stars*, "we have a star of mass about equal to the Sun and radius much less than Uranus". The stability of white dwarfs results from the balance between gravitational attraction and the large degeneracy pressure produced by the relativistic electrons gas within the star. In 1931, Chandrasekhar has proved the existence of a limiting mass, $M_c = 1.44$ $M_\odot$, beyond which white dwarfs cannot exist, because they become unstable against gravitational collapse.

When the initial mass is $M > 4$ $M_\odot$, the higher temperatures needed to bring the the nucleosynthesis reaction chain to its endpoint can be reached. As a consequence, the star develops a core consisting mostly of Iron, the stablest element in nature.

In addition to gravitational attraction, two other processes play a fundamental role driving the star contraction. The *neutronisation*, i.e. the electron capture by protons ($p + e^- \rightarrow n + \nu_e$), with the resulting disappearance of relativistic electrons providing the degeneracy pressure and the appearance of more and more neutron-rich nuclei, and the Iron *photodisintegration* which, being an endothermic reaction, also promotes the star contraction.

When the core mass exceeds the Chandraseckar limit ($M > M_c$), the core collapses in a time of the order of fractions of a second, until it reaches the typical density of atomic nuclei. At this point, the star core behaves as an huge nucleus, almost exclusively composed by neutrons, which resists further compression producing a violent elastic shock wave. The result is the explosion of a *supernova*, the luminosity of which exceeds that of the Sun by a factor $\sim 10^9$ and then decreases by a factor $\sim 10^2$ in few months. The explosion produces a gas cloud, called *nebula*, the centre of which is occupied by what is left: a *neutron star*. Conversely, if the explosion fails, the star collapses further, giving birth to a *black hole*.

Two years after the neutron discovery by Chadwick in 1932, Baade and Zwicky suggested the possibility that a compact star composed by this new particle could lie in the remnant of a supernova explosion. Their hypothesis was based on the persuasion that the collapse of the central nucleus of an high-mass star was the only mechanism capable to produce a stellar explosion visible for weeks, and so violent to throw into the space, with a velocity $v \sim 10^3\,\mathrm{Km/s}$, an amount of matter equal to many solar masses $M_\odot$. Many years before the pulsar discovery, stimulated by the Baade and Zwicky's hypothesis, Oppenheimer, Volkoff and Tolman [12, 13] had brought about the first calculation of neutron star equilibrium properties carried out within General Relativity. Combining Einstein's and hydrostatic equilibrium equations, they showed how the mass of a star composed by non-interacting neutrons cannot exceed the value $M \sim 0.8$ $M_\odot$. However, this value is inconsistent with those obtained by experimental measurements: $M \sim 1.4$ $M_\odot$. This discrepancy can be explained only with the existence of a pressure of dynamical origin, arising from strong interactions between nucleons, the contribution of which cannot be disregarded at the densities typical of neutron stars.

It was only only 34 years after the Baade and Zwicky's hypothesis had been proposed that Hewish and his student Bell [14] observed, for the first time, a pulsar,

i.e. a periodic radio wave source, located outside the solar system. Pulsars were immediately identified as rotating neutron stars, emitting radio wave beams from the magnetic poles. The first evidence of the connection between pulsars and supernovæ came from the discovery of two pulsars placed at the centre of the nebulæ left over by the Vela and Crab supernova explosions. In the 70s, 250 more pulsars were discovered, and nowadays their number is about 1100. Astronomical observations tell us that neutron stars have a mass slightly greater than that of the Sun, $M_\odot$, contained in a spherical volume of radius $R \sim 10\,\mathrm{Km}$. In these conditions, matter density is comparable to the central density of atomic nuclei, namely $\rho \sim 10^{14}\,\mathrm{g/cm^3}$, or 100 million tons per cubic centimeter [15].

1.2 Neutron star structure

Neutron star matter can be considered at zero temperature, because at its typical temperatures, $T \sim 10^9\,\mathrm{K} \sim 100\,\mathrm{KeV}$, and densities, $\rho \sim 10^{14}\,\mathrm{g/cm^3}$, the thermal energy turns out to be much lower than the Fermi kinetic energy of the nucleons, $E_F \sim 10\,\mathrm{MeV}$. Moreover, matter can safely be assumed to be transparent to neutrinos, because their mean free path, obtained from theoretical calculations, is much larger than the typical neutron star radius, $R \sim 10\,\mathrm{Km}$.

The internal structure of a neutron star, schematically represented in Fig. 1.2, features a sequence of layers of different composition. We will now briefly outline the structure of matter in the different layers, moving from the outermost, which is the region of lowest density, to the centre.

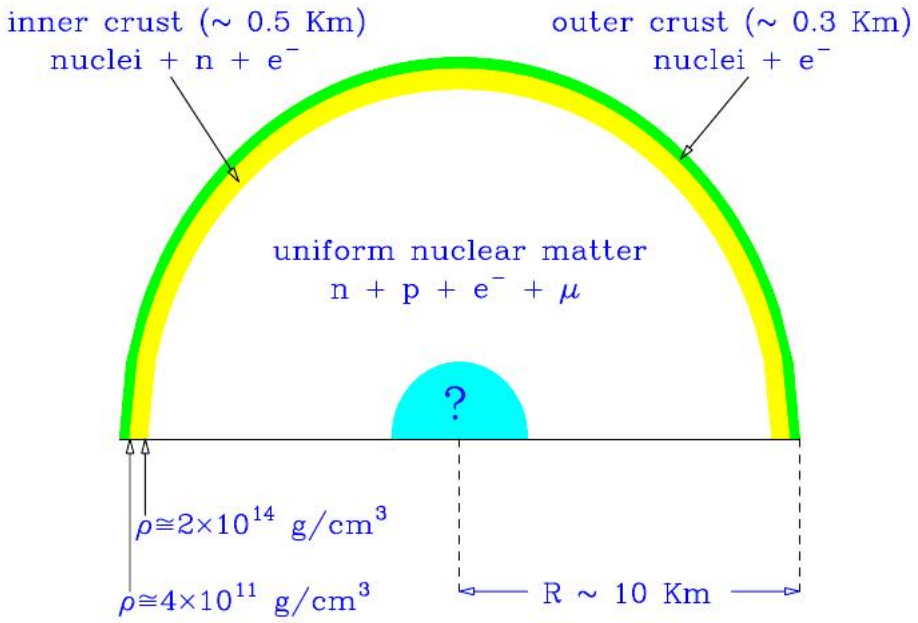

Figure 1.2. Schematic representation of the section of a neutron star.

- ***The outer crust*** has a thickness $\sim 0.3\,\mathrm{Km}$ and a density varying from the superficial value $\rho \sim 10^7\,\mathrm{g/cm^3}$ up to $\rho \sim 4 \times 10^{11}\,\mathrm{g/cm^3}$, at the inner crust

interface. In this region, matter is composed by atomic nuclei localized in a lattice immersed in an electron gas. Owing to *neutronisation*, the nuclear species change as we move towards the centre of the star. When the density increases, so does the electron chemical potential, and electron capture ($p + e^- \to n + \nu_e$) may become energetically favoured, resulting in the appearance of ever neutron-richer nuclei. Neutronisation stops when all negative energy states available in the nuclei are occupied and neutrons are forced to accommodate in positive energy states. This phenomenon is called *neutron drip*. The typical neutron drip density marks the boundary between outer and inner crust. While the properties of matter in the outer crust can be obtained directly from nuclear data, models of the equation of state (EOS) at $4 \times 10^{11} < \rho < 2 \times 10^{14}\,\mathrm{g/cm^3}$ are based on somewhat uncontrolled extrapolations of the available empirical informations, as the extremely neutron rich nuclei appearing in this density regime are not observed on Earth;

- ***The inner crust*** has a thickness $\sim 0.5\,\mathrm{Km}$ and a density varying from the $\rho \sim 4 \times 10^{11}\,\mathrm{g/cm^3}$ up to $\rho \sim 1.4 \times 10^{14}\,\mathrm{g/cm^3}$. In this region, matter is composed by atomic nuclei rich in neutrons, immersed in an electron and neutron gas. For densities $\rho < 4 \times 10^{12}\,\mathrm{g/cm^3}$, the pressure is mainly due to the electron gas, while at $\rho > 4 \times 10^{12}\,\mathrm{g/cm^3}$, neutrons provide the dominant contribution. In the inner crust, neutron star matter exhibits two different phases: *Proton Rich Matter* (PRM) and *Neutron Gas* (NG). The electron gas is present in both phases, in order to guarantee electric neutrality. For densities $4 \times 10^{11}\,\mathrm{g/cm^3} < \rho < 0.35\ \rho_0$, where $\rho_0 = 2.7 \times 10^{14}\,\mathrm{g/cm^3}$ is the typical central density of an atomic nucleus, the state of minimum energy is characterized by PRM spheres, surrounded by electron and neutron gas. As the density increases, tipically $0.35\ \rho_0 < \rho < 0.5\ \rho_0$, the spheres merge to form thin bars and, then, for $0.5\ \rho_0 < \rho < 0.56\ \rho_0$, the bars also merge, to give rise to alternated PRM and NG layers. The appearance of these structure is driven by a complex balance between nuclear volume and surface interactions and the electrostatic forces acting between charged particles;

- ***The outer core*** begins at density values $\rho > 0.56\rho_0$, at which there is no longer separation between PRM and NG; the ground state has the appearance of an homogeneous fluid of neutrons, protons and electrons, in equilibrium with respect to β-decay ($n \to p + e^- + \bar{\nu}_e$) and electron capture ($p + e^- \to n + \nu_e$). For high densities, the electron chemical potential can exceed the muon rest mass ($m_\mu = 105\,\mathrm{MeV}$), making electron decay into muons energetically favoured. Therefore, in general the ground state of matter consists of an homogeneous fluid of neutrons, protons, electrons and muons. The presence of leptons is necessary in order to maintain electric neutrality. As the percentage of charged particles is typically $\lesssim 10\%$, the internal pressure is mainly due to neutrons. As a consequence, modeling neutron star matter in the outer core with pure neutron matter can be regarded as a reasonable approximation. As we have already pointed out, this pressure is dynamical in nature and arises from the strong interaction between neutrons, featuring strong short-range repulsion;

- ***The inner core*** is located at the centre of the star, where the density can be

much higher that ρ_0, the typical value at the centre of atomic nuclei. When the sum of the neutron and electron chemical potentials becomes larger than the rest masses of heavier baryons, such as the Σ^- ($M_{\Sigma^-} = 1197\,\mathrm{MeV}$), which is believed to happen at density value $\rho \sim 2\rho_0$, the production of these heavy strange baryons through nucleon weak interactions (i.e. $n + e^- \to \Sigma^- + \nu_e$) is energetically favoured. A variety of other processes, such as excitation of nucleon resonances and neutron decays into π and K mesons giving rise to Bose-Einstein condensates, are also conjectured to take place. Finally, at extremely high density, typically $\rho \sim 10^{15}\,\mathrm{g/cm^3}$, matter may make a transition to a completely different state, predicted by the fundamental theory of strong interactions (Quantum Chromo Dynamics, or QCD) in which the building blocks of hadrons, the quarks, are deconfined.

Ideally, one may be able to infer the composition and the EOS of neutron star matter from observations. For example, the knowledge of the mass and radius of a neutron star would allow one to severely constrain the EOS. However, while many neutron star masses have been measured with remarkably high accuracy (a compilation of data is shown in Fig. 1.3), the experimental determination of the radii involves serious difficulties and the available estimates are still somewhat controversial.

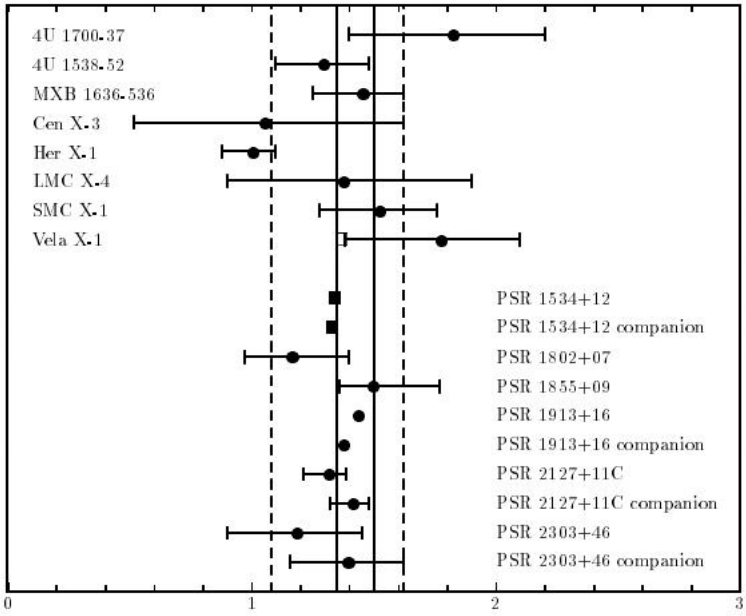

Figure 1.3. Compilation of measured neutron star masses, given in units of solar mass [16].

As pointed out above, the large interferometric gravitational wave detectors are also expected to provide a relevant information on neutron stars [17, 18, 19].

Chapter 2

Superfluidity, superconductivity and Cooper pairs

For a one-component system, superfluidity means zero viscosity, i.e. flux without any form of friction. This phenomenon is totally analogue to superconductivity, as in this case, the absence of friction results into a vanishing electrical resistance. In general, the absence of friction prevents the conversion of the kinetic energy associated with motion into thermal energy.

The superfluid state is characterized by low temperatures: $T < T_c$, where T_c is a critical temperature. The most important property of a superfluid is the presence of an energy gap at the Fermi surface (Fig. 2.1).

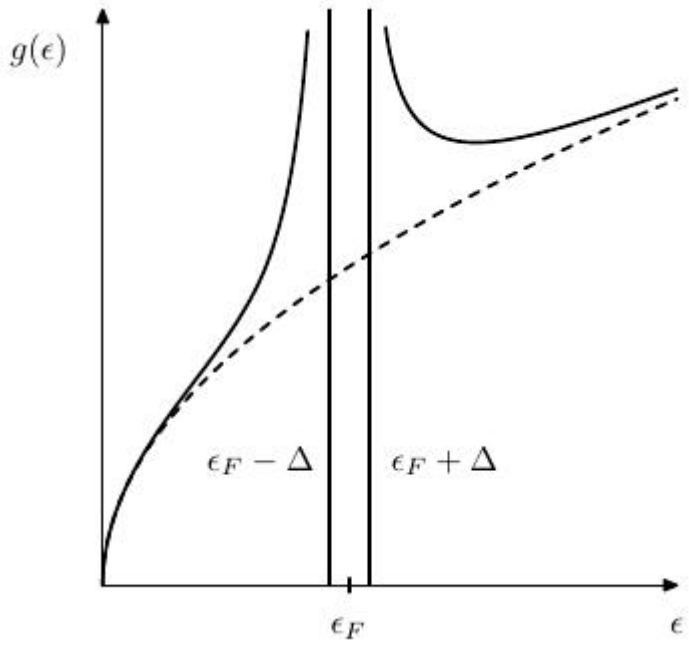

Figure 2.1. Density of states available to electrons, as a function of energy. The onset of superconductivity leads to the appearance of an energy gap of width 2Δ at the Fermi surface [20].

In the case of superconductivity, the gap arises from the coupling of the electrons to lattice oscillations, called phonons. This coupling produces an attractive interaction between the electrons leading to the formation of a bound state, dubbed Cooper pair, and to the appearance of an ordered state in momentum space at low temperature.

In 1956, Landau proposed a semi-phenomenological theory of normal Fermi liquids, i.e. fluids of interacting fermions near $T = 0\,\mathrm{K}$ (note that, as pointed out in Chapter 1, the zero-temperature approximation is suitable for the description of neutron star matter).

The basic assumption underlying Landau theory is that, as interactions are adiabatically switched on, the states of the non interacting system smoothly evolve into interacting states. The elementary excitations of the system are quasi-particles with a well defined dispersion relation $\epsilon(p)$, specific of each fluid. A quasi-particle excitation leads to the appearance of an electron outside the Fermi sphere and an hole inside the same sphere. The system exchanges energy with the environment in the form of quasi-particles. In order satisfy energy and momentum conservation, the Landau criterion of flux stability must be fulfilled. This criterion states that the fluid motion can be damped only for transport velocities greater than a critical value defined as

$$v_c = \min\left\{\frac{\epsilon(p)}{p}\right\} \ . \tag{2.1}$$

As a consequence, the available phase space is reduced and a gap appears in the energy spectrum, between the ground state ($T = 0\,\mathrm{K}$) and the first excited state. Hence, Landau criterion explains why a gas cannot be a superconductor.

The nature of the order in momentum space at low temperatures depends on the statistics of the particles involved:

- In the case of Bose-Einstein statistics, order is established through condensation in the ground state, separated from the first excited state by an energy gap. The condensate states make the system strongly degenerate (for example, ^{4}He);

- In the case of Fermi-Dirac statistics, if the interaction between fermions is attractive, they form bosonic Cooper pairs [21]statistics, which give rise to a condensate as in the previous case (for example any superconductor, or ^{3}He).

To summarize, the main features of the superconducting or superfluid transition are:

- an excitation spectrum compatible with the Landau criterion;

- an ordered state in momentum space at low temperatures.

In the following Sections, we will describe the mechanism leading to the formation of Cooper pairs and the appearance of the energy gap. For simplicity, we will consider the case of normal superconductors and Cooper pairs formed by electrons.

2.1 The electron-phonon interaction

The occurrence of the effective attraction between electrons at the Fermi surface is somewhat counterintuitive, because the elementary electrostatic interaction

$$V(\mathbf{r}-\mathbf{r}') = \frac{\mathrm{e}^2}{4\pi\epsilon_0|\mathbf{r}-\mathbf{r}'|} \ , \tag{2.2}$$

is repulsive for both bare electrons and electron quasi-particles in a metal.

This means that the attraction between electrons due to the presence of lattice phonons is stronger than the Coulomb repulsion.

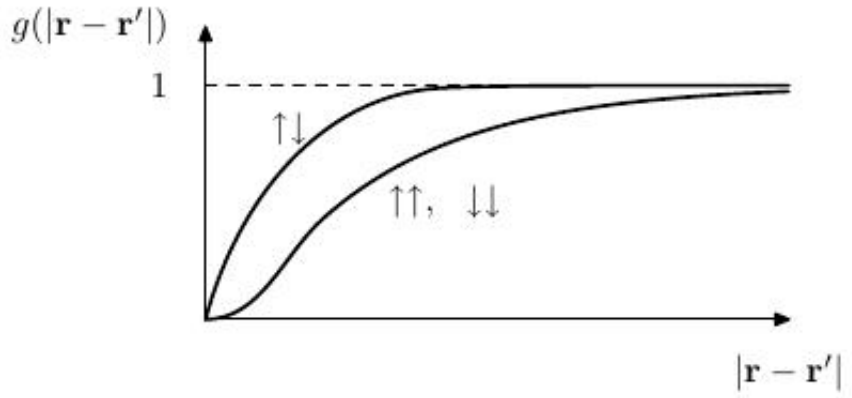

Figure 2.2. The exchange-correlation hole for an electron moving in a metal. The pair correlation function of the electron gas, $g(|\mathbf{r}-\mathbf{r}'|)$, measures the probability of finding two electrons at relative distance $|\mathbf{r}-\mathbf{r}'|$ [20].

We can model the superconductor as a Fermi liquid, because the electrons which compose it are strongly interacting with each other through two mechanisms

- Pauli exclusion principle, implying that two electrons with the same spin projection cannot be in the same position ($g(0) = 0$ for $|\mathbf{r}-\mathbf{r}'| = 0$) (see Fig. 2.2);
- electrostatic repulsion, implying that electrons minimize the Coulomb energy at large distances, whatever their spins (see Fig. 2.2) .

If, in a metal, electrons and their exchange-correlation holes are taken into account, the effective Coulomb force between quasi-particles turns out to be screened. The simplest description of screening in metals is the Thomas-Fermi model, in which the potential (2.2) is replaced by

$$V_{TF}(\mathbf{r}-\mathbf{r}') = \frac{\mathrm{e}^2}{4\pi\epsilon_0|\mathbf{r}-\mathbf{r}'|} e^{\frac{-|\mathbf{r}-\mathbf{r}'|}{r_{TF}}} \ , \tag{2.3}$$

where r_{TF} is the Thomas-Fermi screening length and $V_{TF} \ll V$. It clearly appears that, thanks to the factor $\exp(-|\mathbf{r}-\mathbf{r}'|/r_{TF})$, the effective repulsive force is short ranged: $|\mathbf{r}-\mathbf{r}'| > r_{TF} \Leftrightarrow V_{TF} = 0$.

Electrons interact with each other by interacting with the phonons of the crystalline lattice. An electron in Bloch state $\psi_{n\mathbf{k}}(\mathbf{r})$ first excites a phonon of wave vector $\mathbf{q}$, making a transition to the state of wave vector $\mathbf{k}-\mathbf{q}$

$$\psi_{n\mathbf{k}}(\mathbf{r}) \rightarrow \psi_{n\mathbf{k}'}(\mathbf{r}) \qquad \mathbf{k}' = \mathbf{k}-\mathbf{q}\ . \tag{2.4}$$

Another electron then absorbs the phonon and acquires $\mathbf{q}$ (Fig. 2.3).

This effective interaction between electrons due to exchange of phonons turns out

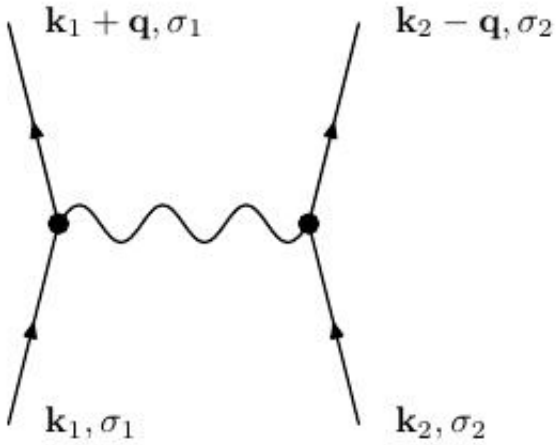

Figure 2.3. Interaction of fermions via exchange of a gauge boson. In Particle Physics, such diagrams could represent interactions between electrons by exchange of photons or W or Z bosons. In superconductors, the same picture can be used to represent the interaction between electrons at the Fermi surface due to exchange of lattice phonons. [20].

to be of the form

$$V_{eff}(\mathbf{q},\omega) = |g_{\mathbf{q}}|^2 \frac{1}{\omega^2-\omega^2_{\mathbf{q}\lambda}}\ , \tag{2.5}$$

where the virtual phonon has momentum $\mathbf{q}$ and energy $\omega_{\mathbf{q}\lambda}$ and $g_{\mathbf{q}}$ is a parameter tied to the matrix element of the electron scattering process $\psi_{n\mathbf{k}}(\mathbf{r}) \rightarrow \psi_{n(\mathbf{k}+\mathbf{q})}(\mathbf{r})$. An important result due to Migdal is that the electron phonon vertex $g(\mathbf{q})$ is of order

$$g_{\mathbf{q}} \sim \sqrt{\frac{m}{M}}\ , \tag{2.6}$$

where m and M denote the electron and ion masses, respectively.

The theory developed by Bardeen, Cooper and Schrieffer (BCS theory) [22], to be discussed in the next Chapter, is based on an highly simplified form of the above effective interaction

- the explicit dependence on the wave vector is removed, by averaging over all values of $\mathbf{q}$;
- $\omega_{\mathbf{q}}$ is replaced by the Debye frequency of the phonons, ω_D;
- the $\mathbf{q}$-dependent electron-phonon interaction vertex, $g_{\mathbf{q}}$, is replaced by a constant, g_{eff}.

With these simplifications, one finds

$$V_{eff}(\mathbf{q},\omega) = |g_{eff}|^2 \frac{1}{\omega^2 - \omega_D^2} \ , \tag{2.7}$$

implying that

- $\omega < \omega_D \Rightarrow V_{eff} < 0$ (attractive interaction) ,
- $\omega > \omega_D \Rightarrow V_{eff} > 0$ (repulsive interaction) .

In BCS theory the repulsive part is not important. We are in fact interested only in electrons which lie within $\pm k_B T$ of the Fermi energy and, at the temperatures of interest to superconductivity, we are in the regime $\omega_D \gg k_B T$. Therefore, the final form for BCS theory reads

$$V_{eff}(\mathbf{q},\omega) = -|g_{eff}|^2 \qquad\qquad |\omega| < \omega_D \ . \tag{2.8}$$

The electron energies involved are all within the range $\pm\omega_D$ of the Fermi surface, i.e.

$$|\epsilon_{\mathbf{k}_i} - \epsilon_F| < \omega_D \ . \tag{2.9}$$

As a consequence, we have interacting electrons near the Fermi surface, but the Bloch states far inside or outside the Fermi surface are unaffected, as shown in Fig. 2.4. The only active electrons are those within this thin shell of states around ϵ_F [20].

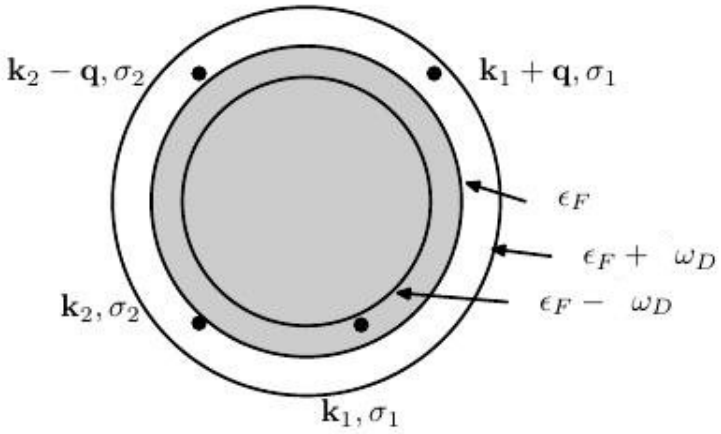

Figure 2.4. The effective electron-electron interaction near the Fermi surface. The electrons with quantum numbers $\mathbf{k}_1$, σ_1 and $\mathbf{k}_2$, σ_2 are scattered to $\mathbf{k}_1 + \mathbf{q}$, σ_1 and $\mathbf{k}_2 + \mathbf{q}$, σ_2. The interaction is attractive provided that all of the wave vectors lie in the range where $\epsilon_{\mathbf{k}}$ is within $\pm\omega_D$ of the Fermi energy [20].

2.2 Origin of the gap and Cooper pairs

Having found that there is an attraction between electrons near the Fermi level is still a long way from a theory of superconductivity. The next key step was carried out by Cooper. He noted that the effective interaction is attractive only near to the Fermi surface, Fig. 2.4, and asked what the effect of this attraction would be for just a single pair of electrons outside the occupied Fermi sea (composed by states with $\mathbf{k} < \mathbf{k}_F$ at T=0). He found that they form a bound state. This result was somewhat unexpected, since two electrons in free space would not be bound with the same weak attractive interaction. This "Cooper problem" idea led the way to the full BCS state, in which every electron at the Fermi surface is part of a pair.

We will now provide a simple explanation of the mechanism leading to the formation of Cooper pairs [21] and the appearance of the associated energy gap [23].

We assume that:

- the two body interaction is attractive;
- the system is strongly degenerate, that is, the active particles occupy energy states within a thin shell with width 2Δ around Fermi surface, Fig. 2.1.

Let us first analyze scattering processes and classify Cooper pairs according to their total momentum $\mathbf{k}$. We want to find out how many pairs could be formed, for given $\mathbf{k}$. For this purpose, we construct two spheres of radius equal to Fermi momentum, $\mathbf{k}_F$, and such that the distance between the two centres is $\mathbf{k}$ (Fig.2.5).

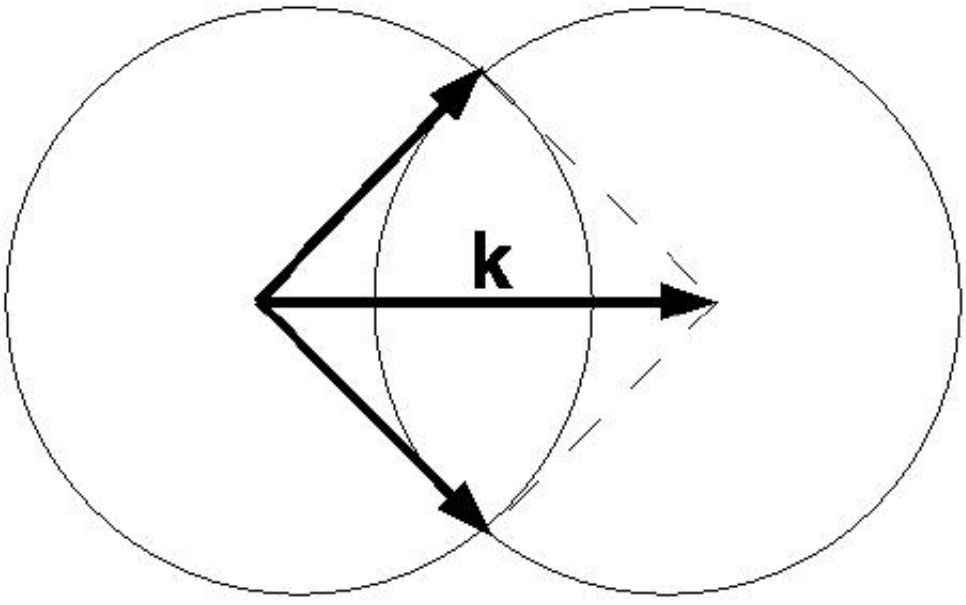

Figure 2.5. Schematic representation of Cooper pair construction. The left sphere is the Fermi sphere, while the right sphere is a geometrical construction.

Figure 2.5 shows that the particles belonging to the pairs correspond to diametrically opposite points lying on the intersection of the two spheres. If Δ is small (that

is to say, the particles are close to Fermi surface), the number of pairs is measured by the half circumference of the circle of intersection. We note that the number of particles is much smaller than the number of particles on Fermi surface. If $\mathbf{k} = 0$, on the other hand, the two spheres are overlapping. The number of pairs is now measured by the half of the area of the Fermi surface. Hence, the number of pairs with $\mathbf{k} = 0$ is much greater than the number of pairs with $\mathbf{k} \neq 0$ and finite.

We now focus on pairs with $\mathbf{k} = 0$ and show how they produce the energy gap. Let us consider a collection of degenerate fermions and select among them a pair with total momentum $\mathbf{k} = 0$ close to Fermi surface. These two particles interact obeying all conservation laws (in particular the total momentum must remain vanishing, $\mathbf{k} = 0$), while the other particles are passive, their role being simply the occupation of all available states within the Fermi sphere (Fig. 2.6). The unperturbed energy of the pair is approximately equal to $2E_F$, where E_F is the Fermi energy.

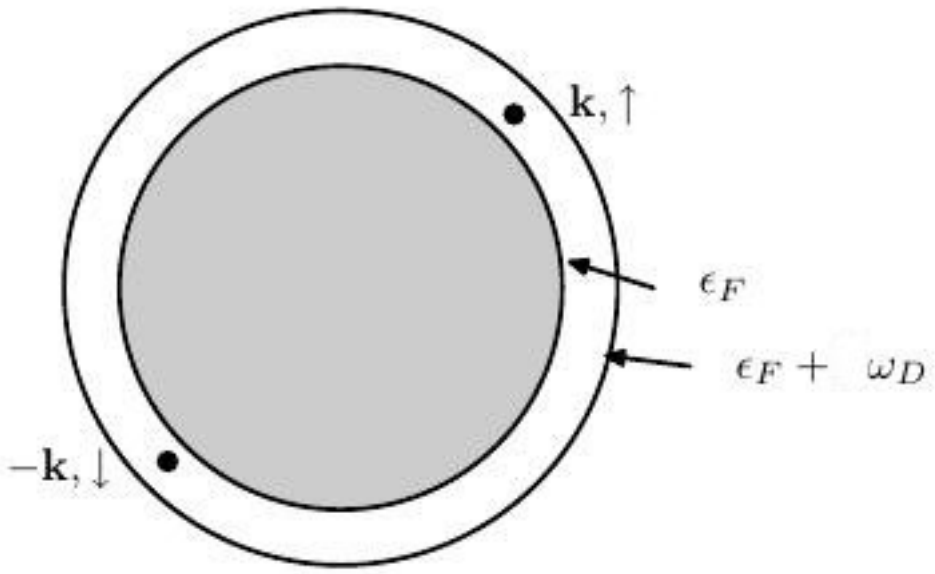

Figure 2.6. The Cooper problem: two electrons outside a fully occupied Fermi sea. The interaction is attractive provided that the electron energies are in the range $\epsilon_F < \epsilon_{\mathbf{k}} < \epsilon_F + \omega_D$ [20].

In order to understand the formation of the bound state, we determine the ground state solving the Schrödinger equation

$$\left[-\frac{1}{2m}\nabla_1^2 - \frac{1}{2m}\nabla_2^2 + v(\mathbf{r}_1, \mathbf{r}_2)\right]\psi = E\psi \ , \tag{2.10}$$

where v is an attractive interaction. Now, we must show that the lowest energy solution of this equation has energy less than $2E_F$. To see this, we expand the wave function ψ in the basis of unperturbed states, setting $v = 0$ and $k > k_F$. These states are products of plane waves with momenta $\mathbf{k}'$ and $-\mathbf{k}'$. In order to simplify the notation, spinors are neglected, because the pair has zero total spin.

Therefore, the wave function can be written as

$$\psi = \sum_{k'>k_F} c_{k'} \frac{e^{i\mathbf{k}'(\mathbf{r}_1-\mathbf{r}_2)}}{\Omega} \ , \tag{2.11}$$

where the coefficients $c_{k'}$ have to been determined. Substitution of Eq. (2.11) into Eq. (2.10) gives

$$\sum_{k'>k_F} c_{k'} \left(E_{k'} - E + v(\mathbf{r}_1, \mathbf{r}_2)\right) \frac{e^{i\mathbf{k}'(\mathbf{r}_1-\mathbf{r}_2)}}{\Omega} = 0 \ . \tag{2.12}$$

Now, we project Eq. (2.12) on the state describing a pair with momentum of magnitude k

$$\left(E_k - E\right) c_k = - \sum_{k'>k_F} c_{k'} v_{k,k'} \ , \tag{2.13}$$

where the matrix elements of potential are

$$v_{k,k'} = \int\int \frac{e^{-i\mathbf{k}(\mathbf{r}_1-\mathbf{r}_2)}}{\Omega} v(\mathbf{r}_1, \mathbf{r}_2) \frac{e^{i\mathbf{k}'(\mathbf{r}_1-\mathbf{r}_2)}}{\Omega} d\mathbf{r}_1 d\mathbf{r}_2 \ . \tag{2.14}$$

For simplicity, we assume that the Fourier transform of the potential reads

$$v_{k,k'} = \begin{cases} -\lambda \text{ for } E_F < E_k, E_{k'} < E_F + \delta \\ 0 \text{ otherwise} \end{cases} \ . \tag{2.15}$$

The above choice implies that we limit the interacting states to those with energies $E_F < E < E_F + \delta$. We also note that the energy gap is not symmetrical around Fermi surface, because a pair cannot penetrate into the fully occupied Fermi sea. Our approximation amounts to substituting $v_{k,k'}$ with a mean value in the considered energetic range. The minus sign implies that the interaction is attractive only if $\lambda > 0$.

Replacing Eq. (2.15) into Eq. (2.13), we find

$$c_k = \frac{\lambda}{E_k - E} \sum_{E_F<E_{k'}<E_F+\delta} c_{k'} \ , \tag{2.16}$$

and by summing both sides of the above equation over the values of k in the considered energetic shell we finally obtain the equation

$$\frac{1}{\lambda} = \sum_{E_F<E_k<E_F+\delta} \frac{1}{E_k - E} \ , \tag{2.17}$$

which must be solved to find the eigenvalues E. We note that for values of the energy $E_F < E_k < E_F + \delta$, the function in the right hand side quickly oscillates between $+\infty$ and $-\infty$, taking once the value $\frac{1}{\lambda}$ at every oscillation. Hence, in this range, we obtain a continuous energy spectrum (Fig. 2.7).

We are interested in the solution with energy less than E_F. Starting from the vertical asymptote at $E = E_F$, the function in the right hand side of Eq. (2.17)

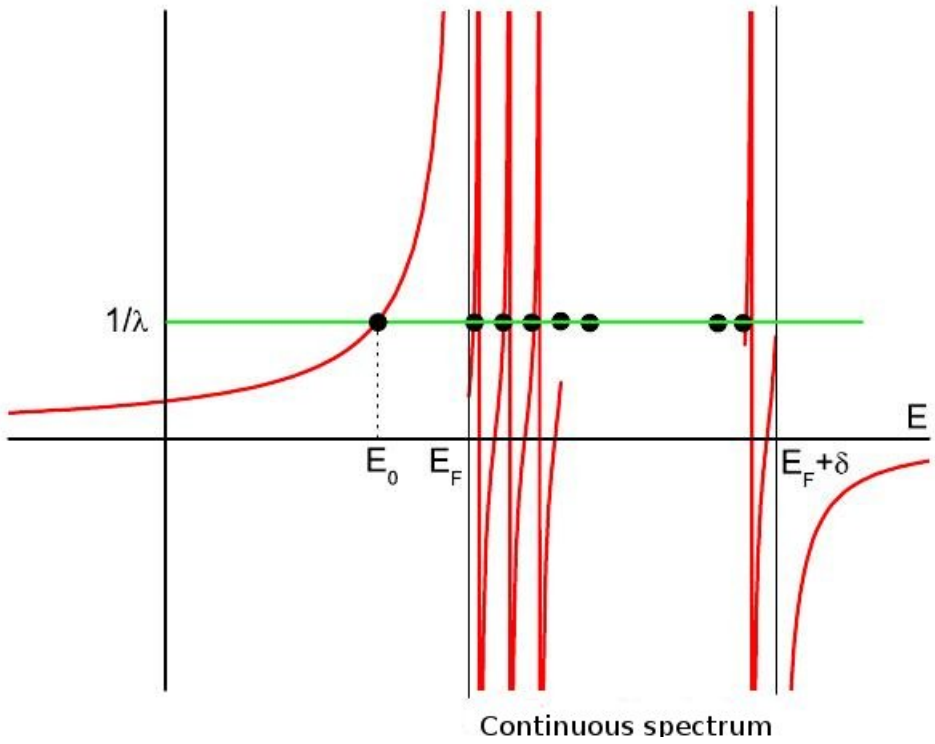

Figure 2.7. Graphical solution of the eigenvalue equation determining the Cooper pair ground state energy.

decreases with E, assuming the value $\frac{1}{\lambda}$ for the energy value corresponding to the ground state, $E = E_0$ (Fig. 2.7).

Since E_k has a continuous spectrum, the sum must be transformed into an integral

$$\frac{1}{\lambda} = \int_{E_F}^{E_F+\delta} dE_k \frac{1}{E_k - E} \ , \tag{2.18}$$

which must be solved to find E. Introducing the energy gap Δ, defined as

$$E_0 = E_F - \Delta \ , \tag{2.19}$$

from Eq. (2.18) we find

$$\Delta = \frac{\delta}{e^{\frac{1}{\lambda}} - 1} \ , \tag{2.20}$$

where, in order to have an attractive interaction (bound state) $\lambda > 0$, which implies $\Delta > 0$. In conclusion, we have seen that the ground state is separated from the continuous spectrum of excited states by a finite energy gap Δ, which makes the superconductor state of the system possible.

Chapter 3

Variational formulation of BCS theory

In this Chapter, we will discuss the BCS theory [22], developed to determine the superconducting ground state and the energy gap within the variational approach. We will first analyze a simplified version of the theory [24], in which the spin is neglected. The complete theory, describing the dynamics of the pairs with vanishing orbital angular momentum and total spin, will then be discussed following Valatin's approach [25].

3.1 BCS theory without spin

The first approximation to BCS theory is based on the assumption that the system can be described by a non-correlated wave function, that is a Slater determinant of plane waves including single particle states of momentum $|\mathbf{k}| < k_F$ and energy $\epsilon(k)$. In BCS theory, when the interaction gives rise to the formation of Cooper pairs (with zero spin and total momentum), the ground state energy is separated from the continuous spectrum by a finite energy gap. In this case, we have a superconducting state.

BCS theory considers a many-particle system, the dynamics of which are described by the Hamiltonian

$$H = \sum_{k_1,k_2 \gtrless 0} \left(t_{k_1 k_2} a^+_{k_1} a_{k_2} \right) + \frac{1}{4} \sum_{k_1,k_2,k_3,k_4 \gtrless 0} \left(\bar{v}_{k_1 k_2 k_3 k_4} a^+_{k_1} a^+_{k_2} a_{k_4} a_{k_3} \right) \ , \tag{3.1}$$

where $t_{k_1 k_2}$ and $v_{k_1 k_2 k_3 k_4}$ are matrix elements of the kinetic energy operator and the interaction potential, respectively.

The wave function must describe a coherent state of many particles in which every electron is paired. For this purpose, it is chosen in the form

$$|BCS\rangle = \prod_{k>0} \left(u_k + v_k a^+_k a^+_{-k} \right) |0\rangle \ , \tag{3.2}$$

where $|0\rangle$ is the vacuum state and u_k and v_k are variational parameters.

Let us now analyze the physical properties of the wave function (3.2).

- as the factors $\left(u_k + v_k a_k^+ a_{-k}^+\right)$ with different momentum commute, the pairs are physically independent. Moreover, by construction, there are only pairs with vanishing total momentum.

- the wave function also describes the unperturbed ground states of non interacting fermions. As a matter of fact, setting

$$\begin{cases} u_k = 1 \\ v_k = 0 \end{cases} \tag{3.3}$$

for $k < k_F$ and

$$\begin{cases} u_k = 0 \\ v_k = 1 \end{cases} \tag{3.4}$$

for $k > k_F$ we obtain

$$|BCS\rangle = \prod_{k>0, k>k_F} \left(a_k^+ a_{-k}^+\right)|0\rangle = \prod_{k>k_F} a_k^+ |0\rangle \ . \tag{3.5}$$

- the wave function does not correspond to a fixed number of particles. This can be easily seen rewriting the BCS state in the form

$$\begin{aligned} |BCS\rangle &= \left(\prod_{k>0} u_k\right)\left[1 + \sum_q \frac{v_q}{u_q} a_q^+ a_{-q}^+ + \sum_{q,l} \frac{v_q}{u_q}\frac{v_l}{u_l} a_q^+ a_l^+ a_{-q}^+ a_{-l}^+ + ...\right]|0\rangle = \\ &= \left(\prod_{k>0} u_k\right)\left[|\phi_0\rangle + |\phi_2\rangle + |\phi_4\rangle + ...\right] \ , \end{aligned} \tag{3.6}$$

where the state $|\phi_N\rangle$, defined as

$$|\phi_N\rangle = \left(\sum_k \frac{v_k}{u_k} a_k^+ a_{-k}^+\right)^{\frac{N}{2}} |0\rangle \tag{3.7}$$

describes $N/2$ electron pairs.

The squared moduli $|v_k|^2$ and $|u_k|^2$ are the probabilities that a given pair with momentum k is occupied or not, respectively. They must be determined through minimization of the ground state energy. The two parameters are not independent, being related by the requirement that the BCS state be normalized to unity. From the equation

$$\langle BCS|BCS\rangle = \langle 0| \prod_{k>0} (u_k^* + v_k^* a_k a_{-k}) \prod_{k'>0} \left(u_{k'} + v_{k'} a_{k'}^+ a_{-k'}^+\right)|0\rangle = 1 \tag{3.8}$$

it follows that (note that pairs of factors with $k \neq k'$ commute)

$$\begin{aligned}\langle BCS|BCS\rangle = \prod_{k>0}\Big[&|u_k|^2 + u_k^* v_k \langle 0|\, a_k^+ a_{-k}^+ \,|0\rangle + u_k v_k^* \langle 0|\, a_k a_{-k} \,|0\rangle \\ &+ |v_k|^2 \langle 0|\, a_k a_{-k} a_k^+ a_{-k}^+ \,|0\rangle\Big] = |u_k|^2 + |v_k|^2 = 1 \ .\end{aligned} \tag{3.9}$$

As the BCS wave function is only determined up to a phase factor, it is always possible to choose the coefficients u_k real and positive. In principle, the phase of v_k must be determined by the variation of the energy expectation value; however, it is possible to prove that, for the interaction potential chosen for our study, real and positive v_k corresponds to the lowest energy. Therefore, the normalization condition becomes

$$u_k^2 + v_k^2 = 1 \ . \tag{3.10}$$

We observe that, while the definition of the BCS state, Eq. (3.2), only involves coefficients with $k > 0$, it is convenient to also define them for $k < 0$. Exploiting the symmetry of the wave function under momentum inversion and the canonical commutation rules (anticommutation for fermions), we find

$$\begin{cases} u_k = u_{-k} \\ v_k = -v_{-k} \ . \end{cases} \tag{3.11}$$

In order to determine the variational parameters u_k and v_k, we have to minimize the energy of BCS state, with the constraint

$$\langle BCS|\, \hat{N} \,|BCS\rangle = 2\sum_{k>0}\left(v_k^2\right) = N \ , \tag{3.12}$$

where the factor accounts for spin degeneracy, expressing the condition that the number of particles is fixed. This condition can be equally imposed, with the introduction of an appropriate term in the Hamiltonian, i.e. replacing

$$H \to H' = H - \mu\hat{N} \ , \tag{3.13}$$

where the Lagrange multiplier μ is the chemical potential of the system, yielding the energy variation due to the variation of the particle number

$$\mu = \frac{dE}{dN} \ . \tag{3.14}$$

We now have to carry out the variational calculation, keeping in mind the normalization and that u_k and v_k are real and positive, which implies that the BCS wave function can be completely determined evaluating v_k. As a consequence, the expression

$$\delta \langle BCS|\, H' \,|BCS\rangle = \delta \langle BCS|\, H - \mu\hat{N} \,|BCS\rangle = 0 \ , \tag{3.15}$$

is equivalent to

$$\left(\frac{\partial}{\partial v_k} + \frac{\partial u_k}{\partial v_k}\frac{\partial}{\partial u_k}\right)\langle BCS|\, H' \,|BCS\rangle = 0 \ . \tag{3.16}$$

In order to solve Eq.(3.16), it is convenient to divide the Hamiltonian into two parts: the single particle contribution

$$\langle BCS|\, H^{(1)}\, |BCS\rangle = \sum_{k_1,k_2 \gtrless 0} t_{k_1 k_2} \langle BCS|\, a^+_{k_1} a_{k_2}\, |BCS\rangle = \sum_{k \gtrless 0} t_{kk} v_k^2 \ , \tag{3.17}$$

and the pair contribution

$$\begin{aligned} \langle BCS|\, H^{(2)}\, |BCS\rangle &= \frac{1}{4} \sum_{k_1,k_2,k_3,k_4 \gtrless 0} \bar{v}_{k_1 k_2 k_3 k_4} \langle BCS|\, a^+_{k_1} a^+_{k_2} a_{k_4} a_{k_3}\, |BCS\rangle = \\ &= \frac{1}{4} \sum_{k_1,k_2,k_3,k_4 \gtrless 0} \bar{v}_{k_1 k_2 k_3 k_4} \langle 0| \prod_{q>0} (u_q + v_q a_q a_{-q}) \\ &\quad a^+_{k_1} a^+_{k_2} a_{k_4} a_{k_3} \prod_{k>0} \left(u_k + v_k a^+_k a^+_{-k}\right) |0\rangle = \\ &= \frac{1}{2} \sum_{k,q \gtrless 0} \bar{v}_{kqkq} v_k^2 v_q^2 + \sum_{k,q>0} \bar{v}_{k-kq-q} v_k u_k u_q v_q \ . \end{aligned} \tag{3.18}$$

Substitution of Eqs. (3.17) and (3.18) into Eq.(3.15) leads to

$$\delta \left\{ \sum_{k \gtrless 0} \left[(t_{kk} - \mu)\, v_k^2 + \frac{1}{2} \sum_{q \gtrless 0} \bar{v}_{kqkq} v_k^2 v_q^2 \right] + \sum_{k,q>0} \bar{v}_{k-kq-q} v_k u_k u_q v_q \right\} = 0 \ . \tag{3.19}$$

Performing the derivative with respect to v_k, we find

$$\begin{aligned} \frac{\partial}{\partial v_k} \langle BCS|\, H'\, |BCS\rangle = &\left[t_{kk} + t_{-k-k} - 2\mu + \sum_{q \gtrless 0} \left(\bar{v}_{kqkq} + \bar{v}_{-kq-kq}\right) v_q^2 \right] v_k + \\ &+ \sum_{q>0} \bar{v}_{k-kq-q} u_q v_q u_k \ , \end{aligned} \tag{3.20}$$

while derivation with respect to u_k yields

$$\frac{\partial}{\partial u_k} \langle BCS|\, H'\, |BCS\rangle = \sum_{q>0} \bar{v}_{k-kq-q} u_q v_q v_k \ . \tag{3.21}$$

Moreover, from the normalization condition it follows that

$$\frac{\partial u_k}{\partial v_k} = \frac{\partial}{\partial v_k} \left(\sqrt{1 - v_k^2} \right) = -\frac{v_k}{\sqrt{1 - v_k^2}} = -\frac{v_k}{u_k} \ . \tag{3.22}$$

Substituting Eqs.(3.20), (3.21) and (3.22) into Eq.(3.16) and multiplying for u_k, we obtain:

$$2\epsilon_k u_k v_k + \Delta_k \left(v_k^2 - u_k^2 \right) = 0 \ , \tag{3.23}$$

where we have introduced the energy ϵ_k, defined as

$$\epsilon_k = \frac{1}{2} \left[t_{kk} + t_{-k-k} + \sum_{q \gtrless 0} \left(\bar{v}_{kqkq} + \bar{v}_{-kq-kq}\right) v_q^2 \right] - \mu \ , \tag{3.24}$$

and the energy gap, Δ_k, defined as:

$$\Delta_k = -\sum_{q>0} \bar{v}_{k-kq-q} u_q v_q \ . \tag{3.25}$$

Using the normalization condition and Eq.(3.23) leads to

$$\begin{cases} u_k^2 = \frac{1}{2}\left(1 \pm \frac{\epsilon_k}{\sqrt{\epsilon_k^2+\Delta_k^2}}\right) \\ v_k^2 = \frac{1}{2}\left(1 \pm \frac{\epsilon_k}{\sqrt{\epsilon_k^2+\Delta_k^2}}\right) \ . \end{cases} \tag{3.26}$$

In the absence of interactions, $\Delta_k = 0$ and the BCS wave function reduces to ground state of the Fermi gas, corresponding to $u_k^2 = 1$ and $v_k^2 = 0$ for $k < k_F$. For this reason, we choose (see Fig. 3.1)

$$\begin{cases} u_k^2 = \frac{1}{2}\left(1 + \frac{\epsilon_k}{\sqrt{\epsilon_k^2+\Delta_k^2}}\right) \\ v_k^2 = \frac{1}{2}\left(1 - \frac{\epsilon_k}{\sqrt{\epsilon_k^2+\Delta_k^2}}\right) \ . \end{cases} \tag{3.27}$$

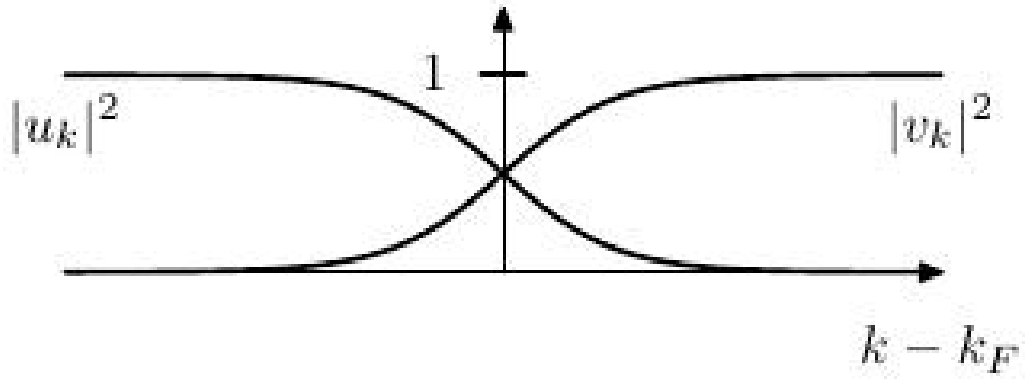

Figure 3.1. Momentum-dependence of the BCS wave function parameters $|u_{\mathbf{k}}|^2$ and $|v_{\mathbf{k}}|^2$ for $|\mathbf{k}|$ close to the Fermi momentum. The state is predominantly electron like well below k_F $\left(|u_{\mathbf{k}}|^2 \approx 1\right)$ and predominantly hole like far above the Fermi surface, $\left(|v_{\mathbf{k}}|^2 \approx 1\right)$. At $|\mathbf{k}| \sim k_F$ quasi-particles exhibit mixed electron and hole character [20].

Finally, substitution of Eq.(3.27) into the definition of Δ_k, Eq.(3.25), yields the BCS gap equation at $T = 0$

$$\Delta_k = -\frac{1}{2}\sum_{q>0} \bar{v}_{k-kq-q} \frac{\Delta_k}{\sqrt{\epsilon_k^2 + \Delta_k^2}} \ . \tag{3.28}$$

In conclusion, we have seen how the variational principle brings to a system of three

equations

- the gap equation (3.28);
- Eq.(3.24) for the energy ϵ_k;
- Eq.(3.27) for v_k^2.

This system can be solved iteratively, keeping in mind the normalization condition.

In the above derivation, we have completely neglected the spin, because Cooper pairs are composed by particles with zero total momentum and spin. We have already seen how the presence of pairs with vanishing total momentum comes about in the construction of the BCS ground state. In the next Section, we will discuss the projection onto states with vanishing total spin, carried out using the Valatin-Bogoliubov transformations.

3.2 Variational Valatin-BCS theory

We will now analyze BCS theory using a system of transformations originally proposed by J.G. Valatin [25] and independently developed by N.N. Bogoliubov [26, 27]. This formalism fits perfectly with the variational method discussed above.

The Hamiltonian

$$H = T + V \ , \tag{3.29}$$

of the theory is the sum of kinetic energy

$$T = \sum_{k,\sigma} \tilde{E}_k a^+_{k\sigma} a_{k\sigma} \ , \tag{3.30}$$

and a two-body non local interaction term

$$V = \frac{1}{2} \sum_{k,k'} \sum_{\sigma,\sigma'} V_{kk'} a^+_{k\sigma} a^+_{-k\sigma'} a_{-k'\sigma'} a_{k'\sigma} \ , \tag{3.31}$$

where we have imposed the condition of zero total momentum of the interacting particles and the indices σ, σ' refer to the spin projections.

Since the theory does not fix the total number of particles, in order to carry out the energy variation, it is convenient to introduce a Lagrange multiplier, as we have made in the previous Section. Hence, we set

$$E_k = \tilde{E}_k - \mu \ . \tag{3.32}$$

The BCS ground state can be written as a product of commuting factors in the form

$$|\phi_0\rangle = \prod_x \frac{1 + g_x a^+_x a_{-x}}{(1 + |g_x|^2)^{\frac{1}{2}}} |0\rangle \ , \tag{3.33}$$

where the index x specifies both spin σ and momentum k ($-x$ indicates the opposite orientations of spin and momentum). The parameter g satisfies the relations

$$g_{k\uparrow} = g_{-k\uparrow} = -g_{k\downarrow} = -g_{-k\downarrow} \tag{3.34}$$

implying

$$g_x = -g_{-x} \ . \tag{3.35}$$

The values of g_x must be determined minimizing the ground state energy.

From the fermion anticommutation rules, we find

$$\begin{cases} a_x \left(1 + g_x a_x^+ a_{-x}\right) |0\rangle = g_x a_{-x}^+ |0\rangle \\ a_{-x}^+ \left(1 + g_x a_x^+ a_{-x}\right) |0\rangle = a_{-x}^+ |0\rangle \ . \end{cases} \tag{3.36}$$

Therefore, it is useful to introduce the new variables

$$\begin{cases} \alpha_x^+ = \frac{a_x^+ - g_x a_{-x}}{(1+|g_x|^2)^{\frac{1}{2}}} \\ \alpha_x = \frac{a_x - g_x^* a_{-x}^+}{(1+|g_x|^2)^{\frac{1}{2}}} \ , \end{cases} \tag{3.37}$$

such that

$$\alpha_x |\phi_0\rangle = 0 \ . \tag{3.38}$$

From the anticommutation relations involving a_x and a_x^+ it follows that

$$\begin{cases} \{\alpha_x, \alpha_{x'}\} = \{\alpha_x^+, \alpha_{x'}^+\} = 0 \\ \{\alpha_x, \alpha_{x'}^+\} = \delta_{xx'} \ . \end{cases} \tag{3.39}$$

Equations (3.37) represent a canonical transformation, as α and α^+ satisfy the same anticommutation rules as the old a and a^+.

We now introduce states of the form

$$|\phi_{x_1 \ldots x_j}\rangle = \alpha_{x_1} \ldots \alpha_{x_j} |\phi_0\rangle \ , \tag{3.40}$$

forming an orthonormal and complete set. From the equations

$$\begin{cases} \alpha_x^+ \left(\frac{1+g_x a_x^+ a_{-x}^+}{(1+|g_x|^2)^{\frac{1}{2}}} \right) |0\rangle = a_x^+ |0\rangle \\ \alpha_x^+ \alpha_{-x}^+ \left(\frac{1+g_x a_x^+ a_{-x}^+}{(1+|g_x|^2)^{\frac{1}{2}}} \right) |0\rangle = \alpha_x^+ \left(a_{-x}^+ \right) |0\rangle = \frac{a_x^+ a_{-x}^+ - g_x^*}{(1+|g_x|^2)^{\frac{1}{2}}} |0\rangle \ , \end{cases} \tag{3.41}$$

it follows that the states $\alpha_x^+ |\phi_0\rangle$ and $\alpha_x^+ \alpha_{-x}^+ |\phi_0\rangle$ correspond to a single-particle excitation and a Cooper pair, respectively.

As mentioned above, the transformations (3.37) have been first obtained by J.G. Valatin. N.N. Bogoliubov has independently derived the same transformations using a different set of variables. To go from one formalism to the other it is sufficient to set

$$\begin{cases} u_x = \frac{1}{(1+|g_x|^2)^{\frac{1}{2}}} \\ v_x = \frac{g_x}{(1+|g_x|^2)^{\frac{1}{2}}} \ , \end{cases} \tag{3.42}$$

where we have assumed that g_x is real and we have introduced the variables u_x and

v_x, in terms of which the BCS ground state (3.33) can be rewritten as

$$|\phi_0\rangle = \prod_x \left(u_x + v_x a_x^+ a_{-x}\right)|0\rangle \ . \tag{3.43}$$

In this formalism, the transformations (3.37) take the form

$$\begin{cases} \alpha_x = u_x a_x - v_x a_x^+ \\ \alpha_x^+ = u_x^* a_x^+ - v_x^* a_x \ . \end{cases} \tag{3.44}$$

It can be easily shown [28, 29, 30] that the above equations describe a rotation in the space of creation and annihilation operators. They can in fact be rewritten as

$$\alpha_x = e^{iS} a_x e^{-iS} \ , \tag{3.45}$$

and the complex conjugate equation, where we have introduced the operator

$$S = -i \sum_k \theta_k \left(a_x^+ a_{-x}^+ - a_{-x} a_x\right) \ . \tag{3.46}$$

The expression of the BCS ground state in terms of the operator S

$$|\phi_0\rangle = e^{iS}|0\rangle \ , \tag{3.47}$$

clearly shows that it can be seen as rotation of the non-interacting ground state.

The previous relations imply that the coefficients u_k and v_k can be expressed as

$$\begin{cases} u_k = \cos\theta_k \\ v_k = \sin\theta_k \ . \end{cases} \tag{3.48}$$

Therefore, there is a single parameter, the rotation angle θ_k, to be determined to minimize the ground state energy.

We now come back to Valatin's formalism. Inverting Eqs. (3.37), we find the relations

$$\begin{cases} a_x^+ = \frac{\alpha_x^+ + g_x^* \alpha_{-x}}{(1+|g_x|^2)^{\frac{1}{2}}} \\ a_x = \frac{\alpha_x + g_x \alpha_{-x}^+}{(1+|g_x|^2)^{\frac{1}{2}}} \ , \end{cases} \tag{3.49}$$

which turn out to be useful to express the operators a_x and a_x^+ in terms of the rotated ones, α_x and α_x^+.

Ordering the operators according to the normal product prescription, i.e. moving the annihilation operators to the right of the creation operator, we obtain constant terms which are the expectation values of operators under consideration in the BCS ground state. For example, for the operator yielding the number of particles in the state x

$$n_x = a_x^+ a_x \ , \tag{3.50}$$

we find

$$n_x = \frac{1}{1+|g_x|^2}\left[\left(\alpha_x^+ + g_x^* \alpha_{-x}\right)\left(\alpha_x + g_x \alpha_{-x}^+\right)\right] \ , \tag{3.51}$$

and the expectation value in the BCS ground state state is

$$\langle\phi_0|\, n_x\, |\phi_0\rangle = h_x = \frac{|g_x|^2}{1+|g_x|^2}\ . \tag{3.52}$$

The properties of $h_x = \langle\phi_0|\, n_x\, |\phi_0\rangle$ follow directly from the properties of g_x

$$h_{k\uparrow} = h_{-k\uparrow} = h_{k\downarrow} = h_{-k\downarrow} = h_k\ . \tag{3.53}$$

Equation (3.52) involves terms proportional to $\alpha_x^+\alpha_{-x}^+$ and $\alpha_{-x}\alpha_x$, with vanishing expectation value on every state of the form $\alpha_{x_1}^+...\alpha_{x_j}^+\,|\phi_0\rangle$. The other terms can be written in the form

$$(n_x)_0 = (1-h_x)\,\Pi_x + h_x\,(1-\Pi_{-x})\ , \tag{3.54}$$

where we have introduced the operator

$$\Pi_x = \alpha_x^+\alpha_x\ , \tag{3.55}$$

yielding the number of elementary excitations in the state x.

Analogously, for pair creation operators, we have

$$a_x^+a_{-x}^+ = \frac{1}{1+|g_x|^2}\left[\left(\alpha_x^+ + g_x^*\alpha_{-x}\right)\left(\alpha_{-x}^+ - g_x^*\alpha_x\right)\right]\ , \tag{3.56}$$

and

$$\left(a_x^+a_{-x}^+\right)_0 = \chi_x^*\,(1-\Pi_x-\Pi_{-x})\ . \tag{3.57}$$

On the other hand, for the pair annihilation operators we find

$$(a_{-x}a_x)_0 = \chi_x\,(1-\Pi_x-\Pi_{-x})\ , \tag{3.58}$$

with χ_x being defined as

$$\chi_x = \frac{g_x}{1+|g_x|^2}\ . \tag{3.59}$$

We can now analyze the spectrum of the theory. Substituting the canonical transformations (3.37) into the Hamiltonian, the latter can be divided into two parts

$$H = H_0 + H_1\ , \tag{3.60}$$

where H_1 has vanishing expectation value in the states of the form $\alpha_{x_1}^+...\alpha_{x_j}^+\,|\phi_0\rangle$, which are eigenstates of H_0. The diagonal operator H_0

$$\begin{aligned} H_0 = &\sum_{k,\sigma} E_k\,(n_{k\sigma})_0 + \frac{1}{2}\sum_{k'\sigma'}(n_{k'\sigma'})_0\sum_{k,\sigma}V_{kk}\,(n_{k\sigma})_0 + \\ &-\frac{1}{2}\sum_{kk',\sigma'}V_{kk'}\,(n_{k\sigma})_0\,(n_{k'\sigma'})_0 + \frac{1}{2}\sum_{kk',\sigma'}V_{kk'}\left(a_{k\sigma}^+a_{-k-\sigma}^+\right)_0(a_{-k'-\sigma}a_{k'\sigma})_0\ , \end{aligned} \tag{3.61}$$

can be rewritten in the form

$$H_0 = W_0 + \sum_x \tilde{E}_x \Pi_x + \sum_{x \neq x'} \tilde{V}_{xx'} \Pi_x \Pi_{x'} \ , \tag{3.62}$$

where the ground state expectation value, W_0, is given by

$$\begin{aligned} W_0 &= 2\sum_k E_k h_k + 2\sum_{k'} h_{k'} \sum_k V_{kk} h_k - \sum_{kk'} V_{kk'} h_{k'} h_k + \sum_{kk'} V_{kk'} \chi^*_{k'} \chi_k = \\ &= \sum_k \left(2E_k h_k + 2\sum_{k'} V_{kk} h_k h_{k'} - \sum_{k'} V_{kk'} h_{k'} h_k + \Delta^*_k \chi_k \right) \ , \end{aligned} \tag{3.63}$$

with

$$\Delta_k = -\sum_{k'} V_{kk'} \chi_{k'} \ . \tag{3.64}$$

Defining also

$$\epsilon_k = E_k - \sum_{k'} \bar{V}_{kk'} h_{k'} \ , \tag{3.65}$$

where

$$\bar{V}_{kk'} = \frac{1}{2} \left(V_{kk'} + V_{k'k} \right) - \left(V_{kk} + V_{k'k'} \right) \ , \tag{3.66}$$

we can finally rewrite the expectation value of the Hamiltonian as

$$W_0 = \sum_k \left(E_k h_k + \epsilon_k h_k - \Delta^*_k \chi_k \right) \ , \tag{3.67}$$

while the excitation energy of the states $\alpha^+_x |\phi_0\rangle$ is given by

$$W_1 = \epsilon_k \left(1 - 2h_k \right) + \left(\Delta^*_k \chi_k + \chi^*_k \Delta_k \right) \ . \tag{3.68}$$

In order to obtain the wave function, we must vary W_0 respect to g^*_k. For this purpose, we observe that the previous definitions, Eqs.(3.52) and (3.59), imply

$$\begin{cases} \frac{\partial h_k}{\partial g^*_k} = \frac{g_k}{\left(1+|g_x|^2\right)^2} \\ \frac{\partial \chi_k}{\partial g^*_k} = -\frac{g_k^2}{\left(1+|g_x|^2\right)^2} \ . \end{cases} \tag{3.69}$$

Hence, carrying out the variation and gathering the resulting terms, we obtain the equation

$$2\epsilon_k g_k + \Delta^*_k g_k^2 - \Delta_k = 0 \ , \tag{3.70}$$

the solution of which is

$$g_k = \frac{1}{\Delta^*_k} \left[-\epsilon_k + \left(\epsilon_k^2 + |\Delta_k|^2 \right)^{\frac{1}{2}} \right] \ , \tag{3.71}$$

where the positive sign of the square root with has been chosen to minimize W_0. Defining now

$$\epsilon^{(1)}_k = \left(\epsilon_k^2 + |\Delta_k|^2 \right)^{\frac{1}{2}} \ , \tag{3.72}$$

we can rewrite Eq. (3.52) in the form

$$h_k = \frac{1}{2}\left(1 - \frac{\epsilon_k}{\epsilon_k^{(1)}}\right) , \tag{3.73}$$

and Eq. (3.59) as

$$\chi_k = \frac{\Delta_k}{2\epsilon_k^{(1)}} . \tag{3.74}$$

Replacing Eqs. (3.73) and (3.74) into Eq. (3.68) and using Eq. (3.72), we find that the energy of an elementary excitation is given by

$$W_1 = \frac{\epsilon_k^2}{\epsilon_k^{(1)}} + \frac{|\Delta_k|^2}{\epsilon_k^{(1)}} = \epsilon_k^{(1)} , \tag{3.75}$$

the quantity ϵ_k being determined by the definition (see Eq. (3.65))

$$\epsilon_k = E_k + \frac{1}{2}\sum_{k'} \bar{V}_{kk'}\left(\frac{\epsilon_k}{\epsilon_k^{(1)}} - 1\right) . \tag{3.76}$$

Finally, we get the equation yielding the energy gap as a function of momentum

$$\Delta_k = -\frac{1}{2}\sum_{k'} V_{kk'}\frac{\Delta_{k'}}{\left(\epsilon_k^2 + |\Delta_k|^2\right)^{\frac{1}{2}}} . \tag{3.77}$$

The coupled equations (3.73), (3.76) and (3.77) form a system which must be solved iteratively in order to determine the wave function of the BCS ground state, its energy and the energy gap necessary associated with the superconducting state (see Fig. 3.2).

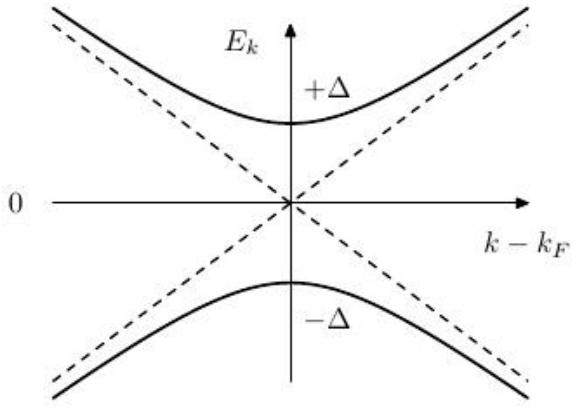

Figure 3.2. Energy spectrum $E_{\mathbf{k}}$ as a function of $|\mathbf{k}|$ near the Fermi surface. The dashed lines show the electron and hole energy levels $\epsilon_{\mathbf{k}} - \epsilon_F$ and $-\epsilon_{\mathbf{k}} + \epsilon_F$ in a normal metal. In a superconductor, these states become hybridized and the resulting energy eigenvalues (relative to ϵ_F) are represented by the solid lines. It clearly appears that there are no states with energy less than $\pm\Delta$ near the Fermi energy [20].

3.3 BCS theory at finite temperature

As we have seen in the previous Section, at $T = 0$ the BCS state is described by a single wave function $|\phi_0\rangle$, given by Eq. (3.33) or the equivalent form of Eq. (3.43), that we will adopt later. On the other hand, at finite temperature, we have to consider a statistical ensemble.

At $T = 0$, only pair states are occupied. We denote $|11\rangle$ the occupied pair state and $|00\rangle$ the unoccupied pair state. Conversely, at finite temperature, we have to consider also mixed states $|10\rangle$ and $|01\rangle$. In particular, we introduce the probability f_k that the state $|01\rangle$, or analogously $|10\rangle$, is occupied. In this way, $1 - 2f_k$ is the occupation probability of the pair state

$$|\psi_k\rangle = \frac{|00\rangle + g_k\,|11\rangle}{(1 + |g_x|^2)^{\frac{1}{2}}} \ . \tag{3.78}$$

Now, the quantity to be minimized is the free energy F, defined as

$$F = \langle H - \mu\hat{N}\rangle - TS \ , \tag{3.79}$$

where H is the Hamiltonian, μ is the chemical potential, $\hat{N}$ is the particle-number operator, S is the entropy and $\langle ...\rangle$ denotes the ensemble average.

The first part of F is simply

$$\langle H - \mu\hat{N}\rangle = \sum_k \left[2f_k E_k + (1 - 2f_k)\, h_k 2E_k\right] \ , \tag{3.80}$$

where the first term is the sum of all contributions due to the occupation of the states $|10\rangle$ and $|01\rangle$, while the second term contains the occupation probabilities of the states $|\psi_k\rangle$, multiplied by the probability amplitude of the state $|11\rangle$.

For simplicity, in this Section we label the states using only the index k, because pairs have vanishing total spin, while the two mixed states $|10\rangle$ and $|01\rangle$ are degenerate.

The average of the potential average has a form similar to that of Eq. (3.63), but, unlike the $T = 0$ case, here we have to introduce a factor $(1 - 2f_k)\,(1 - 2f_{k'})$ because, in order to have the interaction, both $|\psi_k\rangle$ and $|\psi_{k'}\rangle$ must be occupied.

Under the assumption that f_k describes single-particle state, we can write the entropy using the expression suitable for a Fermi gas

$$S = -2k_B \sum_k \left[f_k \ln f_k + (1 - f_k) \ln (1 - f_k)\right] \ . \tag{3.81}$$

Equations (3.79) and (3.81) provide an explicit expression for free energy F in terms of the variational parameters v_k and f_k. The energy gap is defined by the equation

$$\Delta_k = -\sum_{k'} V_{kk'} \chi_{k'}\,(1 - 2f_{k'}) \tag{3.82}$$

which differs from Eq. (3.64), corresponding to $T = 0$, for the introduction of the probabilistic factor $(1 - 2f_{k'})$. With the definition of Δ_k of Eq. (3.82), the

variational equation

$$\frac{\partial F}{\partial g_k^*} = 0 \tag{3.83}$$

becomes totally analogous to Eq. (3.70), derived at $T = 0$. In conclusion, taking into account the probabilistic factor of Eq. (3.82) and performing the same steps leading to Eq. (3.77) in the $T = 0$ case, we obtain the equation

$$\Delta_k = -\sum_{k'} V_{kk'} \frac{\Delta_{k'}}{2\epsilon_k^{(1)}} \left(1 - 2f_{k'}\right) \ , \tag{3.84}$$

where $\epsilon_k^{(1)} = \left(\epsilon_k^2 + |\Delta_k|^2\right)^{\frac{1}{2}}$, the solution of which yields the energy gap for $T \neq 0$. Note that the temperature-dependence of the energy gap Δ_k arises from the presence of f_k.

In conclusion, Eqs. (3.73) and (3.76) which define the wave function and the energy of the system, respectively, can still be derived, but, because of Eq. (3.82), h_k and ϵ_k are now temperature-dependent quantities.

The explicit form of the probability f_k can be obtained using the variational Eq. (3.83) and the definitions of the previous Section. The result is

$$\epsilon_k^{(1)} + k_B T \ln\left[\frac{f_k}{(1 - f_k)}\right] = 0 \ , \tag{3.85}$$

implying

$$f_k = \frac{1}{\left(1 + e^{\frac{\epsilon_k^{(1)}}{k_B T}}\right)} \ . \tag{3.86}$$

The above equation shows that f_k is a Fermi-Dirac distribution describing particles carrying energy $\epsilon_k^{(1)}$. Therefore, $\epsilon_k^{(1)}$ is the excitation energy of a fermion belonging to the system, which justifies the use of Eq. (3.81) for the entropy. As in the $T = 0$ case, Δ_k is the energy gap, but this quantity is temperature dependent, as can be easily seen rewriting Eq. (3.82) in the form [31]

$$\Delta_k = -\frac{1}{2}\sum_{k'} V_{kk'} \frac{\Delta_{k'}}{\left(\epsilon_k^2 + |\Delta_k|^2\right)^{\frac{1}{2}}} \tanh\left(\frac{\left(\epsilon_k^2 + |\Delta_k|^2\right)^{\frac{1}{2}}}{2k_B T}\right) \ . \tag{3.87}$$

The energy gap Δ_k decreases with increasing temperature and vanishes if the temperature reaches its critical value T_c, typical of the transition to the superconducting state (Fig. 3.3). The critical temperature T_c can be estimated using the approximate expression [31]

$$T_c = 0.57\Delta_{k_F}\left(T = 0\right) \ , \tag{3.88}$$

obtained from the gap Eq. (3.87) by taking the limit $\Delta_k \to 0$ and setting $T = 0$. Equation (3.88) is exact in the case of constant Cooper potential. For more realistic interactions, the calculation of the energy gap requires the use of many-body theory [32, 33].

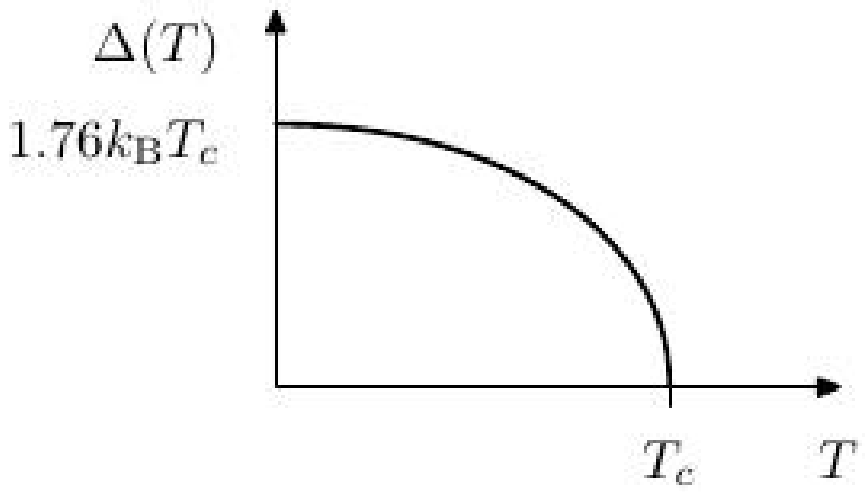

Figure 3.3. Schematic representation of the energy gap Δ as a function of temperature T [20].

3.4 Predictions of the BCS theory

A very important confirmation BCS theory is provided by Andreev scattering, providing evidence of the existence of both Cooper pairs and the BCS energy gap.

Consider the interface between a normal metal and a superconductor and an electron moving in the metal with momentum $\mathbf{k}$ and energy $\epsilon_{\mathbf{k}}$, as shown in Fig. 3.4.

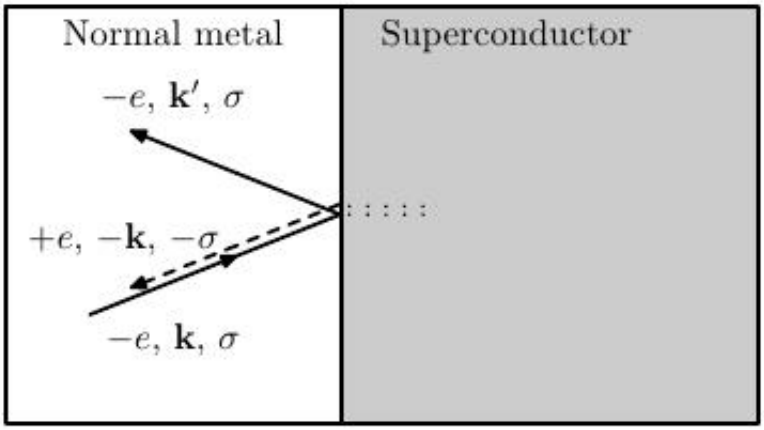

Figure 3.4. Andreev scattering of electrons in a normal metal. The electron incident on the superconductor can either be reflected normally, remaining an electron of the same spin, or it can be Andreev reflected, becoming an hole of opposite momentum and spin. In the Andreev scattering process a net charge of $-e$ is passed into the superconducting condensate. The conductivity of the junction is two times that for electrons with energies V above the gap Δ [20].

If its energy is below the superconductor energy gap, i.e.

$$\epsilon_{\mathbf{k}} - \epsilon_F < \Delta \ , \tag{3.89}$$

the electron cannot propagate into the superconductor, and so it is perfectly reflected at the interface. This is normal particle reflection. But Andreev pointed out that another process is possible. The electron can combine with another electron and form a Cooper pair, which will pass freely into the superconductor. By conservation of charge, an hole must be left behind. By conservation of momentum, this hole will have momentum exactly opposite to that of the original electron, $-\mathbf{k}$. For the same reason, it will also have opposite spin. Therefore, the incoming electron can be reflected either as an electron, with a specularly reflected $\mathbf{k}$ vector, or it can be reflected as an hole of opposite spin and momentum, which travels back exactly along the original electron's path.

Direct evidence of such scattering events can be found by injecting electrons into such an interface, say by electron tunneling. Since the returning hole carries a positive charge and is moving in the opposite direction with respect to the injected electron, the tunnel current is actually twice what it would have been if $\Delta = 0$, or if the tunnelling electron is injected with at a voltage above the energy gap, $V > \Delta$.

An interesting feature of Andreev reflection is that the electron and the hole are in exactly time reversed quantum states,

$$\begin{cases} -e \to e \\ \mathbf{k} \to -\mathbf{k} \\ \sigma \to -\sigma \ . \end{cases} \tag{3.90}$$

This is a manifestation of the fact that Cooper pairs in the BCS wave function are pairs of time reversed single particle states [20].

Chapter 4

Nuclear matter and nuclear forces

As pointed out in the Introduction, nuclear interactions play a critical role in determining the properties of neutron stars. This Chapter is devoted to a review of the available empirical information on nuclear forces and the properties of atomic nuclei and nuclear matter. This information provides the basis of the dynamical model employed in our work, in which neutron star matter is modeled as a uniform, translationally invariant system consisting of neutrons only. While being somewhat oversimplified, this picture can be used to describe both the neutron gas in the inner crust of the star and the β-stable matter in the outer core, in which neutrons largely dominate.

4.1 Empirical information on nuclei and nuclear matter

Nuclear matter can be thought of as a giant nucleus, with given numbers of protons and neutrons interacting through nuclear forces only. As the typical thermal energies are negligible compared to the nucleon Fermi energies, such a system can be safely considered to be at zero temperature.

A quantitative understanding of the properties of nuclear matter, whose calculations is greatly simplified by translational invariance, is needed both as an intermediate step towards the description of real nuclei and for the development of realistic models of matter in the neutron star core.

The large body of data on nuclear masses can be used to extract empirical information on the equilibrium properties of nuclear matter. The binding energy of nuclei of mass number A is defined as the difference between the sum of nucleons masses, which compose the nucleus, and the measured mass of same nucleus. The dependence of binding energy $B(Z, A)$ on protons number Z and mass number A is well described by the semi-empirical formula [34]:

$$B(Z,A) = a_v A - a_s A^{2/3} - a_c \frac{Z^2}{A^{1/3}} - a_A \frac{(A-2Z)^2}{4A} - \lambda a_p \frac{1}{A^{1/2}} \ . \qquad (4.1)$$

The firsts two terms are defined *volume energy* and *surface energy*. They describe the contributions of strong interactions occurring inside the nucleus and on its surface,

respectively. The third term is called *Coulomb term* and takes into account the electrostatic repulsion between protons inside the nucleus. The fourth term is defined as *symmetry energy* and accounts for the observation that symmetric nuclei (consisting of equal numbers of protons and neutrons) are energetically favored. Finally, the last term is the *pairing energy*, the inclusion of which is needed to explain why even-even nuclei (consisting of even numbers of protons and neutrons, Z and $A - Z$, respectively) are more stable than even-odd or odd-odd nuclei.

In the $A \to \infty$ limit, and neglecting the effect of the Coulomb repulsion between protons, the only surviving contribution in the case $Z = A/2$ is the term linear in A. Hence, the coefficient a_v can be identified with the binding energy per particle of isospin symmetric nuclear matter (SNM).

Figure 4.1 shows how, for mass number $A \geq 20$, the measured binding energy per nucleon, $B(A, Z)/A$, of stable nuclei is nearly constant and $\sim 8.5\,\mathrm{MeV}$.

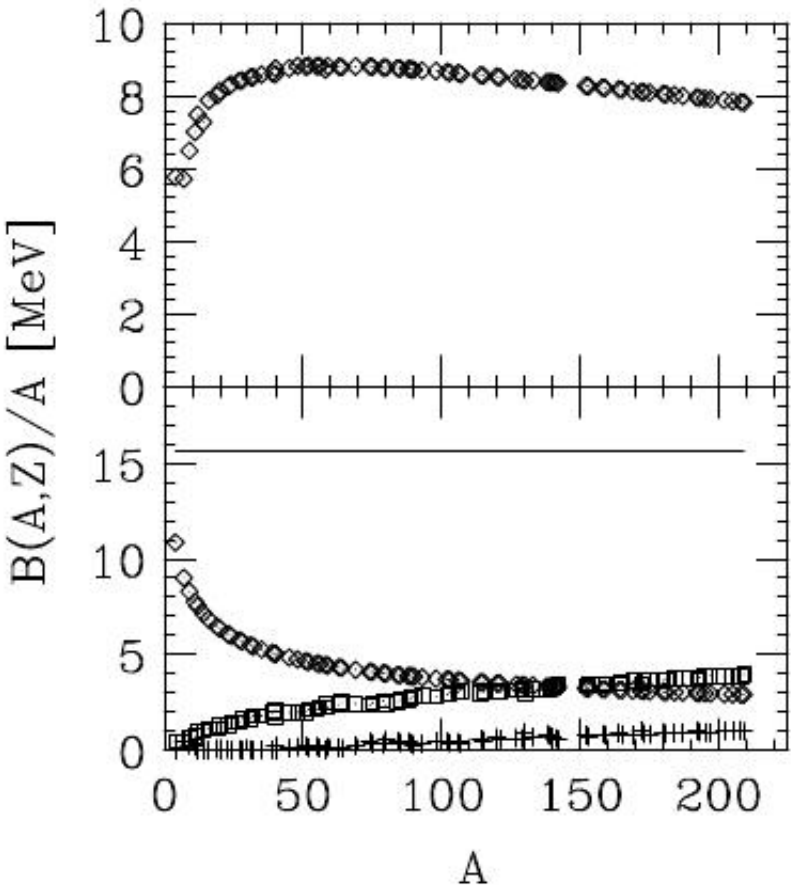

Figure 4.1. Top: A-dependence of binding energy per nucleon of stable nuclei. Bottom: A-dependence of volume (solid line), surface (rhombi), Coulomb (squares) and symmetry (crosses) terms of Eq. (4.1).

The equilibrium density of SNM, ρ_0, can be inferred exploiting the saturation of nuclear densities, i.e. the experimental observation that the central charge density

of atomic nuclei, measured by elastic electron-nucleus scattering, does not depend on A for large A. This property is illustrated in Fig. 4.2. The empirical values of the equilibrium density and binding energy of SNM are:

$$\rho_0 = 0.16\,\mathrm{fm}^{-3}, \qquad B = -15.7\,\mathrm{MeV}\ . \tag{4.2}$$

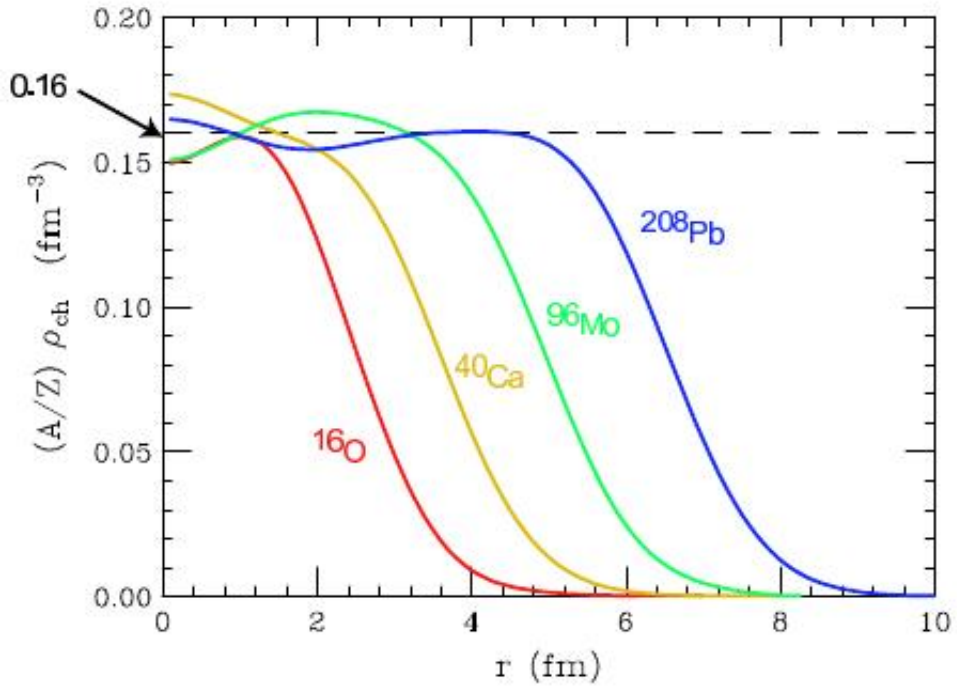

Figure 4.2. Saturation of central nuclear densities measured by elastic electron-nucleus scattering.

In principle, additional information can be obtained from measurements of the excitation energies of nuclear vibrational states, yielding the (in)-compressibility module K. However, the data analysis of these experiments is non trivial and the resulting values of K range from $K \sim 200\,\mathrm{MeV}$, corresponding to more compressible nuclear matter, i.e. to a *soft* equation of state (EOS), to a $K \sim 300\,\mathrm{MeV}$, corresponding to a *stiff* EOS [35].

The main goal of nuclear matter theory is deriving an EOS at zero temperature, i.e. the density dependence of the binding energy per particle $B(\rho)/A$, capable to explain the above data starting from the elementary nucleon-nucleon (NN) interaction. However, many important applications of nuclear matter theory require the development of a formalism flexible enough to describe the properties of matter at finite temperature.

Unfortunately, due to the complexity of the fundamental theory of strong interactions – the quantum chromo-dynamics, or QCD – an *ab initio* description of nuclear matter at finite density and zero temperature is out of reach of the present computational techniques. As a consequence, one has to rely on dynamical models

in which nucleons and mesons play the role of effective degrees of freedom.

In this work, we adopt the approach based on non-relativistic quantum mechanics and phenomenological nuclear Hamiltonians, that allows for a quantitative description of the nucleon-nucleon (NN) system in both bound and scattering states.

4.2 Nuclear forces

The main features of the NN interaction, inferred from the analysis of nuclear systematics, may be summarized as follows.

- The *saturation* of nuclear density (Fig. 4.2), i.e. the fact that density in the interior of atomic nuclei is nearly constant and independent of the mass number A, tells us that nucleons cannot be packed together too tightly. Hence, at short distance, the NN force must be repulsive. Assuming that the interaction can be described by a non-relativistic potential v depending on the inter-particle distance, $\mathbf{r}$, we can then write

$$v(\mathbf{r}) > 0 \quad , \quad |\mathbf{r}| < r_c \ , \tag{4.3}$$

  r_c being the radius of the repulsive core.

- The fact that the nuclear binding energy per nucleon is roughly the same for all nuclei with $A \geq 20$, its value being (Fig. 4.1)

$$\frac{B}{A} \sim 8.5\,\mathrm{MeV} \ , \tag{4.4}$$

  suggests that the NN interaction has a finite range r_0, i.e. that

$$v(\mathbf{r}) = 0 \quad , \quad |\mathbf{r}| > r_0 \ . \tag{4.5}$$

- The spectra of the so called *mirror nuclei*, i.e. pairs of nuclei having the same A and charges differing by one unit (implying that the number of protons in a nucleus is the same as the number of neutrons in its mirror companion) exhibit striking similarities. In these nuclei, the energies of the levels with the same parity and angular momentum are in fact the same, up to small electromagnetic corrections, showing that protons and neutrons have similar nuclear interactions, i.e. that nuclear forces are *charge symmetric*.

Charge symmetry is the manifestation of a more general property of the NN interaction, called *isotopic invariance*. Neglecting the small mass difference, proton and neutron can be viewed as two states of the same particle, the nucleon (N), described by the Dirac equation obtained from the Lagrangian density

$$\mathcal{L} = \bar{\psi}_N \left(i\gamma^\mu \partial_\mu - m \right) \psi_N \ , \tag{4.6}$$

where the nucleon field is described by the isospinor

$$\psi_N = \begin{pmatrix} p \\ n \end{pmatrix} \ , \tag{4.7}$$

p and n being the Dirac spinors associated with the proton and the neutron, respectively. The Lagrangian density of Eq. (4.6) is invariant under the $SU(2)$ global phase transformation

$$U = e^{i\alpha_j \tau_j} \ , \tag{4.8}$$

where $\boldsymbol{\alpha}$ is a constant (i.e. independent of x) vector and the τ_j (j = 1,2,3) are Pauli matrices[1]. The above equations show that the nucleon can be described as a doublet in isospin space with isospin $t = 1/2$. In this formalism, proton and neutron correspond to isospin projections $m_t = +1/2$ and $m_t = -1/2$, respectively.

A nucleon pair is characterized by the total isospin T and its projection M_T. The two-nucleon isospin states $|T, M_T\rangle$ can be summarized as follows (see Appendix C).

$$\begin{aligned} |1,1\rangle &= |pp\rangle \\ |1,0\rangle &= \frac{1}{\sqrt{2}}\left(|pn\rangle + |np\rangle\right) \\ |1,-1\rangle &= |nn\rangle \\ |0,0\rangle &= \frac{1}{\sqrt{2}}\left(|pn\rangle - |np\rangle\right) \ , \end{aligned} \tag{4.9}$$

where we observe that proton-proton and neutron-neutron pairs always have total isospin $T = 1$, whereas a proton-neutron pair may have either $T = 0$ or $T = 1$.

Isospin invariance implies that the interaction between two nucleons separated by a distance $r = |\mathbf{r}_1 - \mathbf{r}_2|$ and having total spin S depends on their total isospin T but not on its projection M_T. For example, the potential $v(\mathbf{r})$ acting between two protons with spins coupled to $S = 0$ is the same as the potential acting between a proton and a neutron with spins and isospins coupled to $S = 0$ and $T = 1$.

4.2.1 The two-nucleon system

The details of the NN interaction can be best understood in the two-nucleon system. There is *only one* NN bound state, the nucleus of deuterium, or deuteron (^{2}H), consisting of a proton and a neutron coupled to total spin and isospin $S = 1$ and $T = 0$, respectively. This is a clear manifestation of the *spin-dependence* of nuclear forces.

Another important piece of information can be inferred from the observation that the deuteron exhibits a non-vanishing electric quadrupole moment, implying that its charge distribution is not spherically symmetric. Hence, the NN interaction is *non-central*: it also depends on the orientation of the inter-particle distance.

Besides the properties of the two-nucleon bound state, the large data base of phase shifts measured in NN scattering experiments (the Nijmegen data base [36] includes $\backsim$ 4000 data points, corresponding to energies up to 350 MeV in the lab frame) provides valuable additional information on the nature of NN forces.

The theoretical description of the NN interaction was first attempted by Yukawa in 1935. He made the hypothesis that nucleons interact through the exchange of a

[1] The main properties of Pauli matrices are summarized in Appendix C.

particle, whose mass μ can be related to the interaction range r_0 according to

$$r_0 \sim \frac{1}{\mu} \ . \tag{4.10}$$

Using $r_0 \sim 1\,\mathrm{fm}$, the above relation yields $\mu \sim 200\,\mathrm{MeV}$ ($1\,\mathrm{fm}^{-1} = 197.3\,\mathrm{MeV}$).

Yukawa's idea has been successfully implemented identifying the exchanged particle with the π meson (or *pion*), discovered in 1947 in cosmic rays, the mass of which is $m_\pi \sim 140\,\mathrm{MeV}$. Experiments show that the pion is a spin zero pseudoscalar particle[2] (i.e. it has spin-parity 0^-) that comes in three charge states, denoted π^+, π^- and π^0. Hence, it can be regarded as an isospin $T = 1$ triplet, the charge states being associated with isospin projections $M_T = +1, 0$ and -1, respectively.

The simplest π-nucleon coupling compatible with the observation that nuclear interactions conserve parity has the pseudoscalar form $ig\gamma^5\boldsymbol{\tau}$. The corresponding interaction Lagrangian reads

$$\mathcal{L}_I = -ig\boldsymbol{\Psi}\gamma_5(\boldsymbol{\tau}\cdot\boldsymbol{\phi})\boldsymbol{\Psi} \ , \tag{4.11}$$

where g is the coupling constant, $\boldsymbol{\Psi}$ is the nucleon field, $\boldsymbol{\tau}$ describes the isospin of the nucleon and $\boldsymbol{\phi}$ is defined in terms of scalar pion fields according to

$$\phi_1 = \frac{(\pi^+ + \pi^-)}{\sqrt{2}}, \qquad \phi_2 = \frac{i(\pi^+ - \pi^-)}{\sqrt{2}}, \qquad \phi_3 = \pi^0 \ . \tag{4.12}$$

With this choice for the interaction vertex, the amplitude of the process depicted in Fig. 4.3 (the calculation of which is described in Appendix B) can be readily written, using standard Feynman's diagram techniques, as

$$\langle f|\, M\, |i\rangle = -ig^2 \frac{\bar{u}(p_2', s_2')\gamma_5 u(p_2, s_2)\bar{u}(p_1', s_1')\gamma_5 u(p_1, s_1)}{k^2 - m_\pi^2} \langle \boldsymbol{\tau}_1 \cdot \boldsymbol{\tau}_2 \rangle \ , \tag{4.13}$$

where $k = p_1' - p_1 = p_2 - p_2'$, $k^2 = k_\mu k^\mu = k_0^2 - |\mathbf{k}|^2$, $u(p,s)$ is the Dirac spinor associated with a nucleon of four momentum $p \equiv (\mathbf{p}, E)$ ($E = \sqrt{\mathbf{p}^2 + m^2}$) and spin projection s and

$$\langle \boldsymbol{\tau}_1 \cdot \boldsymbol{\tau}_2 \rangle = \eta_{2'}^\dagger \boldsymbol{\tau} \eta_2 \eta_{1'}^\dagger \eta_1 \ , \tag{4.14}$$

η_i being the two-component Pauli spinor describing the isospin state of particle i.

In the non-relativistic limit, Yukawa's theory leads to define a NN interaction

[2] The pion spin has been deduced from the balance of the reaction $\pi^+ + {}^2\mathrm{H} \leftrightarrow p + p$, while its intrinsic parity was determined observing the π^- capture from the K shell of the deuterium atom, leading to the appearance of two neutrons: $\pi^- + d \to n + n$.

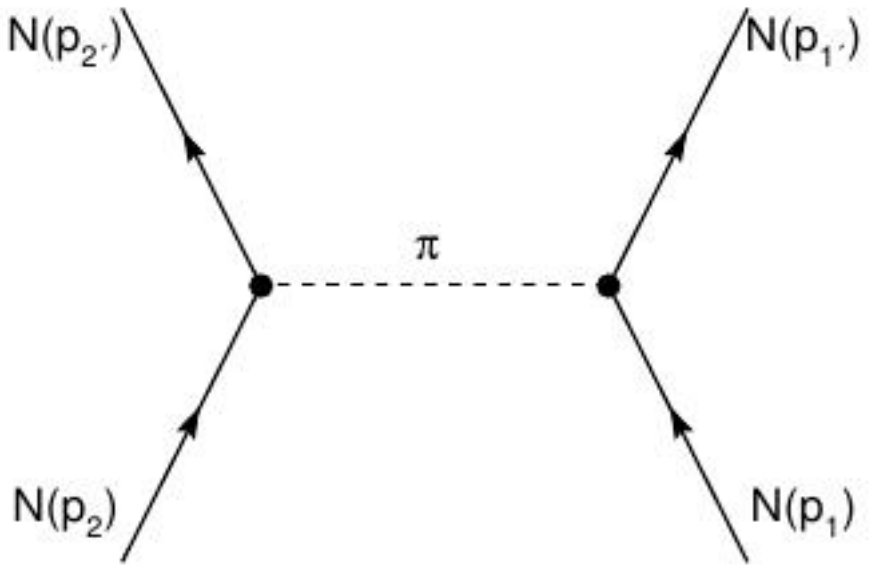

Figure 4.3. Feynman diagram describing the one-pion-exchange process between two nucleons. The corresponding amplitude is given by Eq.(4.13).

potential, that can be written in coordinate space as

$$\begin{aligned} v_\pi &= \frac{g^2}{4m^2}(\boldsymbol{\tau}_1\cdot\boldsymbol{\tau}_2)(\boldsymbol{\sigma}_1\cdot\boldsymbol{\nabla})(\boldsymbol{\sigma}_2\cdot\boldsymbol{\nabla})\frac{e^{-m_\pi r}}{r} \\ &= \frac{g^2}{(4\pi)^2}\frac{m_\pi^3}{4m^2}\frac{1}{3}(\boldsymbol{\tau}_1\cdot\boldsymbol{\tau}_2) \\ &\times\left\{\left[(\boldsymbol{\sigma}_1\cdot\boldsymbol{\sigma}_2)+S_{12}\left(1+\frac{3}{x}+\frac{3}{x^2}\right)\right]\frac{e^{-x}}{x}-\frac{4\pi}{m_\pi^3}\,(\boldsymbol{\sigma}_1\cdot\boldsymbol{\sigma}_2)\,\delta^{(3)}(\mathbf{r})\right\}\,, \end{aligned} \tag{4.15}$$

where $x = m_\pi|\mathbf{r}|$ and

$$S_{12} = \frac{3}{r^2}(\boldsymbol{\sigma}_1\cdot\mathbf{r})(\boldsymbol{\sigma}_2\cdot\mathbf{r}) - (\boldsymbol{\sigma}_1\cdot\boldsymbol{\sigma}_2)\,, \tag{4.16}$$

is reminiscent of the operator describing the non-central interaction between two magnetic dipoles (the properties of the operator S_{12} are given in Appendix C).

For $g^2/(4\pi) \sim 14$, the above potential provides an accurate description of the long range part ($|\mathbf{r}| > 1.5$ fm) of the NN interaction, as shown by the excellent fit of the NN scattering phase shifts in states of high angular momentum. In these states, due to the strong centrifugal barrier, the probability of finding the two nucleons at small relative distances becomes in fact negligibly small.

At medium- and short-range, other more complicated processes, involving the exchange of two or more pions (possibly interacting among themselves) or heavier particles (like the ρ and the ω mesons, whose masses are $m_\rho = 770\,\mathrm{MeV}$ and $m_\omega = 782\,\mathrm{MeV}$, respectively), have to be taken into account. Moreover, when

their relative distance becomes very small ($|\mathbf{r}| \lesssim 0.5\,\mathrm{fm}$) nucleons, being composite and finite in size, are expected to overlap. In this regime, NN interactions should in principle be described in terms of interactions between nucleon costituents, i.e. quarks and gluons, as dictated by QCD.

Phenomenological potentials describing the *full* NN interaction are generally written as

$$v = \tilde{v}_\pi + v_R \ , \tag{4.17}$$

where $\tilde{v}_\pi$ is the one-pion-exchange potential, defined by Eqs. (4.15) and (4.16), stripped of the δ-function contribution, whereas v_R describes the interaction at medium and short range. The spin-isospin dependence and the non-central nature of the NN interactions can be properly described rewriting Eq. (4.17) in the form

$$v(ij) = \sum_{ST} \left[v_{TS}(r_{ij}) + \delta_{S1} v_{tT}(r_{ij}) S_{12} \right] P_{2S+1} \Pi_{2T+1} \ . \tag{4.18}$$

The above expression is applicable at all distances, its behavior at $r_{ij} \to \infty$ being given by Eq. (4.15). In equation (4.18), S and T are the total spin and isospin of the interacting pair, respectively, while P_{2S+1} ($S = 0, 1$) and Π_{2T+1} ($T = 0, 1$) are the spin and isospin projection operators on NN states with definite S and T (the properties of these operators are given in Appendix C). The functions $v_{TS}(r_{ij})$ and $v_{tT}(r_{ij})$ describe the radial dependence of the interaction in the different spin-isospin channels, and reduce to the corresponding components of the one-pion-exchange potential at large r_{ij}. Their shapes are chosen in such a way as to reproduce the available NN data (deuteron binding energy, charge radius and quadrupole moment and the NN scattering data).

An alternative representation of the NN potential, based on the set of six operators (see Appendix C)

$$O_{ij}^{n \le 6} = [1, (\boldsymbol{\sigma}_i \cdot \boldsymbol{\sigma}_j), S_{ij}] \otimes [1, (\boldsymbol{\tau}_i \cdot \boldsymbol{\tau}_j)] \ , \tag{4.19}$$

is given by the expression

$$v(ij) = \sum_{n=1}^{6} v^{(n)}(r_{ij}) O_{ij}^{(n)} \tag{4.20}$$

providing a reasonable account of deuteron properties, as well as of NN scattering in S wave (i.e. in states of angular momentum $L = 0$).

In order to describe P-wave (i.e. $L = 1$) NN scattering, one has to include the two additional $\mathbf{L}$-dependent operators

$$O_{ij}^{n=7,8} = \mathbf{L} \cdot \mathbf{S} \otimes [1, (\boldsymbol{\tau}_i, \boldsymbol{\tau}_j)] \ . \tag{4.21}$$

The potential yielding the best description[3] of the phase shifts included in the Nijmegen database, called Argonne v_{18} potential [37], involves the additional operators

$$O_{ij}^{n=9,\ldots,14} = \left[\mathbf{L}^2, \mathbf{L}^2 (\boldsymbol{\sigma}_i \cdot \boldsymbol{\sigma}_j), (\mathbf{L} \cdot \mathbf{S})^2 \right] \otimes [1, \boldsymbol{\tau}_i \cdot \boldsymbol{\tau}_j] \tag{4.22}$$

[3] Corresponding to χ^2/datum ~ 1.

$$O_{ij}^{n=15,\ldots,18} = [1, \boldsymbol{\sigma}_i \cdot \boldsymbol{\sigma}_j, S_{ij}] \otimes T_{ij}, \qquad (\tau_{zi} + \tau_{zj}) \ , \tag{4.23}$$

where

$$T_{ij} = \frac{3}{r^2}(\boldsymbol{\tau}_i \cdot \mathbf{r})(\boldsymbol{\tau}_j \cdot \mathbf{r}) - (\boldsymbol{\tau}_i \cdot \boldsymbol{\tau}_j) \ . \tag{4.24}$$

The $O_{ij}^{n=15,\ldots,18}$ take care of small charge symmetry breaking effects, due to the different masses and coupling constants of charged and neutral pions.

The typical shape of the NN potential in the state of relative angular momentum $\ell = 0$ and total spin and isospin $S = 0$ and $T = 1$ is shown in Fig. 4.4. The short-range repulsive core, to be ascribed to heavy-meson exchange or to more complicated mechanisms involving nucleon constituents, is followed by an intermediate-range attractive region, largely due to two-pion-exchange processes. Finally, at large inter-particle distance the one-pion-exchange dominates. We recall that the presence of the repulsive core plays a fundamental role for the stability of neutron stars.

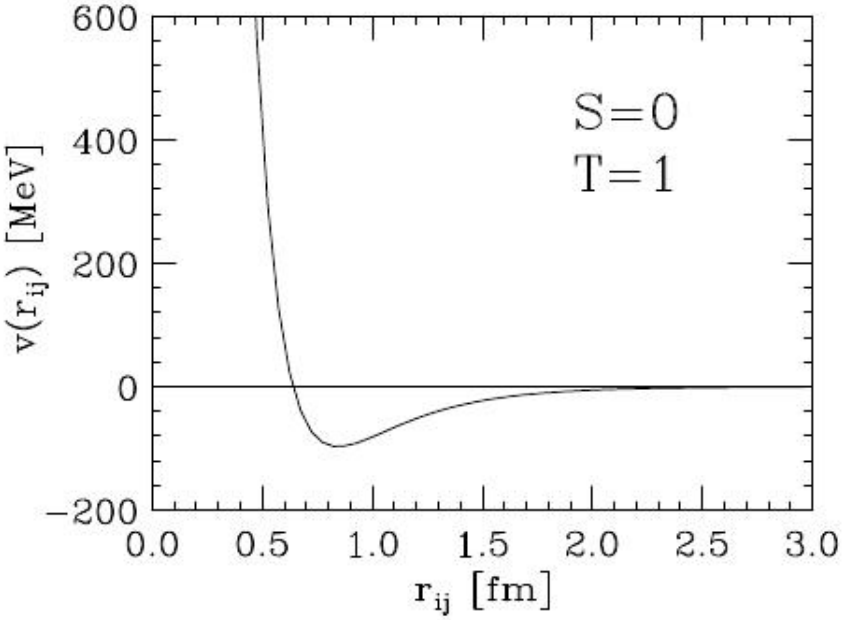

Figure 4.4. Radial dependence of the NN potential describing the interaction between two nucleons in the state of relative angular momentum $L = 0$ and total spin and isospin $S = 0$ and $T = 1$.

The calculations discussed in this Thesis are based on a widely employed potential model, obtained within the phenomenological approach outlined in this Section, generally referred to as Argonne v_{18} potential, which is written in the form

$$v(ij) = \sum_{n=1}^{18} v^n(r_{ij}) O_{ij}^n \ . \tag{4.25}$$

We have used a simplified version of the above potential, v_6', obtained including only the operators $O_{ij}^{n\leq 6}$, to develop the effective interaction described in the next Chapter.

4.2.2 The three-nucleon system

The NN potential determined from the properties of the two-nucleon system can be used to solve the non-relativistic many-body Schrödinger equation for $A > 2$. In the case of $A = 3$, in which the problem can be still solved exactly, the resulting ground state energy, E_0, turns out to be slightly different from the experimental value E_{exp}. For example, for ^{3}He one typically finds $E_0 = 7.6\,\mathrm{MeV}$, to be compared to $E_{exp} = 8.48\,\mathrm{MeV}$. In order to exactly reproduce E_{exp} a term containing three-nucleon interactions described by a potential V_{ijk} of the form

$$V_{ijk} = V_{ijk}^{2\pi} + V_{ijk}^{N} \,, \tag{4.26}$$

has to added to the nuclear Hamiltonian. The first contribution, $V_{ijk}^{2\pi}$, takes into account the two-pion exchange process represented in Fig. 4.5. This mechanism, featuring the excitation of a nucleon resonance in the intermediate state, is dominant at large distances and leads to the appearance of an attractive three-nuclon force. On the other hand, V_{ijk}^{N} is a purely phenomenological repulsive term.

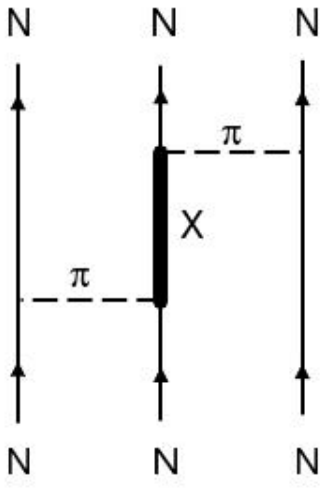

Figure 4.5. Diagrammatic representation of the process providing the main contribution to the three-nucleon interaction. The thick solid line corresponds to an excited state of the nucleon in the intermediate state of the process.

The two contributions entering the definition of the three-body potential V_{ijk} are adjusted to reproduce the properties of ^{3}H and ^{3}He [38]. Note that the inclusion of V_{ijk} leads to a very small change of the total potential energy, the ratio $\langle v_{ij}\rangle/\langle V_{ijk}\rangle$ being $\sim 2\%$.

For $A > 3$ the Schrödinger equation is no longer exactly solvable using deterministic methods. However, very accurate solutions can be obtained using stochastic techniques, such as variational Monte Carlo (VMC) and the Green function Monte Carlo (GFMC) [39] methods.

The GFMC approach has been successfully employed to describe the ground state and the low lying excited states of nuclei with $A \leq 12$. The results of VMC and GFMC calculations, carried out using the Argonne v_{18} NN potential and the state-of-the-art three-nucleon potential model referred to as Urbana IX [38], summarized in Fig. 4.6 for $A \leq 8$. It clearly appears that the non-relativistic approach, based on the dynamics modeled to reproduce the properties of two- and three-nucleon systems, has a remarkable predictive power.

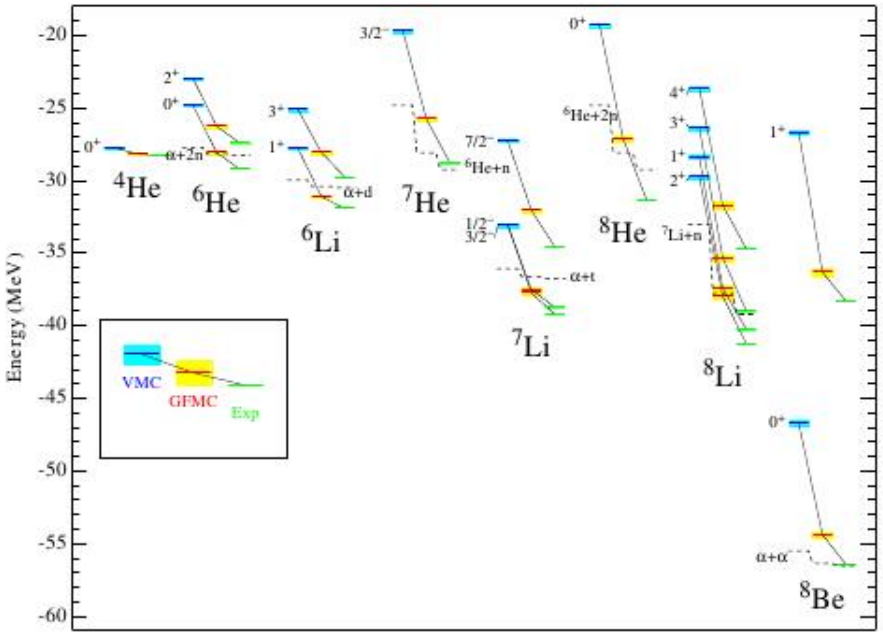

Figure 4.6. Comparison between the VMC and GFMC energies of nuclei with $A \leq 8$ and experimental data [39].

Chapter 5

The CBF effective interaction

In this Chapter, we will outline the main elements of the description of nuclear matter within non- relativistic many-body theory. We will focus on the formalism of correlated basis functions (CBF) and the cluster expansion technique, providing the basis for the derivation of the effective interaction employed to obtain the superfluid gap in neutron matter.

5.1 Non-relativistic many-body theory

Understanding the properties of matter at densities comparable to the central density of atomic nuclei is made difficult by *both* the complexity of the interactions *and* the approximations implied in any theoretical description of quantum mechanical many-particle systems.

Our work has been carried out within the framework of *nuclear many-body theory* (NMBT), providing a theoretical frame suitable to describe a variety of nuclear matter properties starting from the dynamical model described in the previous Chapter. The non-relativistic approximation is based on the observation that, in the relevant density regime, the typical kinetic energy of a nucleon is negligible with respect to the nucleon mass.

Within NMBT, a nuclear system is seen as a collection of point-like nucleons whose dynamics are described by the Hamiltonian

$$H = \sum_{i=1}^{A} \frac{\mathbf{p}_i^2}{2m} + \sum_{j>i=1}^{A} v(ij) + ... \tag{5.1}$$

including the kinetic term, the NN potential $v(ij)$ and additional many-body interactions (see Chapter 4) denoted by the ellipses. The study of such a system involves serious difficulties because of the strong repulsive core of the NN potential $v(ij)$, which cannot be handled within standard perturbation theory. The matrix elements of $v(ij)$ between eigenstates of the non-interacting system are in fact very large, or even divergent.

In order to overcome this difficulty, we substitute the Fermi gas (FG) states, with a new basis of *correlated* states, which include non-perturbative effects arising from the short-range repulsion between nucleons.

5.1.1 Correlated basis function (CBF) formalism

In the *Correlated Basis Function* (CBF) formalism nuclear matter is described by a set of *correlated* states $|n\rangle$, obtained from the Fermi gas (FG) states $|n_{FG}\rangle$ through the transformation [40, 41]

$$|n\rangle = \frac{F\,|n_{FG}\rangle}{\langle n_{FG}|\,F^\dagger F\,|n_{FG}\rangle^{1/2}}\ . \tag{5.2}$$

The operator F, embodying the correlation structure induced by the NN interaction, is written in the form

$$F(1,...,N) = \mathcal{S}\prod_{j>i=1}^{N} f_{ij}\ , \tag{5.3}$$

where $\mathcal{S}$ is the symmetrization operator taking care of the fact that, in general,

$$[f_{ij}, f_{ik}] \neq 0\ . \tag{5.4}$$

The structure of the two-body *correlation functions* f_{ij} must reflect the complexity of the NN potential. Hence, it is generally cast in the form (compare to Eq. (4.20))

$$f_{ij} = \sum_{n=1}^{6} f^n(r_{ij}) O^n_{ij}\ , \tag{5.5}$$

where we have included only the six operators O^n_{ij} defined in Eq. (4.19), which provide a fairly accurate description of the correlation structure of the two-nucleon bound state (i.e. the deuterium). The shape of the radial functions $f^n(r_{ij})$ is determined through functional minimization of the expectation value of the nuclear Hamiltonian in the correlated ground state

$$\langle H\rangle = \langle 0|\,H\,|0\rangle \geq E_0\ , \tag{5.6}$$

with the boundary conditions

$$\begin{aligned} &\lim_{r\to 0} f^n(r) = 0 \\ &\lim_{r\to\infty} f^1(r) = 1 \\ &\lim_{r\to\infty} f^{n\neq 1}(r) = 0\ . \end{aligned} \tag{5.7}$$

The radial functions describing correlations between nucleon pairs with definite S and T can be obtained from the $f^n(r)$ using the transformations discussed in Appendix C. Figure 5.1 illustrates the typical behavior of both the NN potential and the correlation functions – computed in isospin symmetric nuclear matter at equilibrium density – for nucleon pairs with $S = 0,\ T = 0$ and $S = 0,\ T = 1$. We observe how for short interparticle distances the correlation function $f_{TS}(r)$ becomes very small. In particular, for pairs with total spin and isospin $S = 0$ and $T = 0$ the correlation function vanishes, because the corresponding potential $v_{TS}(r)$ exhibits a strong repulsive core. On the other hand, in the case $S = 1$ and $T = 0$, the repulsive part of the potential is less pronounced, and followed by an attractive part. As

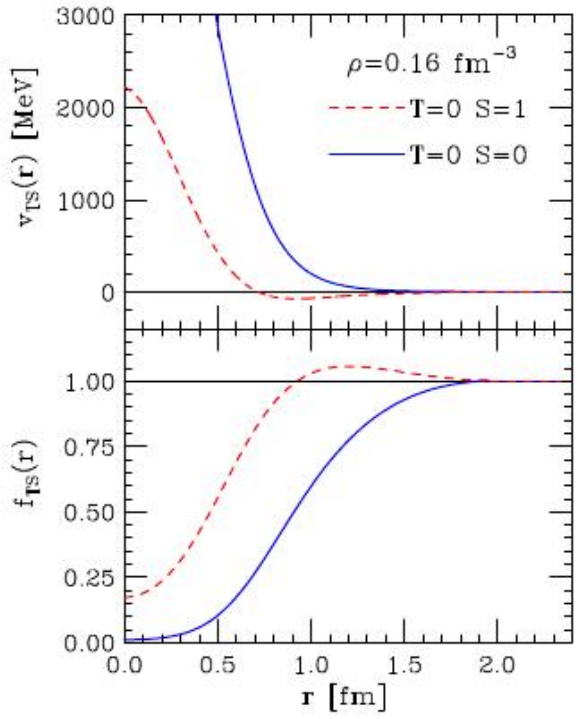

Figure 5.1. The top panel shows the r-dependence of the central component of the Argonne v_{18} potential in the $S = 0$, $T = 0$ (solid line) and $S = 0$, $T = 1$ (dashed line). The corresponding correlation functions $f_{TS}(r)$ are shown in the bottom panel.

a consequence, the correlation function is small but not vanishing at $r = 0$, and exceeds unity at intermediate range.

The correlated states defined in Eq. (5.2) are not orthogonal to one another. However, they can be orthogonalized by a transformation $\hat{T}$ that preserves diagonal matrix elements of the Hamiltonian [42]. Denoting the orthogonalized states by $|n'\rangle$, we can write

$$|n\rangle \to |n'\rangle = \hat{T}\,|n\rangle \ , \tag{5.8}$$

and

$$\langle n'|\,H\,|n'\rangle = \langle n|\,H\,|n\rangle \ . \tag{5.9}$$

Using the orthogonalized basis as defined, we can split the nuclear Hamiltonian according to

$$H = H_0 + H_I \ , \tag{5.10}$$

where H_0 and H_I are defined in terms of their matrix element

$$\begin{aligned} \langle m'|\,H_0\,|n'\rangle &= \delta_{mn}\,\langle m'|\,H\,|n'\rangle \\ \langle m'|\,H_I\,|n'\rangle &= (1-\delta_{mn})\,\langle m'|\,H\,|n'\rangle \ . \end{aligned} \tag{5.11}$$

The above definitions obviously imply that, if the correlated states have large overlaps with the eigenstates of H, the matrix elements of H_I are small, and the perturbative expansions of any observables in powers of H_I is rapidly convergent.

5.1.2 Cluster expansion formalism

The calculation of the matrix elements of many-body operators between correlated states involves severe difficulties, that can be circumvented using a suitable approximation scheme.

The cluster expansion formalism exploits the short range nature of nuclear forces. To take this property of the interaction into account, the correlation operator F of Eq. (5.3) must be defined in such a way that, if any subset of particles, say $i_1, ..., i_p$, is removed far from the remaining $i_{p+1}, ..., i_N$, it factorizes according to

$$F(1, ..., N) \to F_p(i_1, ..., i_p) F_{N-p}(i_{p+1}, ..., i_N) \ . \tag{5.12}$$

The above property is the basis of the cluster expansion formalism [41], allowing one to write the matrix element of a many-body operator between correlated states as a series, the terms of which correspond to contributions arising from isolated subsystems (clusters) involving an increasing number of particles.

Here, we omit the details of the derivation of the cluster expansion, and report only the result for the case of the expectation value of the Hamiltonian in the correlated ground state, which is used to obtain the CBF effective interaction. The expansion can be written in the form

$$\langle H \rangle = \langle 0 | \, H \, | 0 \rangle = T_0 + (\Delta E)_2 + (\Delta E)_3 + ... + (\Delta E)_N \ , \tag{5.13}$$

where T_0 is the ground state energy of the non interacting Fermi gas (FG) and $(\Delta E)_n$ is the contribution of the n-body cluster. Although $(\Delta E)_2$ is the dominant contribution, the contribution of clusters with more than two nucleons is in general not negligible.

The terms of the expansion (5.13) can be represented by diagrams featuring n vertices, representing the nucleons in the cluster, connected by lines corresponding to dynamical and statistical correlations. The terms of the resulting diagrammatic expansion can be classified according to their topological structure, and selected classes of diagrams can be summed up to all orders solving a set of coupled integral equations, called Fermi-hyper-netted-chain (FHNC) equations [41, 43, 44].

5.2 Derivation of the effective interaction

We can define the CBF effective interaction V_{eff} at lowest order of the cluster expansion as (compare to Eq. (5.13)):

$$\langle H \rangle = \langle 0 | \, H \, | 0 \rangle \approx T_0 + (\Delta E)_2 = \langle 0_{FG} | \, T_0 + V_{\mathit{eff}} \, | 0_{FG} \rangle \ . \tag{5.14}$$

As the above equation suggests, this approach is aimed at obtaining a well behaved interaction, suitable to carry out calculations of any nuclear matter observables using perturbation theory in the FG basis.

The explicit expression of V_{eff}, derived and discussed in Refs. [3, 47], is obtained from

$$(\Delta E)_2 = \frac{A(A-1)}{2} \sum_{\mathbf{k}_i, \mathbf{k}_j} \langle \mathbf{k}_i, \mathbf{k}_j | \, v_{\mathit{eff}}(12) \, | \mathbf{k}_i, \mathbf{k}_j \rangle_a \ , \tag{5.15}$$

where the sum includes all occupied states of the Fermi sea and $|ij\rangle_a$ denotes an anti-symmetrized two-nucleon state, i.e. $|ij\rangle_a = (|ij\rangle - |ji\rangle)/\sqrt{2}$. From Eq. (5.15) one obtains

$$V_{\mathit{eff}} = \sum_{i<j} v_{\mathit{eff}}(ij) = \sum_{i<j} f_{ij} \left[-\frac{1}{m} \left(\nabla^2 f_{ij} \right) - \frac{2}{m} \left(\boldsymbol{\nabla} f_{ij} \right) \cdot \boldsymbol{\nabla} + v(ij) f_{ij} \right] . \qquad (5.16)$$

where the Laplacian and the gradient operate on the relative coordinate. Eq. (5.16) clearly shows that the effective potential V_{eff} takes into account the effect of screening of the bare interaction due to correlations, described by the operators f_{ij}. In the zero-density limit, the above effective interaction reduces to the bare potential. Therefore, it reproduces the available two-nucleon data by construction. We also note that $v_{\mathit{eff}}(ij)$ defined by the above equation exhibits a momentum dependence associated with the operator $(\boldsymbol{\nabla} f_{ij}) \cdot \boldsymbol{\nabla}$, yielding contributions to nuclear matter energy through the exchange terms. However, the results of numerical calculations [3] show that these contributions are small, compared those arising from the momentum independent terms [3], and can be neglected. The resulting static interaction reads

$$v_{\mathit{eff}}(ij) = f_{ij} \left(-\frac{1}{m} \nabla^2 + v(ij) \right) f_{ij} = \sum_n v^n_{\mathit{eff}}(r_{ij}) O^n_{ij} . \qquad (5.17)$$

with the operators O^n with $n = 1, ..., 6$ defined in Eq. (4.19).

The definition of v_{eff} by Eqs. (5.16) and (5.17) obviously neglects the contributions of clusters consisting of more than two nucleons, as well as the effects of three-nucleon interactions, the inclusion of which in the Hamiltonian is known to be needed in order to explain the binding energies of the few-nucleon systems and the saturation properties of nuclear matter (see Chapter 4). To circumvent the latter problem, retaining at the same time the simplicity of the two-body cluster approximation, the authors of Ref. [3] used the approach originally proposed by Lagaris and Pandharipande [48], in which the main effect of the three-body force is simulated through a density dependent modification of the two-nucleon potential at intermediate range, where two-pion exchange is believed to be the dominant interaction mechanism. The correlation functions were determined in such a way as to reproduce the results of the highly accurate results obtained from the FHNC approach. From the methodological point of view, this approach can be seen as an *effective theory*, designed to obtain the exact result from a low-order calculation.

In Figure 5.2, the six static components of the effective interaction of Ref. [3] are compared to the corresponding components of the bare Argonne v'_6 potential. The critical role played by NN correlations in screening the bare interaction at short distance is clearly visible.

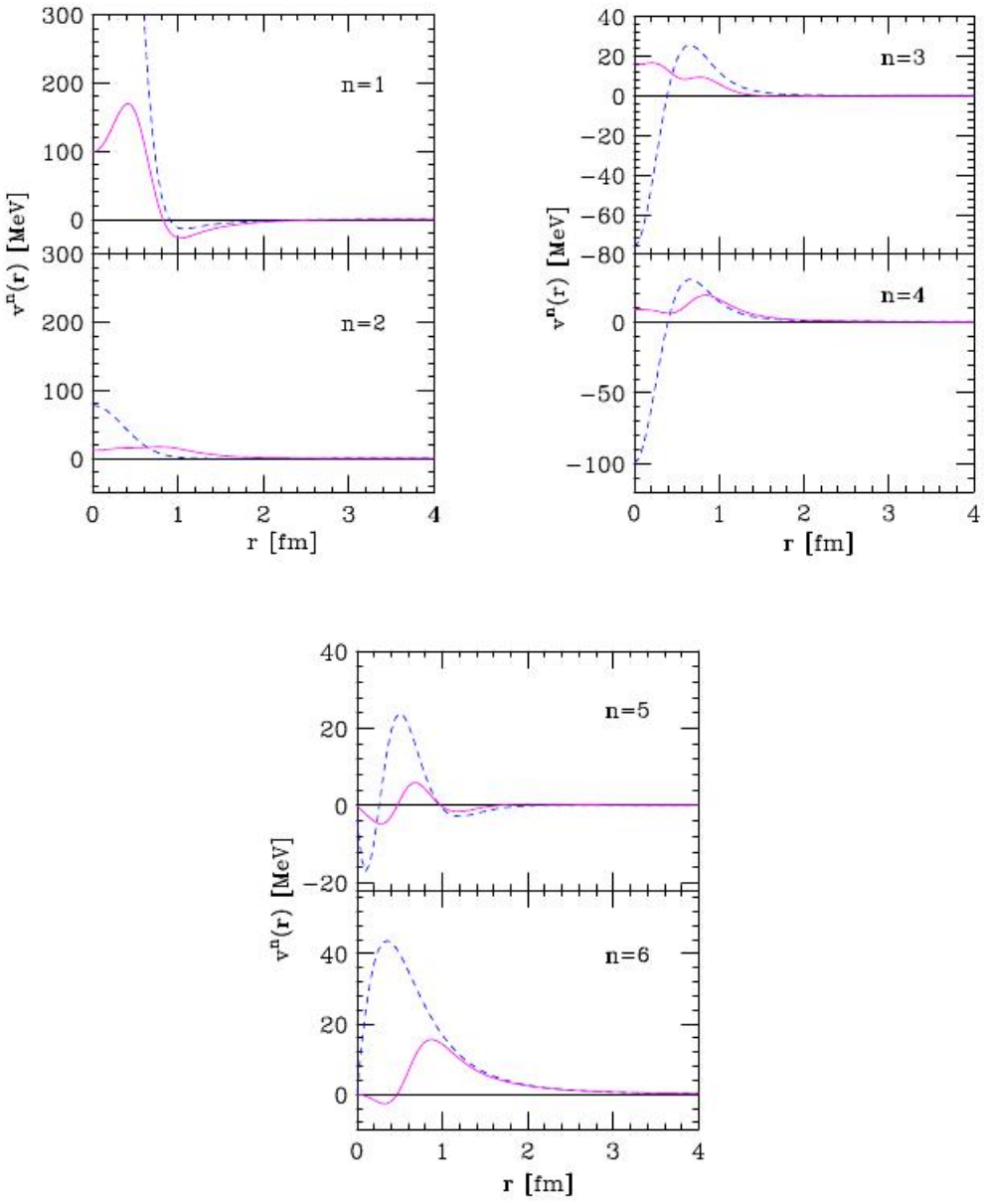

Figure 5.2. Comparison between the components of the bare Argonne v_6' potential (dashed lines) and the effective potential defined by Eq. (5.17) (solid lines), calculated at nuclear matter equilibrium density.

5.3 Binding energy per particle of nucleon matter

The *well behaved* CBF effective interaction discussed in the previous Section can be used to calculate the binding energy per particle of isospin symmetric nuclear matter with arbitrary fractions of spin-up and spin-down protons and neutrons in Hartree-Fock approximation with the FG basis.

Let us consider nuclear matter at density

$$\rho = \sum_{\lambda=1}^{4} \rho_\lambda \tag{5.18}$$

where $\lambda = 1, 2, 3, 4$ labels spin-up protons, spin-down protons, spin-up neutrons and spin-down neutrons, respectively, with the corresponding densities being $\rho_\lambda = x_\lambda \rho$, implying $\sum_\lambda x_\lambda = 1$.

Within our approach, the binding energy per particle of such a system can be obtained from the Hartree-Fock approximation

$$\frac{B}{A} = \frac{3}{5} \sum_\lambda x_\lambda \frac{{p_F^\lambda}^2}{2m} + \frac{\rho}{2} \sum_{\lambda\mu} \sum_n x_\lambda x_\mu \int d^3 r v_{eff}^n \left[A_{\lambda\mu}^n - B_{\lambda\mu}^n \ell\left(p_F^\lambda r\right) \ell\left(p_F^\mu r\right) \right] \ . \tag{5.19}$$

In the above equation, the Fermi momenta are given by $p_F^\lambda = \left(3\pi^2 \rho_\lambda\right)^{1/3}$, while the Slater function ℓ is defined as

$$\ell(p_F^\lambda r) = \frac{1}{N_\lambda} \sum_{|\mathbf{p}| \le \mathbf{p}_F^\lambda} e^{i\mathbf{p}\cdot\mathbf{r}} \ , \tag{5.20}$$

N_λ being the number of particles of type λ. The quantities $A_{\lambda\mu}^n$ and $B_{\lambda\mu}^n$ are the matrix elements of the operators O^n, defined in Eq.(4.19)

$$A_{\lambda\mu}^n = \langle \lambda\mu | \, O^n \, | \lambda\mu \rangle \, , \qquad B_{\lambda\mu}^n = \langle \lambda\mu | \, O^n \, | \mu\lambda \rangle \ , \tag{5.21}$$

where $|\lambda\mu\rangle$ denotes a two-nucleon spin-isospin state. The explicit expressions of these matrix elements are given in Appendix C.

In Fig. 5.3 the results obtained using the effective interaction of Ref. [3] and Eq.(5.19) are compared to those reported in Refs. [49] and [50]. The calculations of Ref. [49] (solid lines) have been carried out using a variational approach based on the FHNC formalism, with an Hamiltonian including the Argonne v_{18} NN potential and the Urbana IX three-body potential [38, 49]. The results of Ref. [50] (dashed line of the lower panel) have been obtained using the Argonne v_8' potential and the same three-body potential within the framework of the Auxiliary Field Diffusion Monte Carlo (AFDMC) approach.

From Fig. 5.3 it clearly appears that the effective interaction provides a fairly reasonable description of the EOS over a broad density range.

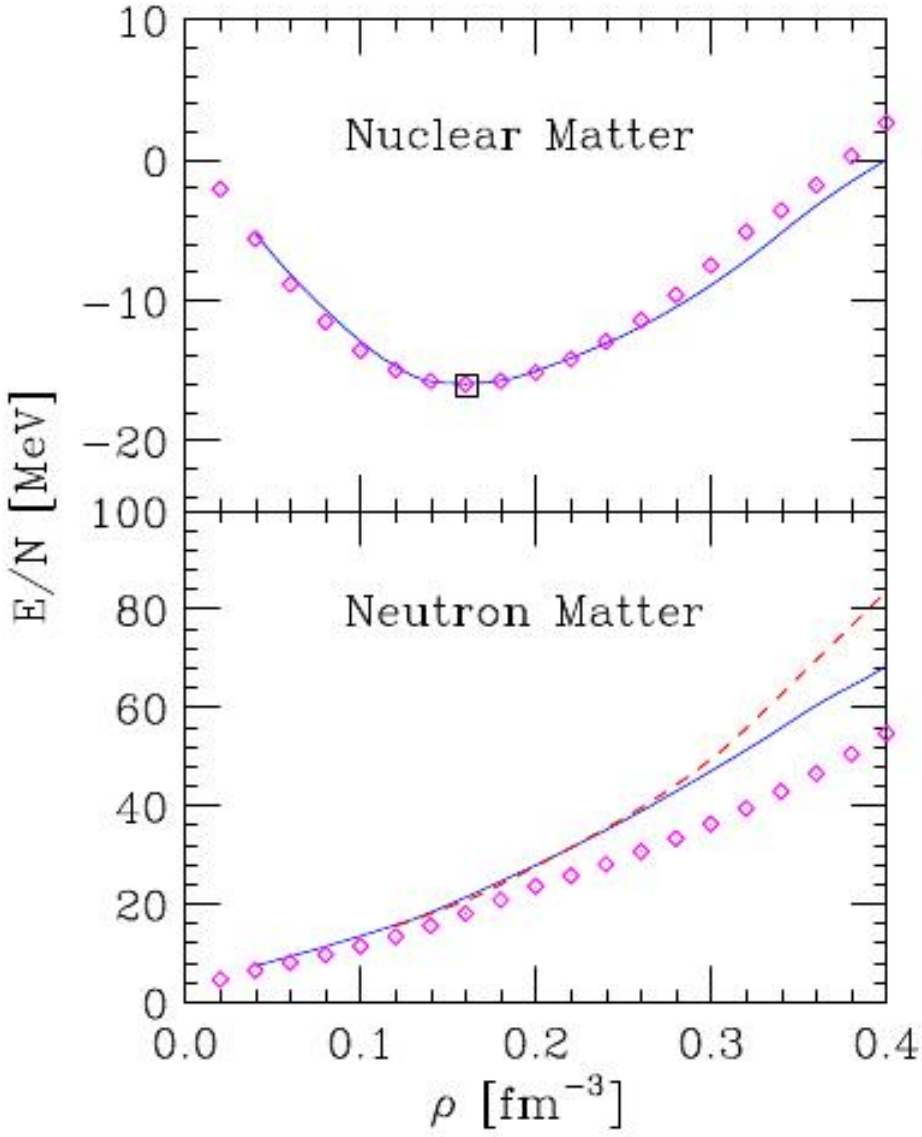

Figure 5.3. Energy per particle of symmetric nuclear matter (SNM, upper panel) and pure neutron matter (PNM, lower panel) as a function of baryon density. The solid line represent the results obtained using Eq.(5.19), whereas the diamonds correspond to the results of Akmal, Pandharipande and Ravenhall [49]. The dashed line of the lower panel shows the results of the AFDMC approach [50]. The square of the upper panel indicates the empirical equilibrium point of SNM.

Chapter 6

Numerical results

In this Chapter we will discuss the results of the numerical calculation of different quantities characterizing the superfluid phase of pure neutron matter, the dynamics of which is modeled using the CBF effective interaction discussed in Chapter 5.

6.1 Neutron-neutron interaction in the $^1S_0$ channel

For any given density, the gap equation corresponding to S-wave coupling has been solved using the procedure outlined in Appendix A. Within the CBF effective interaction approach, the neutron-neutron interaction can be easily projected into the $\ell = 0$ sector. The resulting potential reads

$$v(r) = v^1_{eff}(r) + v^2_{eff}(r) - 3\left[v^3_{eff}(r) + v^4_{eff}(r)\right] \ , \tag{6.1}$$

with the functions $v^n_{eff}(r)$ defined as in Eq. (5.17).

Recent work on the CBF effective interaction has led to the development of improved models, explicitly taking into account three-body cluster contributions and using realistic microscopic models of the three-body force. In this work we have used the effective interaction of Refs. [4, 9], derived from a nuclear Hamiltonian including the Argonne v'_6 NN potential and the Urbana IX three-nucleon potential, discussed in Chapter 4.

6.2 Solution of the gap equation

Figure 6.1 illustrates the shape of the bare (solid line) and effective interactions (dashed line) at baryon density $\rho = 0.025$ fm^{-3} in the $^1S_0$ channel. It clearly appears that, owing to screening arising from nucleon-nucleon correlations, the short ranged repulsive core of the bare interaction is completely washed out. On the scale of Fig. 6.1 the differences between the effective interactions computed with and without inclusion of the three-body force are too small to be visible.

Figure 6.2 shows the momentum-dependence of the function

$$\phi(k) = \frac{\langle k|v|k_F\rangle}{\langle k_F|v|k_F\rangle} \ , \tag{6.2}$$

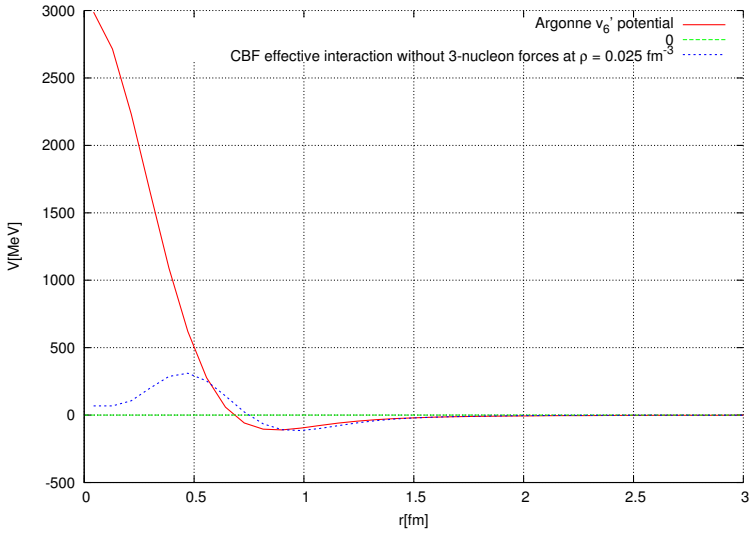

Figure 6.1. Radial dependence of the neutron-neutron potential in the $\ell = 0$ state. The solid line corresponds to the Argonne v_6' potential, while the dashed line show the CBF effective interaction, computed at baryon density $\rho = 0.025$ fm^{-3} without inclusion of three-nucleon forces. The differences between the effective interactions computed with and without inclusion of the three-body force are too small to be visible on the scale of the figure.

as well as of the reduced gap function, obtained at first order of the iterative procedure employed to solve the gap equation

$$\chi(k) = \phi(k) - \frac{1}{\pi} \int \frac{W(k,k')\chi(k')}{\left[\xi^2(k') + \Delta_F^2 \chi^2(k')\right]^{\frac{1}{2}}} k'^2 dk' \ , \tag{6.3}$$

i.e. $\chi^{(1)}$ of Eq.(A.28).

The calculations have been carried out setting $k_F = 0.9$ fm^{-1}, corresponding to baryon density $\rho = 0.025$ fm^{-3} and using both the bare v_6' potential and the CBF effective interactions. In the former case, the single particle spectrum has been assumed to be purely kinetic, setting $U(k) = 0$ in Eq. (A.3), while in the latter $U(k)$ has been consistently computed using the CBF effective interaction and the Hartree-Fock approximation

$$e(k) = \frac{k^2}{2M} + \sum_{\mathbf{k}'} \langle \mathbf{k}\mathbf{k}' | v_{eff} | \mathbf{k}\mathbf{k}' \rangle_a \ . \tag{6.4}$$

The difference between the energies obtained from the above equation and the kinetic energy spectrum is illustrated in Fig. 6.3.

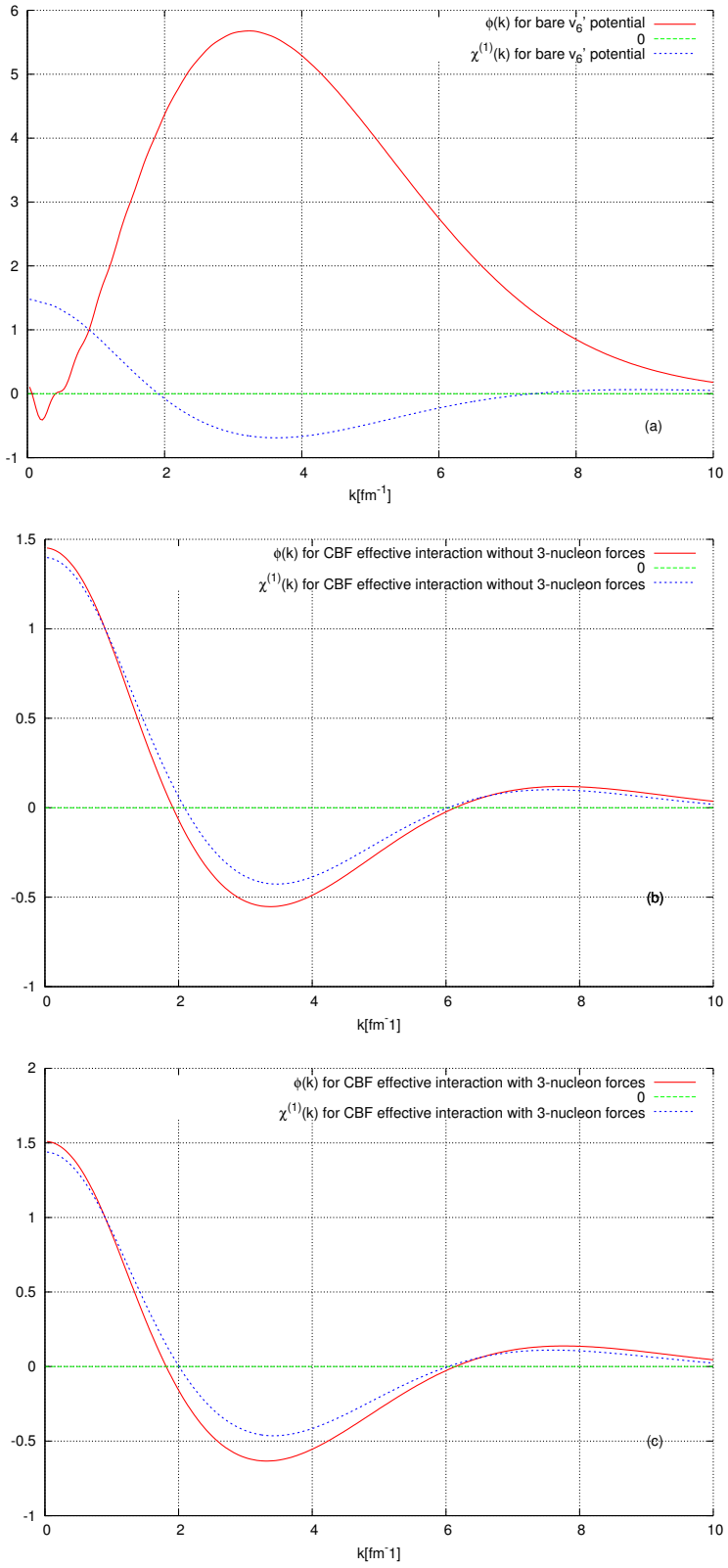

Figure 6.2. Momentum dependence of the functions $\phi(k)$ of Eq.(6.2) and $\chi^{(1)}$ of Eq.(A.28). Panels (a), (b) and (c) show the results obtained using the bare v_6' potential and the CBF effective interaction, without and with inclusion of three-nucleon forces, respectively.

Note that in the case of the effective interaction $v_F = \langle k_F | v_{eff} | k_F \rangle = -21.6$ and -25.3 MeV, with and without inclusion of the three-nucleon force, respectively, while for the bare interaction $v_F = 8.52$ MeV. When the value of v_F at the Fermi surface is negative, the gap integral equation can be trivially solved, as the matrix A_{ij} defined in Appendix A is nearly diagonal and $\chi^{(1)}(k) \approx \phi(k)$. On the other hand, for positive v_F, $\chi^{(1)}(k)$ sizably differs from $\phi(k)$, and solving the gap equation requires the more complex algorithm described in Section A.

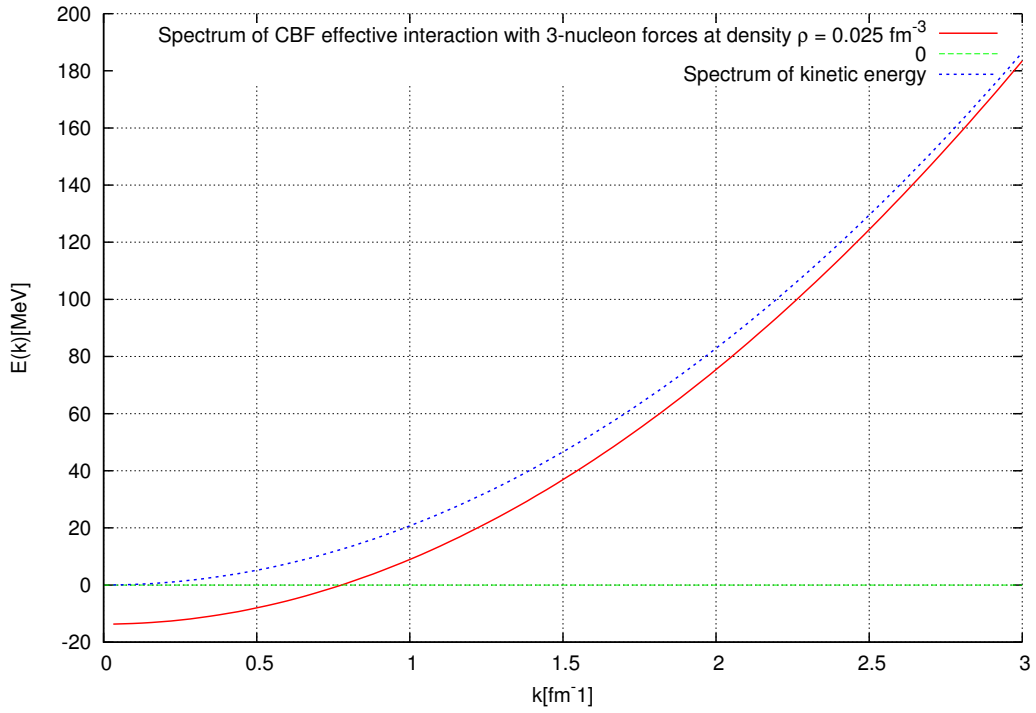

Figure 6.3. Momentum dependence of the quasi-particle energy. The dashed line shows the kinetic energy spectrum, while the solid line has been obtained from Eq. (6.4) using the CBF effective interaction at baryon density $\rho = 0.025$ fm^{-3} and including the UIX three-nucleon potential.

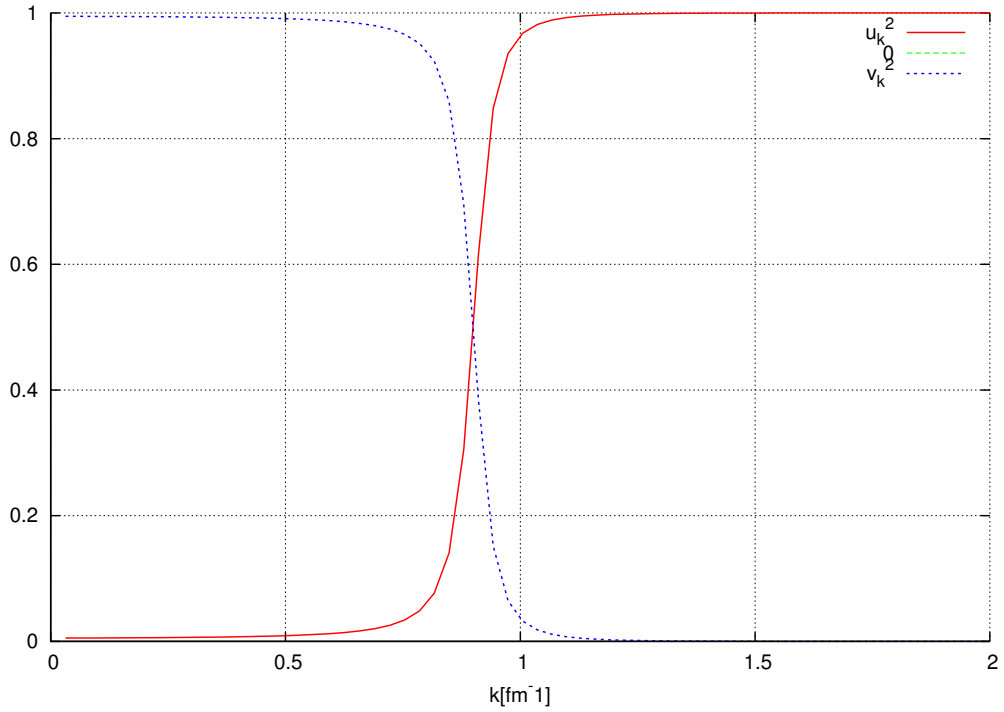

Figure 6.4. Momentum dependence of the BCS wave function parameters u_k^2 and v_k^2, defined in Eq. (3.27). The results have been obtained setting $k_F = 0.9$ fm^{-1} and using the effective interaction including the UIX three-nucleon potential.

Figure 6.4 shows the momentum dependence of the BCS wave function parameters u_k^2 and v_k^2, defined in Eq. (3.27), measuring the mixing of particle and hole character in the quasi-particle state. The results have been obtained setting $k_F = 0.9$ fm^{-1} and using the effective interaction including the UIX three-nucleon potential. Recall that in the normal state $u_k = \theta(k_F - k)$ and $v_k = \theta(k - k_F)$, $\theta(x)$ being the Heaviside step-function.

6.3 Momentum- and density-dependence of the superfluid gap

The superfluid gap at the Fermi surface, $\Delta_F = \Delta(k_F)$ is displayed in Fig. 6.5 as a function of the Fermi momentum, k_F. The dashed line shows the results obtained using the bare v_6' potential and kinetic energy quasi-particle spectrum, while the solid and dot-dashed lines correspond to calculations carried out using the CBF effective interaction, with and without inclusion of the UIX three-nucleon potential, and the Hartree-Fock spectrum of Eq. (6.4).

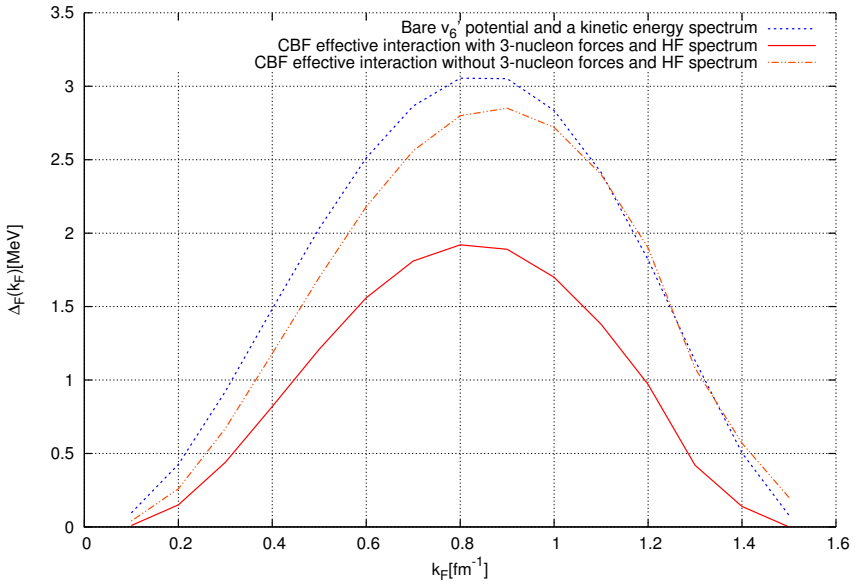

Figure 6.5. Superfluid gap at the Fermi surface, $\Delta_F(k_F)$, as a function of Fermi momentum. The dashed line shows the results obtained using the bare v_6' potential and a kinetic energy quasi-particle spectrum, while the solid and dot-dashed lines correspond to calculations carried out using the effective interaction, with and without inclusion of the UIX three-nucleon potential, and the Hartree-Fock spectrum of Eq. (6.4).

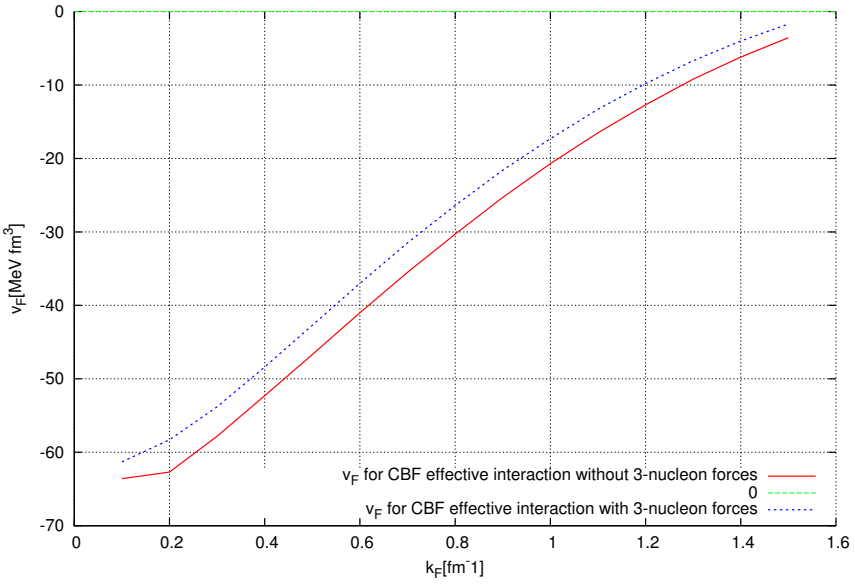

Figure 6.6. Dependence on Fermi momentum of the matrix element $v_F = \langle k_F | v_{eff} | k_F \rangle$. The dashed and solid lines have been obtained from the CBF effective interaction, with and without inclusion of three-nucleon forces, respectively.

It appears that, while the range of Fermi momentum in which $\Delta_F(k_F) \neq 0$ is about the same for the three cases that we have analyzed, the inclusion three-nucleon interactions leads to a sizable reduction of the gap. This is to be ascribed to the effect of the three-nucleon force on the matrix element $\langle \mathbf{k}|v_{eff}|\mathbf{k}'\rangle$ at $|\mathbf{k}| = |\mathbf{k}'| = k_F$, v_F, driving the solution of the gap equation. This feature is illustrated in Fig. 6.6. The momentum dependence of the gap function $\Delta_F(k)$, computed using the CBF effective interaction including three-nucleon forces at $k_F = 0.9$ fm^{-1}, corresponding to the maximum of the solid line of Fig. 6.5 is displayed in Fig. 6.7.

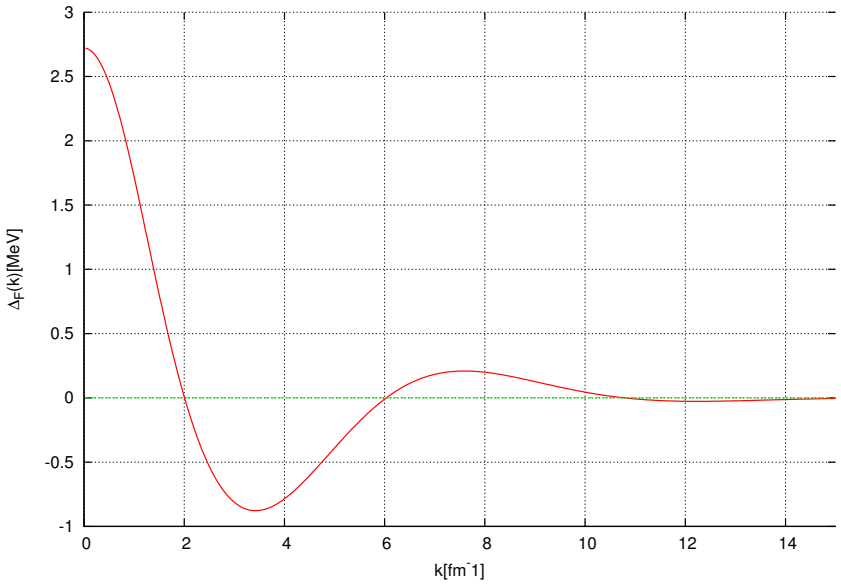

Figure 6.7. Momentum dependence $\Delta_F(k)$ of the gap function at $k_F = 0.9$ fm^{-1}, obtained using the CBF effective interaction including the UIX three-nucleon potential, and the Hartree-Fock spectrum of Eq. (6.4).

The computer codes needed to carry out numerical calculations have been written in FORTRAN language. The typical CPU time required for the solution of the gap equation, involving a Fast Fourier Transform and a matrix inversion, has been of the order of tens of seconds on a personal computer of intermediate level.

Summary and perspectives

We have carried out a calculation of the superfluid gap in pure neutron matter, associated with the formation of Cooper pairs of neutrons in states of total spin $S = 0$ and relative angular momentum $\ell = 0$. The interaction in this channel, which dominates the attractive component of the neutron-neutron force, has been described using an effective interaction derived from the state-of-the-art models of the two- and three-nucleon potentials referred to as Argonne v_6' and Urbana IX, within the formalism based on correlated basis functions.

The main advantage of our approach lies in the fact that, unlike the effective interactions based on the mean field approximation, the CBF effective interaction reduces to the bare interaction in the zero-density limit. As a consequence, it can be used to carry out *consistent* calculations of a number of different properties of neutron star matter, thus allowing for a comprehensive description of equilibrium and non equilibrium properties of neutron star.

Our results show that a superfluid phase develops in the region of low density, $\rho \ll \rho_0$, where $\rho_0 \sim 2.7 \times 10^{14}$ g/cm^3 is the equilibrium density of isospin symmetric nuclear matter. As the maximum of the superfluid gap occurs at density $\rho \sim 0.15\rho_0$, our work is relevant to the description of the neutron gas in the region of the inner crust, extending from $\rho \sim 4 \times 10^{11}$ g/cm^3 to $\rho \sim 2 \times 10^{14}$ g/cm^3.

In the case of $^1S_0$ pairing, the critical temperature of the superfluid transition can be estimated from the value of the gap at $T = 0$, using Eq. (3.88). The resulting maximum values are in the range $1 \leq T_c \leq 2$ MeV, corresponding to $1 \times 10^{10} \leq T_c \leq 2 \times 10^{10}$ K.

Our results, while being interesting in their own right, should be regarded as a first step towards a description of the superfluid and superconductive phases of neutron stars. The interaction between neutrons coupled to total spin $S = 1$ and angular momentum $\ell = 1$ is also attractive. The formation of Cooper pairs of neutrons with these quantum numbers is expected to occur at densities $\rho > \rho_0$ typical of the neutron star outer core. The appearance of a superfluid phase in this region would strongly affect the dissipative processes determining the stability of rotating stars. In addition, the small fraction – typically less that $\sim 10\%$ – of protons are also expected to become superconductive.

The extension of the formalism employed in our work to study neutron superfluidity in the $^3P_2$ channel and proton superconductivity does not involve any conceptual difficulties, and is currently being carried out.

Appendix A

Solution of the gap equation

In this Appendix, we focus on the problem of S-wave pairing in pure, homogeneous neutron matter and, in particular, on the solution of the energy gap equation.

The starting point is the gap equation (3.77), which we rewrite in the form

$$\Delta(k) = -\frac{1}{\pi}\int \frac{v(k,k')\Delta(k')}{[\xi^2(k') + \Delta^2(k')]^{\frac{1}{2}}} k'^2 dk' \tag{A.1}$$

with

$$\xi^2(k) = [e(k) - \mu]^2 \tag{A.2}$$

where, in general, the single-particle energy $e(k)$ can be written as

$$e(k) = \frac{k^2}{2M} + U(k) \ , \tag{A.3}$$

and the chemical potential is the Fermi energy

$$\mu = e(k_F) \ . \tag{A.4}$$

The momentum space matrix elements of the potential $v(x)$, describing neutron-neutron interactions in the $^1S_0$ channel, read

$$v(k,k') = \int dx x^2 j_0(kx) v(x) j_0(k'x) \ , \tag{A.5}$$

the Bessel spherical Bessel function being defined as

$$j_0(kx) = \frac{\sin(kx)}{kx} \ . \tag{A.6}$$

We assume that $v(k,k')$ has no zeros on the Fermi surface, i.e.

$$v_F = v(k_F, k_F) \neq 0 \ . \tag{A.7}$$

The key step of the algorithm employed to solve Eq. (A.1) is a decomposition of $v(k,k')$ into a separable part and a remainder $W(k,k')$ that vanishes when either

argument is on the Fermi surface

$$v(k,k') = v_F\phi(k)\phi(k') + W(k,k') \ . \tag{A.8}$$

It follows that

$$v(k,k_F) = v_F\phi(k)\phi(k_F) + W(k,k_F) \ . \tag{A.9}$$

The above equation is satisfied by

$$\phi(k) = \frac{v(k,k_F)}{v_F} \tag{A.10}$$

with the required conditions

$$W(k,k_F) = W(k_F,k') = 0 \qquad \forall\, k,k' \ . \tag{A.11}$$

In addition, we easily find that

$$\phi(k_F) = 1 \ . \tag{A.12}$$

Using Eq. (A.8) and the definition (A.10), we obtain

$$W(k,k') = v(k,k') - v_F\frac{v(k,k_F)v(k',k_F)}{v_F^2} \ . \tag{A.13}$$

The gap Eq. (A.1) can be cast in the form

$$\begin{aligned}\Delta(k) = &-\frac{1}{\pi}v_F\phi(k)\int\frac{\phi(k')\Delta(k')}{\left[\xi^2(k')+\Delta^2(k')\right]^{\frac{1}{2}}}k'^2dk' \\ &-\frac{1}{\pi}\int\frac{W(k,k')\Delta(k')}{\left[\xi^2(k')+\Delta^2(k')\right]^{\frac{1}{2}}}k'^2dk' \ ,\end{aligned} \tag{A.14}$$

which can be in turn rewritten in terms of the dimensionless gap function (or shape function), defined as

$$\chi(k) = \frac{\Delta(k)}{\Delta(k_F)} = \frac{\Delta(k)}{\Delta_F} \ , \tag{A.15}$$

implying

$$\chi(k_F) = 1 \ . \tag{A.16}$$

The result is

$$\begin{aligned}\chi(k) = &-\frac{1}{\pi}v_F\phi(k)\int\frac{\phi(k')\chi(k')}{\left[\xi^2(k')+\Delta_F^2\chi^2(k')\right]^{\frac{1}{2}}}k'^2dk' \\ &-\frac{1}{\pi}\int\frac{W(k,k')\chi(k')}{\left[\xi^2(k')+\Delta_F^2\chi^2(k')\right]^{\frac{1}{2}}}k'^2dk' \ .\end{aligned} \tag{A.17}$$

Setting $k = k_F$ in the last equation we obtain

$$\chi(k_F) = -\frac{1}{\pi}v_F\phi(k_F)\int\frac{\phi(k')\chi(k')}{\left[\xi^2(k')+\Delta_F^2\chi^2(k')\right]^{\frac{1}{2}}}k'^2dk' = 1 \ , \tag{A.18}$$

leading to

$$-\frac{1}{\pi}v_F\int\frac{\phi(k')\chi(k')}{\left[\xi^2(k')+\Delta_F^2\chi^2(k')\right]^{\frac{1}{2}}}k'^2dk'=1\ . \tag{A.19}$$

Substituting Eq. (A.19) into the gap equation, (A.17), we finally find the integral equation

$$\chi(k)=\phi(k)-\frac{1}{\pi}\int\frac{W(k,k')\chi(k')}{\left[\xi^2(k')+\Delta_F^2\chi^2(k')\right]^{\frac{1}{2}}}k'^2dk'\ . \tag{A.20}$$

The main advantage of the transformation (A.8) is that for $k\to k_F$, the integrand in Eq. (A.20) vanishes and the problem of dealing with a near-singular behaviour is circumvented. The resulting integral turns out to be largely insensitive to any reasonable variations of $\Delta(k')=\Delta_F\chi(k')$ in the denominator. In other words, the shape function $\chi(k)$ is practically independent of $\Delta(k')$. For specified Δ_F, Eq. (A.20) is an integral equation with non-singular kernel, actually a "quasilinear" integral equation, because the non-linearity induced by the presence of $\chi(k')$ in the square root is largely irrelevant.

Equation (A.19) is a non-linear algebraic equation. For both formal and computational purposes, it is advantageous to rewrite it in the form

$$1+\frac{v_F}{\pi}\int\frac{\phi^2(k)}{\left[\xi^2(k)+\Delta_F^2\chi^2(k)\right]^{\frac{1}{2}}}k^2dk-\frac{v_F}{\pi}\int\phi(k)\frac{[\phi(k)-\chi(k)]}{\left[\xi^2(k)+\Delta_F^2\chi^2(k)\right]^{\frac{1}{2}}}k^2dk=0\ , \tag{A.21}$$

observing that the identity $\chi(k_F)=\phi(k_F)=1$ makes the second integral of the left hand side almost independent of the behaviour of $\Delta(k)$, and hence of Δ_F.

Thus, the original gap equation (A.1) has been replaced, without approximations, by the two equivalent equations

$$\begin{cases}-\frac{1}{\pi}v_F\int\frac{\phi(k')\chi(k')}{\left[\xi^2(k')+\Delta_F^2\chi^2(k')\right]^{\frac{1}{2}}}k'^2dk'=1\\ \chi(k)=\phi(k)-\frac{1}{\pi}\int\frac{W(k,k')\chi(k')}{\left[\xi^2(k')+\Delta_F^2\chi^2(k')\right]^{\frac{1}{2}}}k'^2dk'\ .\end{cases} \tag{A.22}$$

This system of equations can be solved iteratively using matrix inversion. The iteration scheme for the determination of the gap function $\Delta(k)=\Delta_F\chi(k)$ is suggested by the extremely weak dependence of the function $\chi(k)$ on the behaviour of the gap. Let us consider discrete momentum values k_i $(i=1,...,N)$ with $k_{i+1}-k_i=h$ and denote

$$\chi(k_i)=\chi_i,\qquad \phi(k_i)=\phi_i,\qquad W(k_i,k_j)=W_{ij}.... \tag{A.23}$$

The iteration scheme involves the following steps:

- Replace the quantity $\Delta_F\chi(k)$ in the denominator of the integrand in Eq. (A.20) by a very small constant scaling factor Δ_0

$$\Delta_F\chi(k)\to\Delta_0\ , \tag{A.24}$$

so that the equation can be rewritten in the form

$$\chi_i^{(1)} = \phi_i - \frac{1}{\pi}\sum_j \frac{W_{ij}\chi_j^{(1)}}{\left[\xi_j^2 + \Delta_0^2\right]^{\frac{1}{2}}} k_j^2 h = \phi_j - \sum_j A_{ij}^{(0)}\chi_j^{(1)} \ , \tag{A.25}$$

where

$$A_{ij}^{(0)} = \frac{1}{\pi}\frac{W_{ij}}{\left[\xi_j^2 + \Delta_0^2\right]^{\frac{1}{2}}} k_j^2 h \ . \tag{A.26}$$

In matrix form

$$\chi^{(1)} = \phi - A^{(0)}\chi^{(1)} \ , \tag{A.27}$$

yielding

$$\chi^{(1)} = \left[\mathbb{1} + A^{(0)}\right]^{-1}\phi \ . \tag{A.28}$$

Solving the above equation we obtain a first approximation to the shape function $\chi(k)$.

- Substitute $\chi^{(1)}(k)$ into Eq. (A.19) and solve the resulting non-linear algebraic equation, to obtain a first approximation $\Delta_F^{(1)}$ for the scaling factor Δ_F.

- Repeat the first step with $\Delta_F^{(1)}\chi^{(1)}(k)$ as input for $\Delta_F\chi(k)$ in the integral term and update the matrix A

$$A_{ij}^{(1)} = \frac{1}{\pi}\frac{W_{ij}}{\left[\xi_j^2 + \left(\Delta_F^{(1)}\chi_j^{(1)}\right)^2\right]^{\frac{1}{2}}} k_j^2 h \ , \tag{A.29}$$

which is needed to generate a second approximation to $\chi(k)$, $\chi^{(2)}(k)$

$$\chi^{(2)} = \left[\mathbb{1} + A^{(1)}\right]^{-1}\phi \ . \tag{A.30}$$

- Repeat the second step in order to get a second approximation to Δ_F, $\Delta_F^{(2)}$. The iterative procedure is carried out until the convergence test

$$|\Delta_F^{(n)} - \Delta_F^{(n-1)}| < \epsilon \tag{A.31}$$

where ϵ is a small number, is passed,

In actual calculations with realistic neutron-neutron interactions the convergence of this algorithm is so rapid that accurate results for $\chi(k)$ and Δ_F are already achieved in the first iteration cycle [51].

Appendix B

Derivation of the one-pion-exchange potential

In this Appendix, we will discuss the calculation of nucleon-nucleon scattering amplitude in the non-relativistic approximation and we will determine an analytical expression for the interaction potential.

B.1 One-pion exchange scattering between two nucleons

We consider the process illustrated in Fig. B.1.

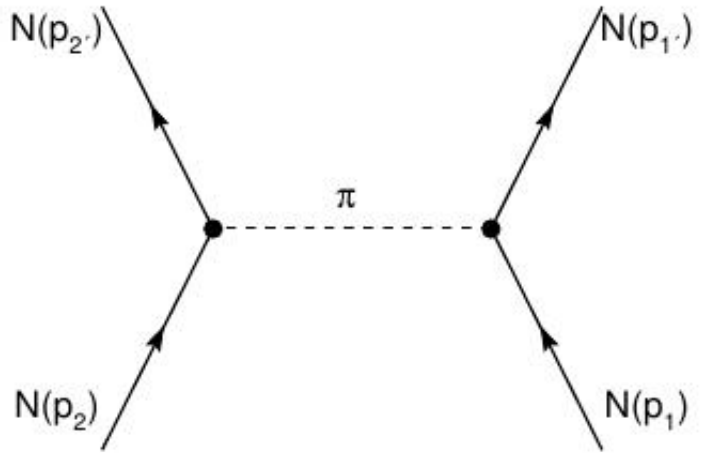

Figure B.1. Feynman diagram describing the one-pion-exchange process between two nucleons. The corresponding amplitude is given by Eq.(4.13).

The corresponding matrix element is

$$\begin{aligned} S_{fi} &= (-ig)^2 \frac{m^2}{(E_1 E_2 E_{1'} E_{2'})^{1/2}} (2\pi)^4 \delta^{(4)}(p_1 + p_2 - p_{1'} - p_{2'}) \\ &\times \eta^\dagger_{1'} \boldsymbol{\tau} \eta_1 \bar{u}_{1'} i\gamma_5 u_1 \frac{i}{k^2 - m_\pi^2} \eta^\dagger_{2'} \boldsymbol{\tau} \eta_2 \bar{u}_{2'} i\gamma_5 u_2 \ , \end{aligned} \tag{B.1}$$

where m_π is the pion mass, $k = p_2 - p_{2'}$ and η_i indicates the two components of Pauli spinor, which describes the isospin state of i-particle.
Introducing $\langle \boldsymbol{\tau}_1 \cdot \boldsymbol{\tau}_2 \rangle = \eta^\dagger_{1'} \boldsymbol{\tau} \eta_1 \eta^\dagger_{2'} \boldsymbol{\tau} \eta_2$, the Eq.(B.1) can be rewritten in the more comfortable form

$$\begin{aligned} S_{fi} &= (-ig)^2 \frac{m^2}{(E_1 E_2 E_{1'} E_{2'})^{1/2}} (2\pi)^4 \delta^{(4)}(p_1 + p_2 - p_{1'} - p_{2'}) \\ &\times \langle \boldsymbol{\tau}_1 \cdot \boldsymbol{\tau}_2 \rangle \bar{u}_{2'} \gamma_5 u_2 \bar{u}_{1'} \gamma_5 u_1 \frac{1}{k^2 - m_\pi^2} \ . \end{aligned} \tag{B.2}$$

We take into account the non-relativistic approximation

$$\begin{aligned} \bar{u}_{2'} \gamma_5 u_2 &= \frac{(E_{2'} + m)^{1/2} (E_2 + m)^{1/2}}{2m} \left[\chi^\dagger_{s'} \frac{\boldsymbol{\sigma} \cdot \mathbf{p}_2}{E_2 + m} \chi_s - \chi^\dagger_{s'} \frac{\boldsymbol{\sigma} \cdot \mathbf{p}_{2'}}{E_{2'} + m} \chi_s \right] \\ &\approx \chi^\dagger_{s'} \frac{\boldsymbol{\sigma} \cdot (\mathbf{p}_2 - \mathbf{p}_{2'})}{2m} \chi_s = \chi^\dagger_{s'} \frac{\boldsymbol{\sigma} \cdot \mathbf{k}}{2m} \chi_s \ , \end{aligned} \tag{B.3}$$

and an analogous expression is available for $\bar{u}_{1'} \gamma_5 u_1$. Always in the non-relativistic limit we can set $E_i \approx E_{i'} \approx m_\pi$ from which $k^2 = (E_i - E_{i'})^2 - |\mathbf{k}|^2 \approx -|\mathbf{k}|^2$, therefore we obtain

$$\frac{1}{k^2 - m_\pi^2} \approx -\frac{1}{|\mathbf{k}|^2 + m_\pi^2} \ . \tag{B.4}$$

Substituting in the matrix element S_{fi}, we have

$$\begin{aligned} S_{fi} &\approx -i \frac{g^2}{4m^2} (2\pi)^4 \delta^{(4)}(p_1 + p_2 - p_{1'} - p_{2'}) \langle \boldsymbol{\tau}_1 \cdot \boldsymbol{\tau}_2 \rangle \\ &\times \chi^\dagger_{1'} \chi^\dagger_{2'} \frac{(\boldsymbol{\sigma}_1 \cdot \mathbf{k})(\boldsymbol{\sigma}_2 \cdot \mathbf{k})}{|\mathbf{k}|^2 + m_\pi^2} \chi_2 \chi_1 \ . \end{aligned} \tag{B.5}$$

The corresponding potential in momentum space is

$$\begin{aligned} v^\pi(\mathbf{k}) &= -\frac{g^2}{4m^2} \frac{(\boldsymbol{\sigma}_1 \cdot \mathbf{k})(\boldsymbol{\sigma}_2 \cdot \mathbf{k})}{|\mathbf{k}|^2 + m_\pi^2} \boldsymbol{\tau}_1 \cdot \boldsymbol{\tau}_2 \\ &= \left(\frac{f_\pi}{m_\pi} \right)^2 \frac{(\boldsymbol{\sigma}_1 \cdot \mathbf{k})(\boldsymbol{\sigma}_2 \cdot \mathbf{k})}{|\mathbf{k}|^2 + m_\pi^2} \boldsymbol{\tau}_1 \cdot \boldsymbol{\tau}_2 \ . \end{aligned} \tag{B.6}$$

In order to obtain the potential expressed in coordinate space $v^\pi(\mathbf{r})$, we have to

carry out the Fourier transform

$$\begin{aligned} v^{\pi}(\mathbf{r}) &= -\frac{f_\pi^2}{m_\pi^2}\int \frac{d^3k}{(2\pi)^3}\boldsymbol{\tau}_1\cdot\boldsymbol{\tau}_2\boldsymbol{\sigma}_1\cdot\mathbf{k}\boldsymbol{\sigma}_2\cdot\mathbf{k}\frac{1}{(|\mathbf{k}|^2+m_\pi^2)}e^{-i\mathbf{k}\cdot\mathbf{r}} \\ &= \frac{f_\pi^2}{m_\pi^2}\boldsymbol{\tau}_1\cdot\boldsymbol{\tau}_2\boldsymbol{\sigma}_1\cdot\boldsymbol{\nabla}\boldsymbol{\sigma}_2\cdot\boldsymbol{\nabla}\int \frac{d^3k}{(2\pi)^3}\frac{1}{(|\mathbf{k}|^2+m_\pi^2)}e^{-i\mathbf{k}\cdot\mathbf{r}} \\ &= \frac{1}{4\pi}\frac{f_\pi^2}{m_\pi^2}\boldsymbol{\tau}_1\cdot\boldsymbol{\tau}_2\boldsymbol{\sigma}_1\cdot\boldsymbol{\nabla}\boldsymbol{\sigma}_2\cdot\boldsymbol{\nabla}y_\pi(r)\ , \end{aligned} \tag{B.7}$$

where we have introduced the *Yukawa function* defined as

$$y_\pi(r) = \frac{e^{-m_\pi r}}{r} = 4\pi\int\frac{d^3k}{(2\pi)^3}\frac{1}{(|\mathbf{k}|^2+m_\pi^2)}e^{-i\mathbf{k}\cdot\mathbf{r}}\ .$$

The Laplacian of Yukawa function can be calculated exploiting the relation

$$(-\nabla^2+m_\pi^2)y_\pi(r) = 4\pi\delta(\mathbf{r})\ , \tag{B.8}$$

therefore, it implies the introduction of a singularity in the origin through the Dirac δ-function. The gradients in Eq. (B.7) must be calculated considering this singularity, thus we rewrite

$$\boldsymbol{\sigma}_1\cdot\boldsymbol{\nabla}\boldsymbol{\sigma}_2\cdot\boldsymbol{\nabla}y_\pi(r) = \left(\boldsymbol{\sigma}_1\cdot\boldsymbol{\nabla}\boldsymbol{\sigma}_2\cdot\boldsymbol{\nabla}-\frac{1}{3}\boldsymbol{\sigma}_1\cdot\boldsymbol{\sigma}_2\nabla^2\right)y_\pi(r)+\frac{1}{3}\boldsymbol{\sigma}_1\cdot\boldsymbol{\sigma}_2\nabla^2y_\pi(r)\ , \tag{B.9}$$

where, in the first addend of the term on the right, the singularity has been removed. Taking into account

$$\partial_x^2\left(\frac{e^{-\alpha x}}{x}\right) = \alpha^2\frac{e^{-\alpha x}}{x}+\frac{3\alpha}{x}\frac{e^{-\alpha x}}{x}+\frac{3}{x^2}\frac{e^{-\alpha x}}{x}\ , \tag{B.10}$$

the first addend of Eq.(B.9) becomes

$$\begin{aligned} &\left(\boldsymbol{\sigma}_1\cdot\boldsymbol{\nabla}\boldsymbol{\sigma}_2\cdot\boldsymbol{\nabla}-\frac{1}{3}\boldsymbol{\sigma}_1\cdot\boldsymbol{\sigma}_2\nabla^2\right)y_\pi(r) \\ &= \left(\boldsymbol{\sigma}_1\cdot\hat{\mathbf{r}}\boldsymbol{\sigma}_2\cdot\hat{\mathbf{r}}-\frac{1}{3}\boldsymbol{\sigma}_1\cdot\boldsymbol{\sigma}_2\right)\left(m_\pi^2+\frac{3m_\pi}{r}+\frac{3}{r^2}\right)y_\pi(r)\ , \end{aligned} \tag{B.11}$$

where $\hat{\mathbf{r}} = \mathbf{r}/r$. The second term of Eq.(B.9), exploiting Eq.(B.8), can be rewritten as

$$\frac{1}{3}\boldsymbol{\sigma}_1\cdot\boldsymbol{\sigma}_2\nabla^2y_\pi(r) = \frac{1}{3}(\boldsymbol{\sigma}_1\cdot\boldsymbol{\sigma}_2)(m_\pi^2y_\pi(r)-4\pi\delta(\mathbf{r}))\ . \tag{B.12}$$

Including all the above terms in the potential (B.7), we finally achieve

$$v^{\pi}(\mathbf{r}) = \frac{1}{3}\frac{1}{4\pi}\frac{f_\pi^2}{m_\pi^2}(\boldsymbol{\tau}_1\cdot\boldsymbol{\tau}_2)\left[S_{12}m_\pi^2\left(1+\frac{1}{rm_\pi}+\frac{3}{r^2m_\pi^2}\right)y_\pi(r)+(m_\pi^2y_\pi(r)-4\pi\delta(\mathbf{r}))\boldsymbol{\sigma}_1\cdot\boldsymbol{\sigma}_2\right]\ , \tag{B.13}$$

which is the same of Eq.(4.15).

Appendix C

Properties of the operators O^n_{ij}

In this Appendix, we discuss the properties of the six operators defined in Eq.(4.19), as well as some useful properties of the Pauli matrices.

C.1 Pauli matrices

In the standard representation, in which σ^3 is chosen to be diagonal, the three Pauli matrices are given by (we specialize here to the spin matrices σ^i: similar properties obviously hold for the isospin matrices τ^i)

$$\sigma^1 = \begin{pmatrix} 0 & 1 \\ 1 & 0 \end{pmatrix}, \quad \sigma^2 = \begin{pmatrix} 0 & -i \\ i & 0 \end{pmatrix}, \quad \sigma^3 = \begin{pmatrix} 1 & 0 \\ 0 & -1 \end{pmatrix} . \tag{C.1}$$

The Pauli matrices satisfy the following properties

$$\sigma^i \sigma^j = \delta_{ij} + i\epsilon_{ijk}\sigma^k , \tag{C.2}$$

$$\epsilon_{ijk}\sigma^j\sigma^k = 2i\sigma^i , \tag{C.3}$$

that can put in the form

$$[\sigma^i, \sigma^j] = 2i\epsilon_{ijk}\sigma^k , \tag{C.4}$$

$$\{\sigma^i, \sigma^j\} = 2\delta_{ij} , \tag{C.5}$$

where ϵ_{ijk} is the totally antisymmetric tensor and i, j, k = 1,2,3. The Eq.(C.4) shows that the Pauli matrices are the generators of an $SU(2)$ algebra.

C.2 Projection operators

Let now $\boldsymbol{\sigma}_1$ and $\boldsymbol{\sigma}_2$ be the vectors of Pauli matrices for particle 1 and 2, respectively (i.e. $\boldsymbol{\sigma}_1 \equiv \{\sigma_1^1, \sigma_1^2, \sigma_1^3\}$). From the properties (C.2)-(C.3), it follows that

$$(\boldsymbol{\sigma}_1 \cdot \boldsymbol{\sigma}_2)^2 = 3 - 2(\boldsymbol{\sigma}_1 \cdot \boldsymbol{\sigma}_2) . \tag{C.6}$$

As $(\boldsymbol{\sigma}_1 \cdot \boldsymbol{\sigma}_2)$ is a scalar quantity, we can interpret the above equation as an algebraic one, with solutions $(\boldsymbol{\sigma}_1 \cdot \boldsymbol{\sigma}_2) = -3$ and $(\boldsymbol{\sigma}_1 \cdot \boldsymbol{\sigma}_2) = 1$. They correspond to the values

of operator $(\boldsymbol{\sigma}_1 \cdot \boldsymbol{\sigma}_2)$ of states of total spin $S = 0$ (spin singlet channel) and $S = 1$ (spin triplet channel), respectively. Thus, it is useful introducing the operators P_{2S+1} (and the analogous Π_{2T+1} for the isospin states), defined as

$$P_{(S=0)} \equiv P_1 = \frac{1 - (\boldsymbol{\sigma}_1 \cdot \boldsymbol{\sigma}_2)}{4} \ , \tag{C.7}$$

$$P_{(S=1)} \equiv P_3 = \frac{3 + (\boldsymbol{\sigma}_1 \cdot \boldsymbol{\sigma}_2)}{4} \ , \tag{C.8}$$

which project onto states of definite total spin 0 or 1, respectively

$$P_{2S+1} \, |S'\rangle = \delta_{SS'} \, |S'\rangle \ . \tag{C.9}$$

The projection operator P_{2S+1} (and its analogous Π_{2T+1}) satisfies all natural properties typical of projection operators:

$$P^2_{2S+1} = P_{2S+1} \ , \tag{C.10}$$

$$P_1 + P_3 = \mathbb{1} \ , \tag{C.11}$$

$$P_1 P_3 = P_3 P_1 = 0 \ , \tag{C.12}$$

where $\mathbb{1}$ is the two-dimensional identity matrix.

C.3 Spin, isospin and exchange operators

Consider the two-nucleon spin states (or the analogous isospin states)

$$\begin{aligned} |00\rangle &= \frac{1}{\sqrt{2}}(|\uparrow\downarrow\rangle - |\downarrow\uparrow\rangle) \ , \\ |1-1\rangle &= |\downarrow\downarrow\rangle \ , \\ |10\rangle &= \frac{1}{\sqrt{2}}(|\uparrow\downarrow\rangle + |\downarrow\uparrow\rangle) \ , \\ |11\rangle &= |\uparrow\uparrow\rangle \ , \end{aligned}$$

where the notation is $|00\rangle \equiv |S = 0, M_S = 0\rangle$ etc., and the inverse relations

$$\begin{aligned} |\uparrow\uparrow\rangle &= |11\rangle \ , \\ |\uparrow\downarrow\rangle &= \frac{1}{\sqrt{2}}(|10\rangle + |00\rangle) \ , \\ |\downarrow\uparrow\rangle &= \frac{1}{\sqrt{2}}(|10\rangle - |00\rangle) \ , \\ |\downarrow\downarrow\rangle &= |1-1\rangle \ . \end{aligned}$$

From property (C.9) and from

$$\begin{aligned} (P_3 - P_1) \, |\uparrow\uparrow\rangle &= |\uparrow\uparrow\rangle \, , \qquad (P_3 - P_1) \, |\downarrow\downarrow\rangle = |\downarrow\downarrow\rangle \ , \\ (P_3 - P_1) \, |\uparrow\downarrow\rangle &= |\downarrow\uparrow\rangle \, , \qquad (P_3 - P_1) \, |\downarrow\uparrow\rangle = |\uparrow\downarrow\rangle \ , \end{aligned}$$

it follows that $P_\sigma \equiv P_3 - P_1$ is the spin-exchange operator, which satisfies

$$P_\sigma \left|SM_S\right\rangle = (-)^{S+1} \left|SM_S\right\rangle \ , \tag{C.13}$$

from which it follows that spin singlet states is antisymmetric under exchange, while spin triplet states are symmetric. A similar exchange operator can be defined for isospin, $P_\tau \equiv \Pi_3 - \Pi_1$, with

$$P_\tau \left|TM_T\right\rangle = (-)^{T+1} \left|TM_T\right\rangle \ . \tag{C.14}$$

Combining the above results we find

$$P_{\sigma\tau} \equiv P_\sigma P_\tau = \frac{1}{4}\left(1 + (\boldsymbol{\sigma}_1 \cdot \boldsymbol{\sigma}_2)\right)\left(1 + (\boldsymbol{\tau}_1 \cdot \boldsymbol{\tau}_2)\right) \ , \tag{C.15}$$

with

$$P_{\sigma\tau} \left|SM_S, TM_T\right\rangle = (-)^{S+T} \left|SM_S, TM_T\right\rangle \ . \tag{C.16}$$

The above equation tells us that, in order to obtain a total antisymmetric state under exchange of particles, the sum of total spin and isospin of pairs, $S + T$, must be odd.

C.4 The tensor operator S_{12}

The tensor operator S_{12} is defined as

$$S_{12} \equiv \frac{3}{r^2}(\boldsymbol{\sigma}_1 \cdot \mathbf{r})(\boldsymbol{\sigma}_2 \cdot \mathbf{r}) - (\boldsymbol{\sigma}_1 \cdot \boldsymbol{\sigma}_2) \ , \tag{C.17}$$

where $\mathbf{r}$ is the relative coordinate of particles 1 and 2 while $r = |\mathbf{r}|$.

Making use of Eq.(C.2), it can be shown that

$$S_{12}(\boldsymbol{\sigma}_1 \cdot \boldsymbol{\sigma}_2) = (\boldsymbol{\sigma}_1 \cdot \boldsymbol{\sigma}_2)S_{12} = S_{12} \ . \tag{C.18}$$

As we have already discussed, $(\boldsymbol{\sigma}_1 \cdot \boldsymbol{\sigma}_2) = 1$ on triplet states, while $(\boldsymbol{\sigma}_1 \cdot \boldsymbol{\sigma}_2) = -3$ on singlet states. Thus, the above equation implies that the tensor operator only acts on triplet states, therefore

$$[S_{12}, P_3] = 0 \ . \tag{C.19}$$

Moreover, from the definition (C.17), we find

$$S_{12}^2 = 6 - 2S_{12} + 2(\boldsymbol{\sigma}_1 \cdot \boldsymbol{\sigma}_2) \ . \tag{C.20}$$

The tensor operator S_{12} is a function of $\mathbf{r}$, whose gradient and Laplacian are

$$\boldsymbol{\nabla} S_{12} = \frac{3}{r^2}\left[\boldsymbol{\sigma}_1(\boldsymbol{\sigma}_2 \cdot \mathbf{r}) + \boldsymbol{\sigma}_2(\boldsymbol{\sigma}_1 \cdot \mathbf{r}) - 2\frac{\mathbf{r}}{r^2}(\boldsymbol{\sigma}_1 \cdot \mathbf{r})(\boldsymbol{\sigma}_2 \cdot \mathbf{r})\right] \ , \tag{C.21}$$

$$\nabla^2 S_{12} = -\frac{6}{r^2} S_{12} \ . \tag{C.22}$$

For any function $u(r)$, Eq. (C.21) implies

$$(\boldsymbol{\nabla} u)\cdot(\boldsymbol{\nabla} S_{12}) = \frac{du}{dr}\frac{\mathbf{r}}{r}\cdot(\boldsymbol{\nabla} S_{12}) = 0 \ . \tag{C.23}$$

Moreover, from Eq.(C.21) and (C.22)

$$(\boldsymbol{\nabla} S_{12})^2 = \frac{6}{r^2}(8 - S_{12}) \ , \tag{C.24}$$

$$[S_{12}, (\boldsymbol{\nabla} S_{12})] = \frac{36}{r^2} i(\mathbf{S}\times\mathbf{r}) \ , \tag{C.25}$$

$$[S_{12}, (\boldsymbol{\nabla} S_{12})]\boldsymbol{\nabla} = \frac{36}{r^2}(\mathbf{L}\cdot\mathbf{S}) \ , \tag{C.26}$$

where $\mathbf{S} = (\boldsymbol{\sigma}_1 + \boldsymbol{\sigma}_2)/2$ and $\mathbf{L} = \mathbf{r}\times\mathbf{p} = -i(\mathbf{r}\times\boldsymbol{\nabla})$ is the orbital angular momentum operator of the relative motion.

From Eq. (C.22), we can calculate

$$[S_{12}, \nabla^2 S_{12}] = 0 \ , \tag{C.27}$$

and

$$(\boldsymbol{\nabla} S_{12})[S_{12}, \boldsymbol{\nabla}] = -(\boldsymbol{\nabla} S_{12})^2 \ . \tag{C.28}$$

C.5 Algebra of the six operators $O_{ij}^{n\leq 6}$

Eqs. (C.6), (C.18) and (C.20) show that the six operators

$$O^{1,\ldots,6} = 1, (\boldsymbol{\tau}_1\cdot\boldsymbol{\tau}_2), (\boldsymbol{\sigma}_1\cdot\boldsymbol{\sigma}_2), (\boldsymbol{\sigma}_1\cdot\boldsymbol{\sigma}_2)(\boldsymbol{\tau}_1\cdot\boldsymbol{\tau}_2), S_{12}, S_{12}(\boldsymbol{\tau}_1\cdot\boldsymbol{\tau}_2) \ , \tag{C.29}$$

close an algebra, i.e. they satisfy

$$O^i O^j = \sum_k K_{ij}^k O^k \ , \tag{C.30}$$

where the coefficients K_{ij}^k are easily obtained by calculating

$$\begin{aligned}
&O^1O^i = O^iO^1 = O^i \Rightarrow K_{1i}^k = K_{i1}^k = \delta_i^k \ , \\
&O^2O^2 = 3O^2 - 2O^2 \Rightarrow K_{22}^k = 3\delta_1^k - 2\delta_2^k \ , \\
&O^2O^3 = O^3O^2 = O^4 \Rightarrow K_{23}^k = K_{32}^k = \delta_4^k \ , \\
&O^2O^4 = 3O^3 - 2O^4 \Rightarrow K_{24}^k = K_{42}^k = \delta_3^k - 1\delta_4^k \ , \\
&O^2O^5 = O^5O^2 = O^6 \Rightarrow K_{25}^k = K_{52}^k = \delta_6^k \ , \\
&O^2O^6 = O^6O^2 = 3O^5 - 2O^6 \Rightarrow K_{26}^k = K_{62}^k = 3\delta_5^k - 2\delta_6^k \ , \\
&O^3O^3 = 3O^1 - 2O^3 \Rightarrow K_{33}^k = 3\delta_1^k - 2\delta_3^k \ , \\
&O^3O^4 = O^4O^3 = 3O^2 - 2O^4 \Rightarrow K_{34}^k = K_{43}^k = 3\delta_2^k - 2\delta_4^k \ ,
\end{aligned}$$

$$
\begin{aligned}
&O^3O^5 = O^5O^3 = O^5 \Rightarrow K^k_{35} = K^k_{53} = \delta^k_5 \ , \\
&O^3O^6 = O^6O^3 = O^6 \Rightarrow K^k_{36} = K^k_{63} = \delta^k_6 \ , \\
&O^4O^4 = 9O^1 - 6O^2 - 6O^3 + 4O^4 \Rightarrow K^k_{44} = 9\delta^k_1 - 6\delta^k_2 - 6\delta^k_3 + 4\delta^k_4 \ , \\
&O^4O^5 = O^5O^4 = O^6 \Rightarrow K^k_{45} = K^k_{54} = \delta^k_6 \ , \\
&O^4O^6 = O^6O^4 = 3O^5 - 2O^6 \Rightarrow K^k_{46} = K^k_{64} = 3\delta^k_5 - 2\delta^k_6 \ , \\
&O^5O^5 = 6O^1 + 2O^3 - 2O^5 \Rightarrow K^k_{55} = 6\delta^k_1 + 2\delta^k_3 - 2\delta^k_5 \ , \\
&O^5O^6 = O^6O^5 = 6O^2 + 2O^4 - 2O^6 \Rightarrow K^k_{56} = K^k_{65} = 6\delta^k_2 + 2\delta^k_4 - 2\delta^k_6 \ , \\
&O^6O^6 = 18O^1 - 12O^2 + 6O^3 - 4O^4 - 6O^6 + 4O^6 \\
&\qquad \Rightarrow K^k_{66} = 18\delta^k_1 - 12\delta^k_2 + 6\delta^k_3 - 4\delta^k_4 - 6\delta^k_4 + 4\delta^k_6 \ .
\end{aligned}
$$

C.6 Matrix elements of operators P_{2S+1} and Π_{2T+1}

We report a number of expectation values of projection operators P_{2S+1} and Π_{2T+1}, in two-nucleon states of definite total spin and isospin, $|SM_S, TM_T\rangle$

$$\langle P_{2S'+1}\Pi_{2T'+1}\rangle = \delta_{SS'}\delta_{TT'} \ , \tag{C.31}$$

$$\langle P_{2S'+1}\Pi_{2T'+1}P_{\sigma\tau}\rangle = (-)^{S+T}\delta_{SS'}\delta_{TT'} \ , \tag{C.32}$$

$$\sum_{SM_S} \delta_{S'1}\langle S_{12}P_{2S'+1}\Pi_{2T'+1}\rangle = \delta_{S'1}\delta_{TT'}\sum_{M_S}\langle 1M_S|\, S_{12}\,|1M_S\rangle = 0 \ , \tag{C.33}$$

$$\sum_{SM_S} \delta_{S'1}\langle S_{12}P_{2S'+1}\Pi_{2T'+1}P_{\sigma\tau}\rangle = 0 \ . \tag{C.34}$$

C.7 Matrix elements of $O^{n\leq 6}_{ij}$

The explicit expressions for the matrices appearing in Eq. (5.19), defined by

$$A^i_{\lambda\mu} = \langle\lambda\mu|\, O^i_{12}\,|\lambda\mu\rangle \ , \qquad B^i_{\lambda\mu} = \langle\lambda\mu|\, O^i_{12}\,|\mu\lambda\rangle \ , \tag{C.35}$$

where $|\lambda\mu\rangle$ denotes the two-nucleon spin-isospin state, can be easily obtained from the above properties of the six operators $O^{n\leq 6}$.

We find

$$A^1 = \begin{pmatrix} 1 & 1 & 1 & 1 \\ 1 & 1 & 1 & 1 \\ 1 & 1 & 1 & 1 \\ 1 & 1 & 1 & 1 \end{pmatrix} \ , \tag{C.36}$$

$$A^2 = \begin{pmatrix} 1 & 1 & -1 & -1 \\ 1 & 1 & -1 & -1 \\ -1 & -1 & 1 & 1 \\ -1 & -1 & 1 & 1 \end{pmatrix} \ , \tag{C.37}$$

$$A^3 = \begin{pmatrix} 1 & -1 & 1 & -1 \\ -1 & 1 & -1 & 1 \\ 1 & -1 & 1 & -1 \\ -1 & 1 & -1 & 1 \end{pmatrix} , \tag{C.38}$$

$$A^4 = \begin{pmatrix} 1 & -1 & -1 & 1 \\ -1 & 1 & 1 & -1 \\ -1 & 1 & 1 & -1 \\ 1 & -1 & -1 & 1 \end{pmatrix} , \tag{C.39}$$

$$A^5 = \begin{pmatrix} 1 & 1 & -1 & -1 \\ 1 & 1 & -1 & -1 \\ -1 & -1 & 1 & 1 \\ -1 & -1 & 1 & 1 \end{pmatrix} (3\cos^2\theta - 1) = A^2(3\cos^2\theta - 1) , \tag{C.40}$$

$$A^6 = \begin{pmatrix} 1 & -1 & -1 & 1 \\ -1 & 1 & 1 & -1 \\ -1 & 1 & 1 & -1 \\ 1 & -1 & -1 & 1 \end{pmatrix} (3\cos^2\theta - 1) = A^4(3\cos^2\theta - 1) , \tag{C.41}$$

$$B^1 = \begin{pmatrix} 1 & 0 & 0 & 0 \\ 0 & 1 & 0 & 0 \\ 0 & 0 & 1 & 0 \\ 0 & 0 & 0 & 1 \end{pmatrix} , \tag{C.42}$$

$$B^2 = \begin{pmatrix} 1 & 0 & 2 & 0 \\ 0 & 1 & 0 & 2 \\ 2 & 0 & 1 & 0 \\ 0 & 2 & 0 & 1 \end{pmatrix} , \tag{C.43}$$

$$B^3 = \begin{pmatrix} 1 & 2 & 0 & 0 \\ 2 & 1 & 0 & 0 \\ 0 & 0 & 1 & 2 \\ 0 & 0 & 2 & 1 \end{pmatrix} , \tag{C.44}$$

$$B^4 = \begin{pmatrix} 1 & 2 & 2 & 4 \\ 2 & 1 & 4 & 2 \\ 2 & 4 & 1 & 2 \\ 4 & 2 & 2 & 1 \end{pmatrix} , \tag{C.45}$$

$$B^5 = \begin{pmatrix} 1 & -1 & 0 & 0 \\ -1 & 1 & 0 & 0 \\ 0 & 0 & 1 & -1 \\ 0 & 0 & -1 & 1 \end{pmatrix} (3\cos^2\theta - 1) , \tag{C.46}$$

$$B^6 = \begin{pmatrix} 1 & -1 & 2 & -2 \\ -1 & 1 & -2 & 2 \\ 2 & -2 & 1 & -1 \\ -2 & 2 & -1 & 1 \end{pmatrix} (3\cos^2\theta - 1) , \tag{C.47}$$

where θ is the angle between $\mathbf{r}$ and the z axis.

C.8 Change of representation

In this Section we discuss the different representations for the operators of the "v_6" algebra and the relations which allow to change representation.
A generic operator x can be written as

$$x = \sum_{p=1}^{6} x_{ij}^{p} O^{p} = x_c + x_\tau(\boldsymbol{\tau}_1\cdot\boldsymbol{\tau}_2) + x_\sigma(\boldsymbol{\sigma}_1\cdot\boldsymbol{\sigma}_2) + x_{\sigma\tau}(\boldsymbol{\sigma}_1\cdot\boldsymbol{\sigma}_2)(\boldsymbol{\tau}_1\cdot\boldsymbol{\tau}_2) + x_t S_{12} + x_{t\tau} S_{12}(\boldsymbol{\tau}_1\cdot\boldsymbol{\tau}_2)\ , \tag{C.48}$$

in the basis of operators (C.29), or as

$$x = \sum_{TS} \left[x_{T0} + \delta_{S1} x_{tT} S_{12}\right] P_{2S+1}\Pi_{2T+1}\ , \tag{C.49}$$

in the "TS-representation".
The transformation matrix is given by

$$\begin{pmatrix} 1 & -3 & -3 & 9 \\ 1 & 1 & -3 & -3 \\ 1 & -3 & 1 & -3 \\ 1 & 1 & 1 & 1 \end{pmatrix} \begin{pmatrix} x_c \\ x_\tau \\ x_\sigma \\ x_{\sigma\tau} \end{pmatrix} = \begin{pmatrix} x_{00} \\ x_{10} \\ x_{01} \\ x_{11} \end{pmatrix}\ , \tag{C.50}$$

$$\begin{pmatrix} 1 & -3 \\ 1 & 1 \end{pmatrix} \begin{pmatrix} x_t \\ x_{t\tau} \end{pmatrix} = \begin{pmatrix} x_{t0} \\ x_{t1} \end{pmatrix}\ , \tag{C.51}$$

or

$$\begin{cases} x_{TS} = x_c + (4T-3)x_\tau + (4S-3)x_\sigma + (4S-3)(4T-3)x_{\sigma\tau}, \\ x_{tT} = x_t + (4T-3)x_{tT}. \end{cases} \tag{C.52}$$

The inverse transformation is given by

$$\frac{1}{16}\begin{pmatrix} 1 & 3 & 3 & 9 \\ -1 & 1 & -3 & 3 \\ -1 & -3 & 1 & 3 \\ 1 & -1 & -1 & 1 \end{pmatrix} \begin{pmatrix} x_{00} \\ x_{10} \\ x_{01} \\ x_{11} \end{pmatrix} = \begin{pmatrix} x_c \\ x_\tau \\ x_\sigma \\ x_{\sigma\tau} \end{pmatrix}\ , \tag{C.53}$$

$$\frac{1}{4}\begin{pmatrix} 1 & 3 \\ -1 & 1 \end{pmatrix} \begin{pmatrix} x_{t0} \\ x_{t1} \end{pmatrix} = \begin{pmatrix} x_t \\ x_{t\tau} \end{pmatrix}\ . \tag{C.54}$$

Bibliography

[1] S.L. Shapiro and S.A. Teukolsky, *Black Holes, White Dwarfs and Neutron Stars. The Physics of Compact Objects* (Wiley, New York, 1983).

[2] J.W. Clark and A. Sedrakian, in *Pairing in Fermionic Systems: Basic Concepts and Modern Applications*, (World Scientific, Singapore, 2006) p.135.

[3] O. Benhar and M. Valli, Phys. Rev. Lett. **99** (2007) 232501.

[4] A. Lovato, O. Benhar, S. Fantoni, A. Yu. Illarionov, and K.E. Schmidt, Phys. Rev. C **83** (2011) 054003.

[5] O. Benhar, A. Polls, M. Valli, and I. Vidaña, Phys. Rev C **81** (2010) 024305.

[6] O. Benhar and A. Carbone, (2009) arXiv: 0912.0129.

[7] O. Benhar and N. Farina, Phys. Lett. **680** (2009) 305.

[8] O. Benhar, A. Cipollone, and A. Loreti, Phys. Rev. C **87** (2013) 014601.

[9] A. Lovato, C. Losa, and O. Benhar, Nucl. Phys. A **901** (2013) 22.

[10] S. Chandrasekhar, Phys. Rev. Lett. **24** (1970) 611.

[11] S. Chandrasekhar, Astrophys. J. **161** (1970) 561.

[12] J.R. Oppenheimer and G.M. Volkoff, Phys. Rev. **55** (1939) 374.

[13] R.C. Tolman, Phys. Rev. **55** (1939) 364.

[14] A. Hewish, S.J. Bell, J.D.H. Pilkington, P.F. Scott, and R.A. Collins, Nature **217** (1968) 709.

[15] N.K. Glendenning, *Compact Stars: Nuclear Physics, Particle Physics, and General Relativity* (Springer, Berlin, 2000).

[16] S.E. Thorsett, Z. Arzoumanian, and J.H. Taylor, Ap. J. **405** (1993) L29.

[17] L. Lindblom and S. Detweiler, Ap. J. Suppl. **53** (1983) 73.

[18] N. Andersson and K.D. Kokkotas, MNRAS **299** (1998) 1059.

[19] O. Benhar, V. Ferrari, and L. Gualtieri, Phys. Rev. D **70** (2004) 124015.

[20] J. F. Annett, *Superconductivity, Superfluids and Condensates* (Oxford University Press, Oxford, 2003).

[21] L.N. Cooper, Phys. Rev. **104** (1956) 1189.

[22] J. Bardeen, L.N. Cooper, and R. Schrieffer, Phys. Rev. **108** (1957) 1175.

[23] N.H. March, W.H. Young, and S. Sampanthar, *The many-body problem in quantum mechanics* (Cambridge University Press, Cambridge, 1967).

[24] P. Ring and P. Schuck, *The Nuclear Many-Body Problem* (Springer-Verlag, Heidelberg, 1980).

[25] J.G. Valatin, Nuovo Cim. **7** (1958) 843.

[26] N.N. Bogoliubov, Soviet Phys. JEPT **34** (1958) 41.

[27] N.N. Bogoliubov, Nuovo Cim. **7** (1958) 794.

[28] R. Tamagaki, Prog. Theor. Phys. **44** (1970) 905.

[29] T. Takatsuka and R. Tamagaki, Prog. Theor. Phys. Suppl. No. **112** (1993) 27.

[30] K. Yosida, Phys. Rev. **111** (1958) 1255.

[31] D.R. Tilley and J. Tilley, *Superfluidity and Superconductivity* (Adam Hilger LTD, Bristol and Boston, BS1, 1986).

[32] M. Baldo, J. Cugnon, A. Lejeune, and U. Lombardo, Nucl. Phys. A **515** (1990) 409.

[33] M. Baldo, J. Cugnon, A. Lejeune, and U. Lombardo, Nucl. Phys. A **536** (1992) 349.

[34] H.A. Bethe, Rev. Mod. Phys. **8** (1936) 139.

[35] S. Shlomo and D.H. Youngblood, Phys. Rev. C. **47** (1993) 529.

[36] V.G.J. Stoks, R.A.M. Klomp, M.C.M. Rentmeester, and J.J. de Swart, Phys. Rev. C **48** (1993) 792.

[37] R.B. Wiringa, V.G.J. Stoks, and R. Schiavilla, Phys. Rev. C **51** (1995) 38.

[38] B.S. Pudliner, V.R. Pandharipande, J. Carlson, and R.B. Wiringa, Phys. Rev. Lett. **74** (1995) 4396.

[39] S.C. Pieper and R.B. Wiringa, Ann. Rev. Nucl. Part. Sci. **51** (2001) 53.

[40] E. Feenberg, *Theory of quantum fluids* (Academic Press, New York, NY, 1969).

[41] J.W. Clark, Prog. Part. Nucl. Phys. **2** (1979) 89.

[42] S. Fantoni and V.R. Pandharipande, Phys. Rev. C **37** 1697 (1988) 1697.

[43] S. Fantoni and S. Rosati, Nuovo Cimento A **25** (1975) 593.

[44] V.R. Pandharipande and R.B. Wiringa, Rev. Mod. Phys. **51** (1979) 821.

[45] S. Cowell, Ph.D. Thesis, University of Illinois at Urbana-Champaign (2004).

[46] S. Cowell and V.R. Pandharipande, Phys. Rev. C **70** (2004) 035801.

[47] N. Farina, PhD in Physics Thesis, "Sapienza" University of Rome (2009). arXiv: 0901.2507.

[48] I. Lagaris and V.R. Pandharipande, Nucl. Phys. A **359** (1981) 349.

[49] A. Akmal, V.R. Pandharipande, and D.G. Ravenhall, Phys. Rev. C **58** (1998) 1804.

[50] A. Sarsa, S. Fantoni, K.E. Schmidt, and F. Pederiva, Phys. Rev. C **68** (2003) 024308.

[51] V.A. Khodel, V.V. Khodel, and J.W. Clark, Nucl. Phys. A **598** (1996) 390.

Ringraziamenti

Scrivere una Tesi non comporta solo forza di volontà, studio, impegno, speranza e insonnia, ma richiede anche la presenza di persone che siano in grado di dare un valido sostegno nei momenti più difficili. Qui di seguito, vorrei, appunto, ringraziare queste persone che mi sono state vicine in questi ultimi mesi ma anche in questi lunghissimi, intensissimi e soprattutto bellissimi anni universitari, senza le quali, probabilmente, non avrei raggiunto la mia "meta".

Innanzitutto, desidero ringraziare il mio relatore Prof. Omar Benhar Noccioli per avermi fatto intravedere cosa significa veramente fare Ricerca: un processo di crescita in cui si impara a correggere i propri errori e come ciò risulti ancora più difficile in Italia dove non si finanzia mai abbastanza. Per quanto riguarda il lato umano, lo vorrei ringraziare per avermi insegnato che, per riuscire a raggiungere i propri obiettivi, non basta solo l'impegno e la forza di volontà, ma serve anche una componente fondamentale nei momenti di crisi e di emergenza: l'ottimismo, ciò che fa la differenza molte volte. E ciò si è dimostrato immancabilmente vero, proprio con la mia Tesi. Vorrei ringraziarlo, inoltre, per l'aspetto tecnico: per non avermi ostacolato nello scrivere la Tesi in una lingua diversa dalla mia (idea da molti giudicata completamente folle) ma, anzi, di avermi seguito nella correzione, anche linguistica. Infine, lo ringrazio per la sua multidisciplinarietà, che poi è stato il motivo principale nella mia scelta di questa Tesi: il fatto di non porre mai dei limiti né alla conoscenza, né alla curiosità.

Ringrazio vivamente anche il mio relatore della Tesi triennale, Dr. Carlo Luciano Bianco, che è stato un' inesauribile fonte di consigli preziosi. In particolare, senza il suo aiuto, non avrei mai risolto alcuni dei problemi del mio programma di simulazione e molti grafici di questa Tesi non avrebbero mai visto la luce, né un layout accettabile.

Vorrei ringraziare anche il Prof. Massimo Testa che mi ha permesso di essere il suo incubo per un intero semestre e mi ha seguito nella mia preparazione dell'esame di Meccanica Quantistica Relativistica. Se certi fondamenti della Fisica Teorica mi sono molto chiari, lo devo soprattutto alle sue risposte alle mie domande senza fine.

Ringrazio mia sorella Francesca, detta Tata, per due ragioni molto profonde: la prima è che, nonostante il suo odio per la Fisica, mi ha trasmesso l'amore per la Scienza. Grazie a lei, infatti, da bambina ho capito cosa mi sarebbe piaciuto fare da grande. La seconda, grazie per Diego: è il miglior nipote che si possa desiderare. Proverò a insegnargli qualcosa di utile nella vita.

Ringrazio di cuore anche il Prof. Alessandro Ercoli, che è stato un ottimo insegnante di Liceo. Se non lo avessi incontrato, non mi sarebbe mai venuto in mente di fare il fisico da grande. Grazie anche per essermi stato vicino nei momenti più duri degli anni universitari, quelli in cui si voleva gettare la spugna, ma alla fine non si è mai fatto perché, "in cima alla salita, la soddisfazione è sempre doppia".

Grazie ai miei genitori per la loro straordinaria e umana imperfezione. Grazie per non essere stati d'accordo, all'inizio, con alcune delle mie scelte. Solo dalla lotta, ho capito quanto queste fossero importanti per me. Se potessi tornare indietro, ripercorrerei le stesse strade, perché ne è valsa la pena. Grazie, inoltre, per non essere stati mai autoritari: ho imparato a pensare con la mia testa, senza accettare nulla ciecamente e a rifiutare l'omologazione, in difesa della diversità.

Ringrazio anche tutte le mie coinquiline che in questi anni hanno condiviso il tetto e le loro vite con me. In particolare, grazie a Mariagiovanna, Natalie, Camilla, Petra, Marzia e Sara. Grazie a voi ho imparato ad apprezzare la diversità e a imparare da essa. Senza etichette, né contenitori in cui racchiudere le persone. Non ha senso dividere l'umanità in sottoinsiemi. Grazie per le serate estive passate in terrazza, per le cene distruttive sudcoreane e non e per le uscite per Roma. Normalmente, le persone scelgono con cui vivere. Io non vi ho scelto, ma se avessi potuto, l'avrei fatto.

Un ringraziamento veramente speciale va a Sarah, amica da una vita, coinquilina e collega. Grazie per aver cucinato per me quando ero sotto esame e per aver tentato di insegnarmi ad accendere la lavatrice da sola. Grazie per essere stata la mia sempiterna compagna di laboratorio, luogo alquanto cupo e buio, per quelli come me che, appunto, non riescono neanche ad accendere una lavatrice, figuriamoci a far funzionare un circuito! Grazie per aver creduto nelle mie capacità, quando io stessa avevo perso ogni speranza. Ti ringrazio per aver curato ogni mia paranoia, però, in quanto a paranoie, anche tu ne avevi abbastanza e, infatti, siamo cresciute assieme, sostenendoci a vicenda quando tutto andava storto, quando la salita non finiva mai e quando nulla andava come avevamo sognato...almeno all'inizio. Ho imparato che quando il cammino è difficile, non si può viaggiare da soli, ma c'è bisogno di un valido compagno che sappia sollevarci quando cadiamo, curarci quando ci facciamo male e sostenerci quando perdiamo di vista la meta. Sei uno dei pochi fisici che io conosca a essere sia teorico che sperimentale, quando tutti decidono di diventare l'uno o l'altro, perché si rendono conto di essere completamente negati in una cosa, come me. Ti stimo.

Grazie anche a Elena, altra coinquilina e collega, che condivide con me la negazione per la lavatrice e per il laboratorio. Grazie per aver studiato con me Meccanica Quantistica Relativistica che non era più un esame, ma una sfida. Ringrazio anche Giovanna Chiara, la cui bravura e intelligenza non finiranno mai di stupirmi. E' da lei che ho imparato la filosofia del "I can do it!". In questi mesi, ogni volta che entravo in saletta laureandi teorici e voi eravate lì, c'era un vivace scambio di cose-che-non-tornano-con-la-Tesi-e-non-si-sa-il-perché...Ho capito che è importante condividere i propri problemi, perché si comprende come, in realtà, "siamo tutti sulla stessa barca" e quindi non bisogna disperarsi, ma tentare di risolverli, magari assieme.

Ringrazio anche la mia eterna compagna di banco, Laura, che mi ha visto crescere in ben 13 anni di scuola. Grazie per aver scelto di condividere con me fatti tragici e allo stesso tempo straordinari in grado di sconvolgere una vita da un giorno all'altro. Grazie per Matilde. Ora sono anche una zia "adottiva".

In chiusura, ringrazio anche tutti i miei amici vecchi, nuovi e ritrovati di Viterbo. Senza di voi il mio ritorno a casa poteva essere drammatico. Grazie per avermi sostenuto in questi ultimi mesi di disastri emotivi-sentimentali-esistenziali. Avete tenuto la mia mente lontana dai pensieri che potevano farmi del male: siete stati le mie "morfine" viventi. Grazie a Virginia, Roberta detta Roby, Jacopo e a tutti gli altri che bazzicano per il 2 Righe Book Bar. In particolare, Virginia, per i 19 anni sempre assieme e Roby, per avere in comune con me un insieme infinito di cose. A queste due ultime persone, aggiungo anche Maria Laura e Amelio, detto Junior, Juju o Ju, per completare la squadra delle glitterate all'Elletì Bar del Venerdì,

che si trasformano sempre in sedute psicoanalitiche per tentare di risolvere tutti i nostri dilemmi. Probabilmente, in un'altra vita, eravamo degli Esistenzialisti. Aggiungendo la presenza di Elisabetta ed il suo memorabile Tiramisù al cioccolato bianco, si completa così la compagnia di quelli che giocano a Dixit (alquanto da strizzacervelli!).

Dicono che nella vita ci vuole fortuna. La mia non è legata tanto a quello che mi è capitato finora, quanto al fatto di aver incontrato queste persone, ognuna delle quali mi ha insegnato qualcosa e mi ha permesso di intraprendere alcune strade e non altre. E' come se ognuna di loro mi avesse donato un pezzo di sé, che io custodisco gelosamente come se fosse un tesoro. Io sono la somma di questi pezzi, che ancora tento di mettere assieme e di dare un senso al tutto. Sono un work-in-progress. Ho ancora molto da imparare. Sono ancora in viaggio: e questo è più eccitante di qualsiasi meta.